Neural dynamics and their relationship to learning behavior in response to stimulation with a cortical neuroprosthesis

Dissertation

zur Erlangung des akademischen Grades

doctor rerum naturalium
(Dr. rer. nat.)

genehmigt durch die Fakultät für Naturwissenschaften
der Otto-von-Guericke-Universität Magdeburg

von Dipl. Biol. Matthias Deliano

geb. am 7. April 1972 in München

Gutachter: Prof. Dr. med. Henning Scheich

                Prof. Dr. rer. nat. Klaus-Peter Hoffmann

                Prof. Dr. med. Hans-Jochen Heinze

eingereicht am: 11. November 2004

verteidigt am: 15. November 2005

Abstract

Replacing lost sensory function with a cortical neuroprosthesis would be a promising alternative to interfacing earlier stages of the afferent sensory pathways, e.g. with cochlear or retinal implants. In bypassing the afferent pathways altogether, expectedly a wider range of patients would benefit from a cortical neuroprosthesis including those with damages at any level of the afferent sensory pathways. The critical step for the development of a sensory cortical neuroprosthesis is the generation of meaningful structured perception on the basis of spatially and temporally patterned electrical stimulation of sensory cortex. In this respect, previous attempts in the development of such neuroprostheses focusing on the encoding of environmental stimuli into patterns of electrical stimulation have been rather unsuccessful. The present thesis tries to go beyond this simple coding approach by investigating how the meaningful interpretation of neuroprosthetic stimulation arises from its interaction with the ongoing cortical dynamics through learning. For this, intracortical microstimulation (ICMS) was applied to the auditory cortex of Mongolian gerbils (*Meriones unguiculatus*) via a simple unidirectionally operating cortical implant. Animals were trained in a GO/(NO-GO)-paradigm to discriminate stimulation sites in the low and high frequency region of the tonotopic map of the primary auditory cortex. The ongoing cortical activity was measured by concurrently recording the electrocorticogram (ECoG) at high spatial resolution parallel during discrimination learning of electrical stimuli. Spatial cortical activity patterns associated with the behaviorally relevant stimulus classes were identified in the β- and γ-band (15 Hz to 80 Hz) of the ongoing ECoG by a multivariate pattern classification procedure. Patterns identified in this way were found in late epochs about 1 or 2 seconds after stimulus onset, i.e. in the time range between the end of the electrical stimulus and the behavioral response. They were neither precisely time-locked to the stimulus, nor to the response, emerged over training sessions and were not present in training sessions before the animals reached significant behavioral discrimination performance. Furthermore, classification performance in the late epochs after the end of the electrical stimulus was significantly correlated with the behavioral discrimination performance, indicating that the emergence of late cortical activity patterns was related to learning. The observed patterns shared many properties with late cortical activity patterns emerging with discrimination and categorization learning

of acoustic stimuli, which are thought to reflect the subjective perceptual sorting of stimuli into classes relevant in the context of the behavioral contingencies. However, the analysis of the spatial organization of the late cortical activity patterns by a discriminant analysis based on a bootstrapping procedure showed that late cortical activity patterns emerging with discrimination learning of electrical stimuli were more focal compared to the distributed patterns found with acoustic discrimination learning. This indicates principle differences in the modes how cortical dynamics is recruited to form discernable percepts when using acoustic or electrical stimuli. To restore the mode of cortical operation seen with meaningful acoustic stimulation, a proper timing of electrical stimulation in reference to changing cortical states might be crucial. This could be achieved by an interactive, bidirectional cortical neuroprosthesis that guarantees for the proper timing of the electrical stimuli conditional on the momentary cortical state, and by this improve the perceptual interpretation of stimuli delivered by the neuroprosthetic device.

Zusammenfassung

Die Wiederherstellung verloren gegangener sensorischer Funktionen mit Hilfe einer corticalen Neuroprothese ist eine viel versprechende Alternative zur Bereitstellung von Schnittstellen mit weiter peripher lokalisierten Stationen der afferenten sensorischen Bahnen, wie sie z.B. Cochlea- oder Retinaimplantate darstellen. Durch die vollständige Umgehung afferenter sensorischer Bahnen würde ein größerer Patientenkreis von einer sensorischen Cortexporthese profitieren, so z.B. auch alle Patienten bei denen frühere Verarbeitungsstationen auf dem Weg zum Cortex geschädigt sind (Normann et al., 1999).

Die Entwicklung einer corticalen Neuroprothese ist eine große Herausforderung, nicht nur wegen der weitreichenden sozialen und ethischen Implikationen einer solchen Technologie. Der entscheidende Schritt in der Entwicklung einer corticalen Neuroprothese ist die Erzeugung einer Wahrnehmung von bedeutungsvollen Objekten und Szenen, von denen sich blinde oder taube Personen in ihren Alltagshandlungen leiten lassen können. Diesbezüglich sind frühere Versuche, eine corticale Neuroprothese allein auf der Grundlage einer geeigneten Kodierung von Umweltreizen in elektrische Stimulationsmuster zu entwickeln, weitgehend gescheitert (Brindley & Lewin, 1968; Schmidt et al., 1996). In der hier vorliegenden Arbeit wird daher versucht, diesen reinen „Kodierungsansatz" zu überwinden und sich direkt mit der Frage auseinanderzusetzen, wie an den Cortex übertragene elektrische Stimuli wahrgenommen und durch Lernen bedeutungsvoll interpretiert werden können. Dazu ist es notwendig, ein besseres Verständnis für die Interaktion zwischen neuroprothetischer Stimulation und der endogenen corticalen Dynamik zu gewinnen, durch die eine erlernte bedeutungsvolle Interpretation elektrischer Stimuli hervorgebracht wird.

In einem ersten Schritt wurde in der vorliegenden Arbeit ein Tiermodel entwickelt, mit dem sich die Interaktion zwischen neuroprothetischer Stimulation und endogener corticaler Dynamik in frei beweglichen und lernenden Mongolischen Wüstenrennmäusen (Meriones unguiculatus) untersuchen lässt. Über eine einfache, unidirektionale neuroprothetische Schnittstelle wurde dabei an einzelnen Stellen im auditorischen Cortex eine intracorticale Mikrostimulation (ICMS) appliziert (Scheich & Breindl, 2002). Die Schnittstelle zum Cortex bestand aus zwei Stimulationselektroden

(~700 µm Elektrodenabstand), die chronisch in die Tiefe des auditorischen Cortex, nahe der corticalen Eingangsschicht IV, implantiert wurden. Die ICMS wurde durch die Stimulationselektroden an einem von zwei Stimulationsorten entlang des tonotopen Gradienten des auditorischen Cortex appliziert und beschränkte sich somit auf einzelne Stellen im Cortex. Dadurch sollten erst einmal einfache Prinzipien der Interaktion zwischen ICMS und endogener corticaler Dynamik untersucht werden, die vermutlich aber auch für die bedeutungsvolle Interpretation von elektrischen Stimulationsmustern durch gleichzeitige ICMS an mehreren Stellen im Cortex eine grundlegende Rolle spielen.

Um die räumliche und zeitliche Spezifität der ICMS zu bestimmen, wurde in einer Testmessung vor Trainingsbeginn ein räumlich hoch aufgelöstes Elektrocorticogram (ECoG) des auditorischen Cortex über ein chronisch implantiertes 6x3 epidurales Oberflächen-Array abgeleitet (~600 µm Elektrodenabstand). Elektrisch evozierte Potentiale in Antwort auf einzelne Strompulse wurden analysiert. Generell spiegeln diese Potentiale die transsynaptische Aktivierung wieder, die aus der direkten Erregung der am Stimulationsort vorbeiziehenden axonalen Fasern resultiert (Nowak & Bullier, 1998a, b).

Die durch einzelne Strompulse elektrisch evozierten Potentiale besaßen eine typische Wellenform, die einer gedämpften, frequenz-modulierten Oszillation ähnelte. Dabei fielen die Peak-Amplituden innerhalb 150 ms nach der Reizung stark ab und erreichten den Rauschpegel. Die Frequenz der Oszillation nahm in dieser Zeit von etwa 80 Hz auf etwa 20 Hz ab. Ein mit einer Latenz von etwa 12 ms auftretender negativer Peak des durch Einzelpulse elektrisch evozierten Potentials zeigte in seiner Topographie einen Aktivitätsfokus mit maximalen Peak-Amplituden am Ort der elektrischen Stimulation. Die räumliche Ausdehnung der fokalen, elektrisch evozierten Aktivität überstieg den theoretisch geschätzten Bereich der effektiven Stromausbreitung, d.h. den Bereich in dem neuronale Elemente direkt durch ICMS erregt werden (Tehovnik, 1996). Insgesamt zeigten die Ergebnisse, dass die räumlich und zeitlich begrenzte Anregung durch ICMS zu einer räumlich und zeitlich ausgedehnten transsynaptischen Aktivierung führte. Daher scheint die räumliche und zeitliche Spezifität der ICMS vor allem von den intrinsischen corticalen Verbindungen, also vom Radius und der Geometrie der direkt angeregten exzitatorischen und inhibitorischen Fasern, und vom sich daraus ergebenden

postsynaptischen Wechselspiel aus Exzitation und Inhibition abzuhängen (Butovas & Schwarz, 2003). Durch die damit verbundene räumliche Ausbreitung der transsynaptischen Anregung werden große Zellpopulationen aktiviert, die sich zum Teil zwischen den Stimulationsorten überlappen.

Nach der Testmessung wurden sechs Mongolische Wüstenrennmäuse in einer Shuttle-Box mit Hilfe eines GO/(NO-GO)-Paradigmas trainiert. Sie mussten lernen, elektrische Pulszüge voneinander zu unterscheiden, mit denen zwei Regionen, welche tiefe and höhere Frequenzen in der tonotopen Karte des auditorischen Cortex repräsentierten, angeregt wurden (Scheich et al., 1993). An einem der zwei Stimulationsorte wurde ein elektrischer Pulszug als positiv konditionierter Stimulus (CS+) appliziert und am jeweilig anderen ein Pulszug, der als negativ konditionierter Stimulus (CS-) diente. Trotz der beträchtlichen Überlappung der an den Stimulationsorten transsynaptisch aktivierten Neuronenpopulationen (Butovas & Schwarz, 2003), waren alle Tiere in der Lage, die Diskriminierungsaufgabe zu bewältigen. Die Tiere lernten, die beiden Stimulationsorte innerhalb von vier oder fünf Trainingstagen zu unterscheiden. Wie die Analyse ihres Verhaltens zeigte, waren die Tiere offensichtlich in der Lage, einfache neuroprothetische Stimulation in bedeutungsvoller Weise zu interpretieren (Scheich & Breindl, 2002).

Um die Interaktion zwischen neuroprothetischer Stimulation und der endogenen corticalen Dynamik zu untersuchen, wurde ein räumlich hoch aufgelöstes ECoG vom auditorischen Cortex in Antwort auf elektrischen Pulszüge abgeleitet, die als CS+ und CS- während dem Training präsentiert wurden. Wie schon bei den durch einzelne elektrische Pulse evozierten Potentialen der Testmessung vor dem Training, evozierten die CS+ und CS- Pulszüge eine gedämpfte, frequenz-modulierte Oszillation. Zum Ende des Pulszuges hin fielen die Peak-Amplituden rapide ab. Manchmal jedoch überdauerte das elektrisch evozierte Potential den elektrischen Stimulus. Mit einem Frequenzabfall von etwa 20 Hz auf etwa 5 Hz war die Oszillation generell langsamer verglichen mit der Einzelpulsstimulation. Im elektrisch evozierten Potential trat nach einer Latenz von etwa 30 ms ein negativer Peak auf, dessen maximalen Amplituden am Ort der Stimulation lokalisiert waren.

Corticale Aktivitätsmuster in Verbindung mit dem CS+ und dem CS- ließen sich im β- und γ-Band (15 Hz bis 80 Hz) des ECoG mit Hilfe eines multivariaten Klassifikationsverfahrens identifizieren (Barrie et al., 1996). Die Klassifikation wurde

in 180 ms Zeitfenstern durchgeführt, die in 20 ms Schritten über dem Signal verschoben wurden. Für jedes 180 ms Zeitfenster wurde eine räumliche Verteilung der Signalleistung im β- and γ-Band anhand von Root Mean Squared (RMS) Amplituden bestimmt, die für jeden Ableitkanal berechnet wurden. Über Euklidische Abstände wurde festgestellt, ob sich eine resultierende räumliche Aktivitätsverteilung näher an einem CS+- oder näher an einem CS- Centroid befand. Für jeden Zeitschritt wurde die Klassifikationsleistung als Prozentsatz der korrekt klassifizierten Trials bestimmt und die Signifikanz der Klassifikationsleistung mit Hilfe einer Binomialstatistik evaluiert. Epochen signifikanter Musterklassifikation fanden sich früh, währen der Präsentation der elektrischen Stimuli, und spät, in der Zeit zwischen dem Ende des elektrischen Stimulus und der Verhaltensantwort.

Frühe corticale Aktivitätsmuster konnten durch Epochen hochsignifikanter Musterklassifikation in den ersten 100 ms nach Stimulusbeginn identifiziert werden. Sie fanden sich in festem Zeitbezug zum Stimulus und traten an allen Trainingstagen auf, unabhängig vom Lernzustand und der Lerngeschichte des Tieres. Frühe Epochen hochsignifikanter Musterklassifikation koexistierten mit der frühen negativen Welle im elektrisch evozierten Potential. Aufgrund des fokalen Maximums am Stimulationsort stellte die räumliche Variation der negativen Peak-Amplitude ein Muster dar, das gut zwischen CS+ und CS- unterscheidbar war. Offensichtlich spiegelten die frühen corticalen Aktivitätsmuster die fokale Topographie des durch ICMS transsynaptische evozierten, künstlichen sensorischen Inputs wieder.

Späte corticale Aktivitätsmuster im β- and γ-Band des ECoG wurden anhand von Epochen signifikanter Musterklassifikation in der Zeit zwischen Stimulusende und Verhaltensantwort identifiziert. Späte corticale Aktivitätsmuster fanden sich in keinem festen Zeitbezug, weder zum elektrischen Stimulus noch zur Verhaltensantwort. Sie traten im Laufe des Trainings auf, fanden sich aber nicht an Trainingstagen, an denen das Tier noch keine signifikante Lernleistung zeigte. Dass die Klassifikationsleistung in den späten Epochen signifikant mit der Lernleistung korreliert war, ließ darauf schließen, dass die späten corticalen Aktivitätsmuster lerniduziert waren. In den elektrisch evozierten Potentialen wurde keine Aktivität gefunden, durch die sich die signifikante Musterklassifikation in den späten Epochen

hätte erklären lassen können. Die Muster bestanden aus räumlichen Amplituden-Modulationen einer aperiodischen Trägerwelle im β- and γ-Band des ECoG und wurden offensichtlich von der endogenen corticalen Aktivität hervorgebracht.

Die späten corticalen Aktivitätsmuster, die mit dem Diskriminierungslernen elektrischer Stimuli auftraten, ähnelten in vielerlei Hinsicht späten corticalen Aktivitätsmustern die beim Diskriminierungslernen akustischer Stimuli gefunden und in Beziehung zur bedeutungsvollen Interpretation dieser Stimuli gebracht wurden (Ohl et al., 2003a, b). Entsprechend könnten auch die durch elektrisches Diskriminierungslernen hervorgebrachten späten corticalen Aktivitätsmuster mit der subjektiven, perzeptuellen Einordnung der elektrischen Stimuli in verhaltensrelevante, bedeutungsvolle Stimulusklassen zu tun haben, wie dies im Falle akustischer Reizung mit Hilfe eines Ansatzes gezeigt werden konnte, der sich die subjektive Bildung von Kategorien zu Nutze machte (Ohl et al., 2001).

In Bezug auf ihre räumliche Organisation wurden jedoch auch deutliche Unterschiede zwischen den durch elektrisches und akustisches Lernen induzierten corticalen Aktivitätsmustern gefunden. Die räumliche Organisation corticaler Aktivitätsmuster wurde mit Hilfe einer auf einem Bootstrapping Verfahren beruhenden Diskriminanzanalyse erfasst (Ohl et al., 2003a). Die Ergebnisse zeigten, dass die späten corticalen Aktivitätsmuster die beim Diskriminierungslernen elektrischer Stimuli auftraten fokal waren, im Gegensatz zu den räumlich verteilten Mustern, die beim akustischen Lernen beobachtet wurden (Ohl et al., 2003a). Gleichzeitig ließ sich die fokale räumliche Organisation der elektrisch induzierten späten corticalen Aktivitätsmuster nicht direkt mit der fokalen transsynaptischen Aktivierung am Stimulationsort in Verbindung bringen. Dies könnte bedeuten, dass die endogene corticale Dynamik von elektrischen Stimuli in einer anderen Weise rekrutiert wird als mit akustischer Stimulation.

Die hoch synchrone Aktivierung großer, gemischter Neuronenpopulationen im Cortex durch ICMS könnte einen großen Einfluss auf den corticalen Funktionsmodus ausüben. Darüber hinaus kann ICMS durch diese hoch synchrone Anregung plastische Veränderungen im Cortex auslösen (Maldonado & Gerstein, 1996a; Sakai & Suga, 2002; Valentine & Eggermont, 2003), wodurch die lerninduzierte Musterbildung möglicherweise verzerrt werden kann. Der generelle Anstieg der Amplitude des elektrisch evozierten Potentials über die Trainingstage könnte ein

Hinweis auf solche ICMS induzierten plastischen Veränderungen sein. Des weiteren traten im Verlauf der Trainingstage Epochen signifikanter Musterklassifikation zu späteren Zeitpunkten während der Präsentation der elektrischen Stimuli auf. Da der Zuwachs and Klassifikationsleistung in dieser Zeit nicht signifikant mit der Lernleistung des Tieres korreliert war, wurden die der Klassifikation unterliegenden Muster möglicherweise durch die ICMS selbst induziert. Schließlich ist zu beachten, dass, durch die Umgehung afferenter sensorischer Bahnen, unidirektional applizierte ICMS zeitlich nicht mit möglichen endogenen corticalen Zustandsänderungen abgestimmt ist (Freeman & Barrie, 2000; Ohl et al., 2001). Dies könnte ebenso zu einer veränderten Funktionalität des Cortex unter elektrischer Stimulation führen.

Durch die Entwicklung einer interaktiven, bidirektionalen corticalen Neuroprothese wäre es möglich eine passende zeitliche Abstimmung zwischen ICMS und endogener corticaler Dynamik zu erreichen und somit die Möglichkeiten einer bedeutungsvollen Interpretation neuroprothetischer Stimulation zu verbessern. Ein grundlegendes Verständnis der Interaktion zwischen neuroprothetischer Stimulation und endogener corticaler Dynamik ist auf jeden Fall eine wichtige Vorraussetzung, um den entscheidenden Schritt in der Entwicklung einer corticalen Neuroprothese zu tun: der Erzeugung einer bedeutungsvoll strukturierten Wahrnehmung mit Hilfe räumlicher und zeitlicher Muster elektrischer Cortexstimulation.

Content

1. Introduction

1.1. Preface: of men and machines

In 1960 the medical engineer Manfred Clynes and the psychiatrist Nathan Kline invented the term cyborg to describe their vision of augmenting the human body by technical devices to be better adapted to an extraterrestrial environment during space travel (Clynes & Kline, 1960). Since then the development of technology for the interfacing between men and machines has been more than an ordinary scientific project most often involving a vision about the future of being human. This is why the cyborg became such a major theme in science fiction literature and movies. Altering our perception and our action, brain machine interfaces (BMIs) are a central issue here, because they apparently have the widest reaching consequences among interfaces between men and machines.

Figure 1: Hopes and fears related to brain machine interfaces (BMIs) illustrated by characters from the science fiction television series Star Trek. Commander Geordi LaForge from the starship Enterprise represents the positive perspective on BMI technology. Although born blind, he has visual capabilities which even transcend normal human vision by using a technical device called visor directly connected to his visual cortex (left). The Borg (right) stand for a negative vision of BMI technology. Humans connected to the BMI of the Borg become part of a cybernetic super-organism. Loosing their identity they turn into unhuman monsters (adapted from http://en.wikipedia.org/wiki/Geordie_LaForge and http://en.wikipedia.org/wiki/Borg).

Science fiction expresses both the hopes and fears related to this kind of technology. On the one hand BMI technology promises to let paralyzed people walk, blind people see, or deaf people hear again. This enthusiastic view on BMI technology is

illustrated by the character Geordi LaForge from the science fiction television series Star Trek, who is a Commander of the starship Enterprise. Born blind he is able to see by using a technical device called visor. The visor consists of an implant in his visual cortex which is connected at the temples to a half-moon shaped optical sensor positioned over his eyes (figure 1, left). Although painful, the visor allows him to perceive throughout the electromagnetic spectrum from infrared to radio frequencies and thus to even transcend normal human vision. On the other hand BMI technology provokes fears that our subjective experience might be unwillingly controlled by a machine without even being recognized by us. This negative perspective is illustrated by the Borg in the Star Trek series. Humans connected to the BMI of the Borg are assimilated by a cybernetic super-organism. With their actions controlled to serve the intentions of this super-organism, they turn into unhuman monsters (figure 1, right). Similar to the miracles described in the bible, BMI technology ultimately nourishes our spiritual desire to transcend our abilities beyond the limits of our biological destiny. By transforming ourselves into renewable machines we might finally reach immortality. However, this could come at a high price, as we might also loose our human identity along such a transformation.

That the hopes and fears might not only dwell on unrealistic fiction is shown by the advances in BMI technology during the last decades. With the use of inner ear prostheses (cochlear implants) electrically stimulating the 8th cranial nerve, deaf people can have the legitimate hope to regain speech understanding again. Also, children born deaf have a good chance to acquire spoken language with such a device. Otherwise, a recent experiment by Talwar and colleagues (2002) has provoked a highly controversial debate about the potential dangers of BMI technology. As implied by the authors, this experiment demonstrates that the navigation of a rat through a 3D environment could be remote-controlled by signals transmitted to the brain via a BMI. To move the rat forward, the experimenters delivered electrical stimulation of the medial forebrain bundle, which is known to arouse appetitive motivational behavior. Virtual touch sensations to the left or right whiskers evoked by electrical stimulation of the corresponding representations of the somatosensory cortex were used as signals to turn the animal either left or right.

However, in questioning our human self-understanding the concerns about BMIs go far beyond the actual possibilities of the state of the art of this technology. BMI technology is based on neuroscientific research that explains our perception and our actions from a third person perspective as directed by biological mechanisms. It is still an unresolved issue how this view relates to the first person perspective of our subjective experiences characterized by intentional action in a meaningful world – a perspective which seems to defy current mechanistic explanations of brain functioning. With the invasion of BMI technology into our brains, this issue comes to a head. What ultimately is this hybrid creature called a cyborg, an externally directed machine or a self-determined human? To resolve this opposition will require new scientific concepts of brain functioning that take serious our first person lived experience (Varela & Shear, 1999). But, it will also afford to take the challenge in transforming our conception of what it is meant to be human. This will inevitably involve a redefinition of ourselves in relation to the machines we live with, or as the feminist philosopher Donna J. Haraway puts it: "The machine is not an it to be animated, worshipped, and dominated. The machine is us, our processes, an aspect of our embodiment" (Haraway, 1991, p.180). How the interaction between a neuroprosthesis and the brain via a BMI is conceptualized is therefore not only important for guiding experimental research, but has far reaching social, political and ethical implications, which are inherent in these concepts and not only imposed by external discourses.

This becomes obvious from the "ratbot" experiment described above (Talwar et al. 2002). With the objective of transmitting control-signals to the passively receiving brain by electrically stimulating at different sites, the result of this experiment seems frightening. Otherwise, taking serious the active part of the animal in generating the "remote-controlled" behavior, the controversy about this experiment is resolved to a great deal. A closer look at the experimental design shows that the rat was not truly remote-controlled like an unwilling robot. Rather the rat had to learn to interpret the "forward/left/right"' meaning of the electrical stimulation delivered to its brain during repeated training sessions requiring the active participation of an autonomous subject. The potential danger showing up with this experiment is thus not so much the general possibility of an external control of behavior by electrical stimulation of the brain via a BMI. Rather, it points to the long known fact that electrical or

pharmacological intervention with certain brain regions like the limbic structures can alter the internal emotional states of a subject with severe consequences for the subject. Thus, the experiment by Talwar and colleagues (2002) confirms what has been known for a long time, i.e. that animals can learn to exhibit a vigorous appetitive searching behavior in response to MFB stimulation. Clearly such a highly restricted behavior, as it is also seen with the addiction to certain drugs, is open for any kind of external control not only through a BMI.

Currently, most of the BMI research is carried out in the field of neuroprosthetics, i.e. in the context of medical rehabilitation. Although this research is mainly justified by its expected benefit for handicapped subjects, this does not permit an escape from the social and ethical area of conflict stated above. This is because what is considered as beneficial for a handicapped person will also depend on the scientific concepts explaining the functioning of the neuroprosthesis. Again, if the functioning of a neuroprosthesis is based on information transfer to the passively receiving brain, a handicapped person must be seen as defective simply benefiting from the replacement of lost sensory information. Otherwise, if the functioning of a neuroprosthetic device is based on an active dynamic coupling between brain, body, and environment, the focus of research shifts from quantitative differences in the information transfer to qualitative differences in the perceptual modes which arise from the loss of sensory function or with the use of the neuroprosthetic device. From this perspective the benefit of a neuroprosthesis cannot be predefined by the researcher, but only in close cooperation with handicapped persons. This actually means to give true respect for the world as it is experienced and lived by handicapped persons.

1.2. Restoring lost function in the central nervous system

In the adult mammalian central nervous system the capacity for the intrinsic repair of damage following destructing disease or injury is limited for several reasons: no substantive axonal regeneration is initiated in response to neural damage, and with a few exceptions neurons finally lost after the damage will not be replaced. Although recent findings indicate that neurogenesis from endogenous stem cells occurs in certain regions of the adult brain (Gage, 2002), the number of newly generated

neurons may not be sufficient to replace lost neuronal tissue (Cao et al., 2002). Therefore, the loss of neural function[1] caused by the damage of neurons in the adult CNS often persists or is at best compensated by plastic reorganization of the brain with the neural functions often remaining impaired.

Classical treatment of the resulting symptoms consists of substitution rather than restoration of the impaired or lost function. In that way, deaf patients do not acquire new hearing but learn lip reading, blind patients do not acquire new vision but learn Braille-reading, and paralyzed patients do not acquire new movement ability, but learn to use the wheelchair instead. The alternative is the restoration of nervous system function by technical devices interfacing with selected parts of the nervous system, so called neuroprostheses.

In the human CNS, neuroprostheses are already applied with great success for suppressing pathological neural activity. For example, neural activity leading to tremor and movement arrest in Parkinson patients can be interrupted by deep brain stimulation, i.e. chronic electrical stimulation delivered through electrodes implanted into the globus pallidus interna or into the subthalamic nuclei lying deep in the brain (Volkmann, 2004; McIntyre et al., 2004a, b; Tass et al. 2003a, b). Cortical stimulation might be also used in the future to suppress epileptic seizures predicted from neural recordings (Lehnertz et al., 2001; Le van Quyen, 2001). Promising results have been recently obtained in the field of central motor neuroprostheses demonstrating that it is possible to record neural activity from the motor cortex that can be transformed into signals for controlling external devices (for a review see Schwartz, 2004). Via this kind of interfaces, paralyzed patients might once be able to control robotic arms or their own limbs by functional electrical stimulation.

A number of different types of neuroprostheses for restoring lost sensory functions, e.g. in the visual or auditory system, are currently probed in clinical contexts (Heiduschka & Thanos, 1998; Chapin & Moxon, 2001; Prochazka, 2001). However, the only sensory neuroprosthesis that is commercially manufactured and successfully applied in the clinic is the inner ear prosthesis (cochlear implant or CI) which interfaces the 8th cranial nerve to restore hearing (Rubinstein & Miller, 1999; Wilson

---

[1] The term function can refer to different levels of observation like single cells, networks, systems, or behavior and cognition. In the work presented here "function" always refers to a systems level which can be related to the level of cognition and behavior.

et al., 2003). Although currently over 30,000 deaf patients worldwide are implanted with this type of neuroprosthesis, there are numerous factors of a patient's individual anamnesis which can render the implantation of a CI unfeasible. Also, different types of retinal prostheses for restoring vision in the blind are currently under development (Alteheld et al., 2004). Similar to the CI, their application is restricted to a subgroup of blind patients with specific etiologies that leave intact the retinal ganglion cells.

It has long been recognized that sensory neuroprostheses interfacing higher levels of the sensory pathways would be an alternative to cochlear or retinal implants. Recently clinical trials have been started with auditory brainstem implants (ABI) (Lenarz et al., 2001; Lenarz et al., 2002; Kuchta, 2004). Bypassing the cochlea and the 8th cranial nerve, the ABI is applicable to a wider range of etiologies than the CI. However, the implantation of technical devices along the afferent sensory pathways is often surgically difficult and can be highly dangerous, as in the case of the brain stem.

Thus, a promising approach is to directly interface sensory cortex bypassing the sensory afferent pathways altogether (Normann et al., 1999; Donoghue, 2002). Expectedly, a higher percentage of patients would benefit from a sensory cortical neuroprosthesis (figure 2) including those with damages at any level of the afferent sensory pathways. Another great advantage is that all sensory cortices can be accessed easily and safely under surgical procedures. Different from the retina, the stimulation site is mechanically quite stable, and the skull can serve as a rugged housing for the implant. The sensory cortices also provide enough space for the implantation of high-count multichannel interfaces, which might be crucial for restoring lost sensory function. Still, the development of a cortical neuroprosthesis is a great challenge both due to the complexities of cortical functioning and the possible negative societal perception of this kind of technology (see section 1.1.).

In contrast to the development of neuroprostheses for suppressing pathological neural activity, or central neuroprostheses for motor control, the design of neuroprostheses for restoring lost sensory function is much more difficult. Compared to the suppression of pathological neural activity, a well functioning sensory neuroprosthesis necessarily involves the delivery of spatially and temporally patterned stimulation via a high-count, high-density multichannel interface. Whereas

a lot is known about how to record and extract information from neural activity patterns recorded via such an interface, the reverse, namely how patterned stimulation leads to perceptual and behavioral effects, is poorly understood.
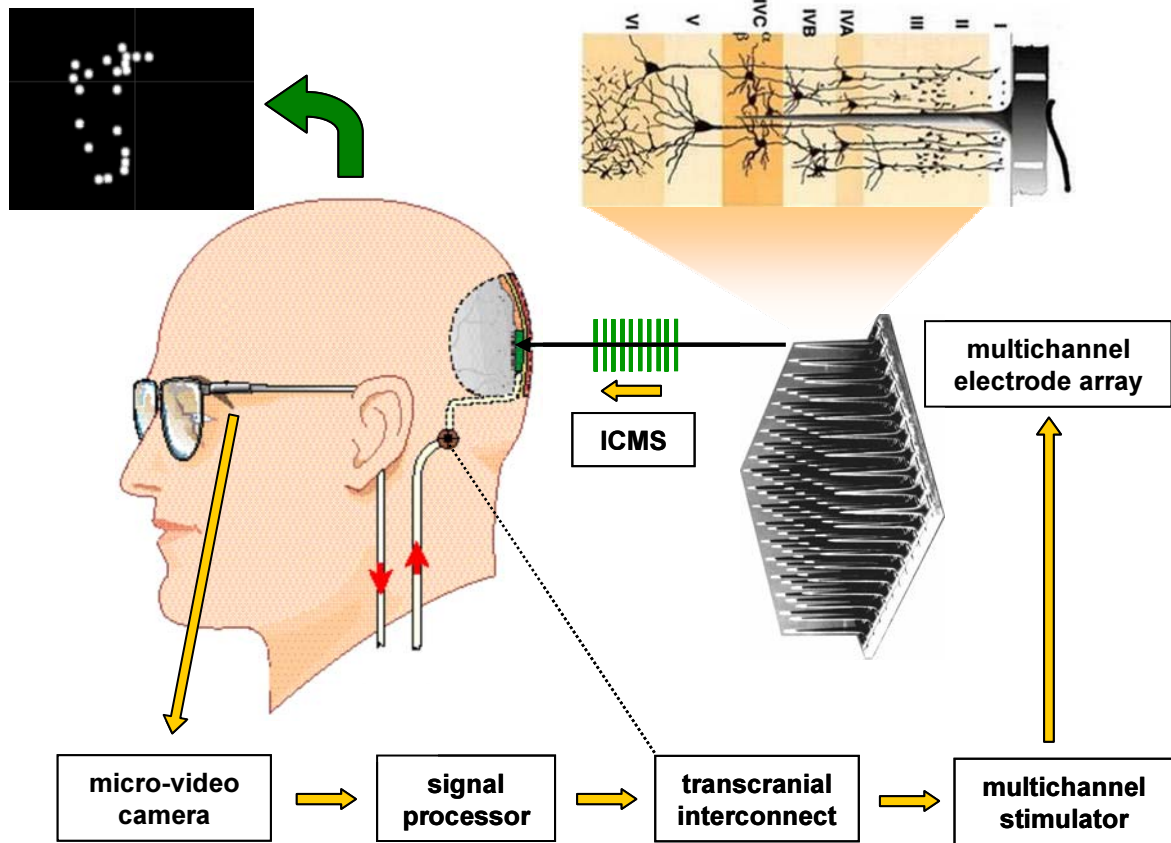
Figure 2: Concept of a visual cortical neuroprosthesis. Visual scenes are recorded by a micro-video camera and encoded by a signal processor into a spatial pattern of 10x10 pulse trains. Via a transcranial connector or a radio-frequency transmitter the signals are passed on to an implanted multichannel stimulator where they are transformed into trains of current pulses which are delivered to the input layer (IVC) of visual cortex via a multichannel interface, e.g. a 10x10 microelectrode array. Intracortical microstimulation (ICMS) applied through one of the microelectrodes leads to the sensation of a little spot of light (phosphene), which is localized in the visual field corresponding to the electrode's position in the retinotopic map. Patterns of phosphenes evoked by multi-site ICMS (black inset) could then be interpreted as pixelized "on" and "off" images of visual scenes recorded by the micro-video camera (adapted from Normann et al., 1999).

In most sensory neuroprostheses, the interface consists of implanted multichannel electrode arrays through which patterned electrical stimulation can be delivered to the neural tissue. In the cortex electrical stimulation mainly excites conglomerates of axonal fibers spreading the electrically evoked neural activity, which finally results in

transsynaptic input to various cell types at many different sites in the cortex and also in subcortical structures (Butovas & Schwarz, 2003). In contrast to the electrical activation of axons, more specific stimulation of neural tissue could be achieved by the controlled administration of small amounts of neurotransmitter at multiple, well defined locations in the CNS directly mimicking synaptic input. Such a different kind of neural interface, called artificial synapse chip, is currently under development consisting of arrays of electroosmotic minipumps (Peterman et al., 2004).

Completely different approaches for restoring lost function in the CNS currently arise from the field of regenerative medicine (Peterson, 2004; Cao et al., 2002). In one approach it is tried to replace lost neurons in the CNS by pharmacologically promoting the proliferation, migration, and differentiation of endogenous neural stem cells (Picard-Riera et al. 2004). In another approach, genetically and pharmacologically engineered stem cells are grown in vitro to yield multipotent neuronal graft tissue which can be transplanted into the brain (Harrower & Barker, 2004). Migrating to the damaged site and further differentiating in situ, the transplanted cells might finally integrate into the brain replacing the lost neurons. Various studies have demonstrated that transplanted, multipotent cells survive, migrate, differentiate, and even form synaptic connections in the CNS. Beyond this structural integration of transplanted multipotent cells into the CNS circuitry, it remains an open question whether these cells will functionally integrate in a way that efficiently restores lost neural function for a prolonged time without disturbing the remaining functions (Kempermann et al., 2004). Furthermore, there still is a considerable risk that transplanted multipotent cells migrate within the CNS in an uncontrolled manner or might even form tumors, whereas a neuroprosthetic device can be removed from the CNS in the case of failure leaving only minor damage in the brain. This is currently not possible with transplanted multipotent neural tissue.

Thus, rather than being outdated, the neuroprosthetic approach is likely to combine with regenerative medicine in the future. The development of electrode interfaces already moves into the direction of regenerative medicine, today. Electrodes are bathed in media containing neurotrophic factors (Kennedy et al., 1992, Kennedy & Bakay, 1998) or are coated with cell signaling molecules (Zhong et al., 2001) that promote the outgrowth of neurites from the host tissue and direct them towards the electrode. This way, a better electrical contact between electrode and tissue is

established. Also, if only a few neurites would be attracted by a single electrode, such an interface could achieve high spatial selectivity for interaction with only a few neurons per electrode.

Types of neuroprosthetic devices can be imagined which are designed to promote functional integration of transplanted neural graft tissue into brain circuitry by applying patterned electrical stimulation. After the successful integration, such a device could be removed again. Finally, neuroprosthetic devices and neuronal graft tissue might be one day combined in a biohybrid implant. The cells of the graft could be directly grown on the neuroprosthetic device in vitro prior to implantation. By this, cell-specific contacts could be established between electrodes and cultured neurons which have well defined electrical properties. After implantation, neurites outgrowing from the graft could synaptically connect to the host tissue. This would result in a spatially dense interface with the CNS, via which neurons could be electrically stimulated and/or recorded in a highly specific manner (Hutzler & Fromherz, 2004; Fromherz, 2002).

Besides these more technical problems of designing a suitable interface with the cortex, the major problem is how to interact with the highly complex physiological processes underlying perception in a functionally proper way. This is the central issue of the present thesis.

1.3. Interfacing sensory cortex: the coding approach

1.3.1. Early work: an overview

The idea of restoring lost sensory function by interfacing the sensory cortex has a long history in neuroscientific research. Medical experiments to restore vision in blind subjects by electrical stimulation of the cerebral cortex date back to the 18th century (LeRoy, 1755, cited from Uhlig et al., 2001)[2]. Though, the first well documented and often cited scientific study demonstrating that the cerebral cortex is electrically

---

[2] These experiments were possible after the construction of a prototypic electrostatic generator by Otto von Guericke in 1672 and the Leyden jar in 1745, which permits to store electrical charge similar to today's capacitors. By these technical inventions, it was possible for the first time to apply electrical stimuli to the nervous system in a controlled manner.

excitable stems from Fritsch and Hitzig (1870), who evoked muscle contraction in dogs by electrical stimulation of the motor cortex. However, it took until the beginning of the 20th century that advances in neurosurgery made possible the systematic investigation of sensations electrically evoked in sensory cortices. Löwenstein and Borchardt (1918) performed a surgery on a war-injured patient, in order to remove bone fragments caused by a bullet wound. During the surgery they electrically stimulated the surface of the left occipital lobe and reported that the patient perceived a flickering in the right visual field. While removing an occipital epileptic focus, Förster (1929) reported that on electrical stimulation of the occipital cortex the patient saw a little spot of light. The localization of this light spot varied systematically with the site of stimulation on the surface of the occipital lobe which for the first time demonstrated the retinotopic organization of the visual cortex. These electrically evoked spots of light, later called phosphenes[3], could still be elicited by the electrical stimulation of the deafferented visual cortex in a hemianopic patient (Krause & Schum, 1931) and also by electrical stimulation of the visual cortex in a blind subject (Urban, 1937). In their extensive studies on a large group of epileptic patients, Penfield and colleagues (Penfield & Rasmussen, 1950; Penfield & Jasper, 1954) mapped the functional topographies of various parts of cerebral cortex by applying electrical stimuli. They extended the observations reviewed above to other cortical areas like the auditory and the somatosensory cortex providing a systematic description of functional topographic maps like the famous homunculus of the somatosensory cortex.

In the beginning, electrical stimulation of the cortex was applied mainly in the context of epilepsy research. However, already 1953, Krieg proposed that due to its retinotopic organization concurrent electrical stimulation of many sites in the visual cortex could produce a single coherent image. This lead to the compelling idea, that vision could be restored in blind subjects by multi-site electrical stimulation of the visual cortex. Following the tradition of the research reviewed above, early experiments on such a cortical neuroprosthesis were mainly situated in the realm of neurosurgery. Thus most of these early experiments were carried out in awake humans who were only locally anesthetized and thus were able to give conscious report about perceptual phenomena. Button and Putnam (1962) built the first cortical neuroprosthesis, in which the amplitude and the frequency of an electrical stimulus

---

[3] The word phosphene stems from the conjunction of the Greek words phos meaning light and phainein meaning to show (Oster, 1970).

applied through a cortical surface electrode were controlled by the strength of the illumination of a photocell. Even with this simple device, the subjects were able to grossly determine the location of an illuminated object by scanning the visual space with the photocell held in their hand. The first attempt to demonstrate the feasibility of a multichannel cortical neuroprosthesis exploiting the retinotopic organization of the visual cortex was undertaken by Brindley and Lewin (1968). In a carefully prepared study, they chronically implanted an array of 80 platinum disc electrodes subdurally onto the pial surface of the visual cortex of a female volunteer, who had been blind for more than a year. It was demonstrated that at 32 electrodes spatially discernable phosphenes could be evoked. The location of a phosphene grossly corresponded to the position of the stimulating electrode. Also, small sets of phosphenes could be evoked by concurrently stimulating at a few electrodes. In the following years several blind volunteer subjects were chronically implanted with cortical surface electrode arrays by Brindley and colleagues as well as by other groups (Brindley et al., 1972; Dobelle et al., 1974a, b; Dobelle et al., 1979a; Pollen, 1975). Phosphene positions were mapped, phosphene thresholds were determined, and different stimulus parameters were tried. Also, some attempts were made to combine single phosphenes into crude visual patterns. For example, Dobelle and colleagues (1976) concurrently evoked phosphene patterns arranged in a 3x2 raster, which could be interpreted as Braille letters. However, reading rates were much lower than obtained by tactile Braille. Dobelle and colleagues also extended the cortical prosthesis approach to the auditory cortex (Dobelle et al., 1973). They studied auditory sensations evoked from the lower lip of the Sylvian fissure in eight normal hearing volunteer subjects, whose temporal cortex was exposed during tumor surgery. From their results, they proposed that an auditory cortical neuroprosthesis could be designed by the combination of simple electrically evoked auditory sensations, which they called audenes by analogy with phosphenes evoked by electrical stimulation of the visual cortex.

The research on cortical neuroprostheses in humans was very enthusiastic at the beginning. However, it soon became clear that besides the technical progress the experiments remained largely unsuccessful in restoring vision or hearing. Only crude perceptual patterns could be generated with these prototypic devices, far from the perception of meaningful objects and scenes, which could guide the actions of blind or deaf persons in their everyday life. A recent report by Dobelle (2000) shows that

since the early research of the 1970s there has been no substantial progress with cortical surface stimulation in humans (Dobelle et al., 1979b). Therefore, human experiments involving the chronic implantation of cortical neuroprostheses are currently not justifiable, both for ethical and scientific reasons.

1.3.2. Recent research: the coding approach and its difficulties

Since the early work on cortical neuroprostheses in humans, the focus of research has gradually shifted from clinical to engineering aspects. The current approach is heavily drawing on classical information theoretical concepts. Accordingly, a cortical neuroprosthesis is operationalized as a device which either encodes external stimuli and transmits the encoded information to the cortex, or decodes information received from the cortex, in order to derive signals for controlling external devices. Promising results have been obtained with the latter approach in the design of motor cortical prosthesis. For example, it has been demonstrated that single unit activity and local field potentials recorded from multiple sites within the motor cortex of monkeys can be transformed into control signals by which a robotic arm can be directed along the 3D trajectory of the arm movement intended by the monkey (Chapin et al., 1999; Wessberg et al., 2000; see Nicolelis, 2003; Chapin, 2004; and Schwartz, 2004 for review).

It is often assumed that, in the reverse direction, perception can be restored through a sensory cortical neuroprosthesis solely by transmitting information from the external environment to the cortex. During the last decades, it has been found that sensory cortical areas are organized in a multitude of overlying functional topographic maps representing various features of external stimuli. Thus, the general idea is to decompose visual or auditory scenes into these features, which in turn are encoded into neural activity via patterns of electrical stimulation activating the cortical sites that represent the feature.

The most salient feature of a phosphene is its localization within the visual field depending on the stimulation site within the retinotopic map of the visual cortex. Whereas the most salient feature of an audene is its spectral pitch, i.e. its localization within auditory spectral space, according to the stimulation site within the tonotopic

map of the auditory cortex. For example, a visual scene recorded by a camera can then be decomposed into an "on" and "off" pixelized image. With each pixel encoded by electrical stimulation of the retinotopic site corresponding to its position in the visual field, the pixelized image can be transmitted to the visual cortex. Like the lighted bulbs in a score-board, groups of phosphenes evoked by multi-site electrical stimulation are thought to combine into a perceptual pattern partially reconstructing the original scene (figure 2). Similarly a sound could be decomposed into its frequency components and transmitted to the auditory cortex by applying electrical stimulation at the corresponding sites of the tonotopic map. Like in a synthesizer simultaneously evoked audenes representing the frequency components of the sound could be combined to reconstruct the sound.

The early attempts of developing a cortical neuroprosthesis as reviewed above had great difficulties in eliciting meaningful perceptual patterns by multi-site electrical stimulation (Brindley & Lewin, 1968; Dobelle et al., 1973; Dobelle et al., 1976). It is now often believed that the spatial accuracy of electrical stimulation of the cortical surface applied in all these studies was too low to guarantee for a large enough number of independent channels by which information, e.g. a pixel coded image, could have been transmitted. This view was supported by psychophysical studies on pixelized vision in normal sighted subjects (Hayes et al., 2003), which have demonstrated that a total of 25x25 pixels can provide sufficient visual information for reading and navigation in complex visual environments (Cha et al., 1992a, b, c). Recent studies have therefore focused on increasing the number of discernable sensations that can be evoked independent from each other (Normann et al., 1999). This was attempted by making electrical stimulation spatially more specific in using intracortical microstimulation (ICMS) delivered through penetrating micro-electrodes (figure 7). Bak and colleagues applied ICMS to the visual cortex of normal sighted human volunteers undergoing epilepsy surgery (Bak et al., 1990). In a follow up study (Schmidt et al., 1996), a volunteer subject who had been blind for 22 years, was chronically implanted with 38 micro-electrodes through which ICMS was applied. Both in the normal sighted and in the blind subjects, ICMS elicited phosphenes similar to those seen with cortical surface stimulation. Though, the phosphenes evoked by ICMS seemed to be more compact with current thresholds much lower than with surface stimulation. They did not flicker as it often occurred with surface stimulation, and they were sometimes colored, mostly at low stimulus intensities.

These results were also promising in indicating the feasibility of increasing the channel densities for information transfer, especially because the minimal interelectrode distances from which separate alternating phosphenes could be evoked by ICMS were about 0.5 mm compared to about 2.4 mm with surface stimulation (Brindley & Lewin, 1968). The two-point resolution with ICMS was thus about five times greater than with surface stimulation. Accordingly, much of the current research on cortical neuroprostheses is focused on increasing the density of stimulation sites by the development of high-count microelectrode arrays (Normann et al., 1999, see also figure 2).

However, many difficulties already encountered with cortical surface stimulation could not be resolved by using ICMS. Phosphenes electrically evoked in the visual cortex often were not salient and appeared to be vague to the subject (Bak et al., 1990; Schmidt et al., 1996). Also, phosphene properties other than location like intensity or size could be only crudely modulated by varying the stimulus parameters. Simultaneously evoked phosphenes often interacted in a highly nonlinear manner. If two phosphenes were spaced too closely, light "filled in" between the phosphenes. Additionally, phosphene location was not stable, but moved in the direction of the eye movements which made the interpretation of groups of phosphenes even more difficult. As a result, multi-site electrical stimulation of the visual cortex often generated rather meaningless blobs of light than meaningfully structured percepts (Troyk et al., 2003). Therefore, even with ICMS, the coding approach failed at the same critical point as in the earlier experiments. It could not be demonstrated that patterned multi-site electrical stimulation of sensory cortex results in the perception of meaningful objects or scenes.

1.4. Beyond coding: towards the generation of meaning with a cortical neuroprosthesis

1.4.1. Why the coding approach fails

A properly functioning cortical neuroprosthesis has to provide its user with meaningfully structured perception. Thereby, meaning refers to the whole of a percept, a Gestalt (Köhler, 1967). The coding approach to cortical neuroprostheses

does not explicitly address the question of how meaning arises from electrical stimulation of the cortex. Rather, it follows along the traditional lines of information theory developed by Claude Shannon, who stated: "The fundamental problem of communication is that of reproducing at one point either exactly or approximately a message selected at another point. Frequently, the messages have meaning; that is they refer to or are correlated according to some system with certain physical or conceptual entities. These semantic aspects of communication are irrelevant to the engineering problem " (Shannon, 1948, p.1). However, decomposing visual or auditory scenes into features, and transmitting the encoded feature information to the cortex via a cortical neuroprosthesis, irrespective of its meaning to the animal, leads to the binding problem: How can the activated cortical representations of the features bind into a Gestalt, e.g. an object or scene meaningful to the subject, again. The coding approach to cortical neuroprostheses tries to pragmatically put aside the binding problem in focusing on the replacement of lost sensory input. It remains the task of the brain to reconstruct objects and scenes in a computational process carried out on the neural representations of the features activated by the artificial sensory input. In this respect, the question of how meaning is attributed to the electrical stimuli seems to be irrelevant for the development of a cortical neuroprosthesis. Though, in the experiments on patterned multi-site electrical stimulation of sensory cortices in humans (Brindley & Lewin, 1968; Schmidt et al., 1996), electrically evoked phosphenes or audenes did not easily combine into meaningfully structured percepts, which shows that the binding problem obviously cannot be circumvented with the coding approach.

The key problem seems to be that phosphenes and audenes are far from representing simple features that can be arbitrarily bound together into a Gestalt. One reason for this is that single electrically evoked phosphenes and audenes can be meaningful by themselves in the sense that they attract the attention and guide the behavior of a subject. In animals, the behavioral interpretation of electrical stimulation at the same cortical site varies with the behavioral context, i.e. the behavioral contingencies, the learning history, and the actual behavioral and physiological state of the animal (Doty, 1969).

In human subjects, phosphenes evoked by electrical stimulation of the visual cortex are often described as "stars", "wheels", "discs", "spots", "streaks", or "lines" (Penfield & Jasper, 1954). For audenes electrically evoked in the auditory cortex, words like "buzz", "hum", "knocking", "crickets", and "wavering" were often used in the subjects' descriptions (Penfield & Perrot, 1963; Dobelle, 1973). From these verbal reports of the human subjects responding to electrical cortical stimulation, it can be at inferred that phosphenes and audenes have dynamic properties and posses a certain degree of autonomy, which is they are difficult to control in their properties by the experimenter or the subject.

Phosphenes and audenes already form Gestalts by themselves structuring the whole perceptual space. In this respect the dark background of a phosphene is not just absence of visual content, but is involved in the constitution of a phosphene as a figure segregated from a ground (Merleau-Ponty, 1962). This corresponds to the finding that simultaneously evoked phosphenes often are not independent, but interact in a highly nonlinear manner. Altogether, such electrically evoked sensations cannot be atoms of vision or audition from which meaningfully structured percepts can be synthesized.

In the introductory chapter of his "Phenomenology of Perception" (1962), Merleau-Ponty summarizes this point as follows: "Let us imagine a white patch on a homogenous background. All points in the patch have a certain 'function' in common, that of forming themselves into a 'shape'. The colour of the shape is more intense, and as it were more resistant than that of the background; the edges of the white patch 'belong' to it, and are not part of the background although they adjoin it: the patch appears to be placed on the background and does not break it up. Each part arouses the expectation of more than it contains, and this elementary perception is therefore already charged with a meaning. But if the shape and the background, as a whole, are not sensed they may be sensed, one may object, in each of their points. To say this is to forget that each point in its tern can be perceived only as a figure on a background. … The perceptual 'something' is always in the middle of something else, it always forms part of a field." (Merleau-Ponty, 1962).

Phosphenes and audenes appear to be phenomenally rich in themselves. However, this richness seems to be difficult to grasp by the human subjects in their verbal description, which is highly constrained by the experimental protocols. In such cases, in which it was possible to simultaneously evoke crude patterns of phosphenes, a variety of different meanings was given to these patterns by the subjects largely depending on the experimental context. In free verbal association, subjects often described multiple electrically evoked phosphenes as "stars in the sky". Primed by the scientific inquiry of the experimenters, the subjects were able to interpret phosphenes evoked in a group as visual Braille letters (Dobelle, 1976) or as adequate to form a letter of the alphabet (Schmidt et al., 1996)[4]. Clearly, it is the meaning which makes these patterns of electrically evoked sensations viable to a subject. How meaning is attributed to sensations electrically evoked in the cortex is therefore a crucial question that cannot be ignored in the development of a cortical neuroprosthesis.

1.4.2. The generation of meaning by the interplay of brain, body, environment and a cortical neuroprosthesis

For solving the difficulties with the coding approach, it will be necessary to develop new concepts upon which the research on sensory cortical neuroprostheses can be based. Dwelling on the tradition of phenomenology developed in the European philosophy during the mid 20th century by Husserl, Heidegger, and Merleau-Ponty, a growing number of researchers in the field of cognitive neuroscience have emphasized that perception is an observational act and not the passive representation of environmental aspects. From this notion there currently emerges a new theoretical framework in cognitive neuroscience called embodied cognition (Varela et al., 1992; Chiel and Beer, 1997; Clark, 1999; Nunez & Freeman, 2000; Beer, 2000; Thompson & Varela, 2001; O'Regan & Noë, 2001), in which perception

---

[4] Phosphene sensations similar to those evoked by cortical stimulation are also elicited by migraine attacks, focal epileptic seizures or with certain drugs (Oster, 1970). Sometimes, these sensations were interpreted as mystical visions. A particular rich description of such phenomena was given, for example, by Hildegard von Bingen, a nun and influential religious woman philosopher living 1098 to 1180 AD (Sacks, 1998, p. 166-172).

in particular and cognition in general are viewed as the situated, embodied action of a subject. Such a conceptualization of perception as "enacted" (Varela et al., 1992) has regained actuality in the field of robotics during the 1980s (Brooks, 1999), where it has proven to be highly successful in the development of autonomous robots. Embodied cognition could also provide a theoretical background for the development of a cortical neuroprosthesis and will thus be shortly sketched in the following.

Situatedness of perception refers to the immediate situation of a subject in an environment which dynamically changes in (real) time depending on the actions of the subject. What the subject senses is thus a function of how it moves, and, vice versa, how it moves is a function of what it senses. If sensory input is intimately linked to the actions of the subject (Varela, 1997), it is an exceedingly complex task to start perception with a detailed internal representation of the environment and finally compute an adequate motor response from this representation. An alternative is to begin perception with the formation of a behavioral action directed towards the future goals of a subject depending on its pre-experience and expectation (Freeman, 2000a, c). Environmental complexity would then be greatly reduced due to the constraints imposed on the sensory input by the selection of environmental aspects through the intentional behavior of the subject.

Freeman (2000a, c) further pointed out that the intentional actions of a subject are self-selected under the constraint of a context which is provided by the current emotional state and by the pre-experience instantiated through the memory systems of the subject. In behavioral experiments the current emotional state depends on the behavioral contingencies and the pre-experience on the learning history of the subject. Additionally, inter-subjective interactions can provide a social and cultural context in which individuals mutually codetermine each others perception by gestures, social behavioral expression, or language, in a shared social reality. The meaning of the subject's perception arises from its intentional actions and, by this, only exists in relation to the psychobehavioral and sociocultural context the subject lives in.

Most importantly, perception requires that a subject learns from the consequences of its intentional actions, by which it acquires of knowledge about the sensorimotor contingencies emerging from its behavior. For solving a behavioral task it is then not

necessary to integrate detailed "snapshot" representations over time. Instead, the aspects in the environment relevant for the task can be directly accessed through explorative attentive behavior mediated by the knowledge and mastery of the sensorimotor contingencies related to this behavior (O'Reagan & Noë, 2001). As has been shown by O'Regan and Noë (2001), characterizing perception in this way accounts well for its qualitative properties and can explain the differences in the perceptual modes between the sensory modalities.

In the framework described above, it is emphasized that cognition is embodied in the sense that it arises from the coordinate action of brain, body, and environment (Chiel & Beer, 1997). Thereby brain, body, and environment are described as mutually embedded dynamical systems, which are coupled to each other in a coherent and complementary fashion due to their co-evolution and co-development during phylo- and ontogenesis, respectively. Accordingly, the embodied approach to cognition uses rather the language of dynamical systems theory than the language of theory of computation (Port & van Gelder, 1995). The brain plays an important role in mediating sensorimotor contingencies, but perception as a whole involves a dynamics which "cuts across brain-body-environment divisions" (Thompson & Varela, 2001), rather than brain-bound neural events.

Growing empirical evidence supports the view on perception described above. Particularly telling experiments have been carried out in the field of crossmodal "sensory substitution", where it is tried to replace or augment a lost sensory modality by transforming stimuli characteristic of the lost modality to stimuli of another modality. For example Bach-Y-Rita and colleagues (1969) developed a tactile vision substitution system (TVSS), which converts an image captured by a video camera into a "tactile image" produced by a matrix of 20 x 20 vibrotactile or electrotactile stimulators. If the camera was positioned by the experimenter, blind or blindfolded subjects were immediately able to discriminate different patterns of tactile stimulation derived from the camera images. Simple geometric shapes could be recognized by the subjects after some learning (Epstein et al., 1986; Epstein et al. 1989; Bach-Y-Rita, 2004). The subjects reported that they achieved this by different successive patterns of tickling or irritating sensations on their skin at the sites of tactile stimulation. However, when the subjects were allowed to operate the camera by themselves for exploring their environment, the mode of perception changed

fundamentally. After about 10 hours of exploration, the subjects perceived objects in an external space in front of them, as confirmed by their reports, and as it could be also inferred from their behavior[5]. In this perceptual mode, subjects neglected the tactile input most of the time and were only aware of stable distant objects in front of them. When asked to concentrate on the tactile sensations, subjects were nevertheless able to become aware of the tactile input and distinguished it from object perception. Despite the limited spatial resolution of the TVSS, subjects managed to localize objects in a three-dimensional space, to characterize the shape of an object, and to recognize objects, even faces. The perception of external objects never occurred when subjects were not able to explore their environment by manipulating the camera. Furthermore, the performance in object recognition tasks was better than chance, only if the subjects received feedback about the success of their responses. For the spatial localization as well as the recognition of external objects, the subjects had to learn how variations in the tactile sensations are related to their actions, i.e. to acquire knowledge about the sensorimotor contingencies related to their exploratory behavior. Thus, what the subjects perceived was not derived from the representation of invariants in the sensory information, but rather from knowledge about invariants in the sensorimotor contingencies related to their specific intentional behavior (O'Reagan & Noë, 2001).

The sensory substitution experiments demonstrated that perception is structured by a subject's intentional action and by perceptual learning, but also they also showed that it is not always better to have access to more information (Lenay et al., 2003). The use of additional tactile information in sensory substitution does not make the qualitative difference of blind compared to normal sighted persons disappear. It rather creates new differences, as the "visual" perceptual mode emerging from the use of a TVSS is still too different, as to be shared with normal sighted subjects. There is no color, and spatial resolution is very low. This prevents the build up of emotional value and social meaning leaving the user isolated with his particular mode of perception. It is mainly for this reason that sensory substitution devices are not widely used by blind people in their daily life, beside of their bulky design. Thus, rather than quantitative differences in information it is the qualitative differences in

---

[5] For example, if the camera was zoomed without informing the subject leading to a sudden expansion of the tactile image, subjects moved backwards and raised their arms as if the protected themselves from the impact of an approaching object.

experience that prevents the widespread use of these devices. Although involving invasive surgery, a sensory cortical neuroprosthesis might have a deciding advantage in this respect. The use of a cortical neuroprosthesis could provide a blind person with a perceptual experience, which is qualitatively more similar to that of normal sighted or normal hearing persons, and it might thus be possible to share it with others.

In most of the experiments on sensory cortical neuroprostheses, electrical stimulation is applied in a similar way as in passive tactile sensory substitution. The perceptual mode arising in this setting mainly refers to the structure of the sensory apparatus itself (O'Reagan & Noë, 2001). For example, the phosphenes evoked by electrical stimulation of the visual cortex reflect the topographic organization of the sensory epithelium with the phosphenes changing their locations together with the eye movements. It is apprently difficult for the subjects to refer to attributes of external objects or scenes solely on the basis of these features. However, restoring vision or hearing a sensory cortical neuroprosthesis must enable a blind or deaf person to relate to external objects and scenes in a meaningful way. As can be inferred from the research on TVSS reviewed above, this requires attentive action and considerable perceptual learning by the subject using a sensory cortical neuroprosthesis. Owing to the coding approach, issues of active perception and perceptual learning have been largely neglected in the field of neuroprosthetics. Embodied cognition might provide a theoretical framework to overcome the limitations of the coding approach.

That the proper functioning of a cortical neuroprosthesis might require a quite dramatic relearning of perception, is demonstrated by the following example. Fine and coworkers (2003) reported the case of a 43 year old man whose visual sensory input was perfectly restored by a corneal implant after more than 40 years of blindness. In an accident at the age of three and a half years he lost one eye completely and was blinded due to a chemical and thermal damage of the cornea of the other eye. Although this patient regained sight immediately, was able to recognize simple shapes, and was successful at many motion tasks, he had continuing difficulties to interpret what he saw in a meaningful way, e.g. as objects in a three dimensional visual space.

This case study demonstrates that even the perfect replacement of lost sensory input is not sufficient for a proper functioning of a cortical neuroprosthesis. Rather, the research has to focus on the development of training and stimulation strategies that promote a relearning of perception in blind or deaf persons during rehabilitation. A better understanding of physiological processes underlying learning and perception will be an important prerequisite for this.

1.4.3. Taking into account ongoing cortical dynamics

According to the theoretical framework and the experiments on sensory substitution reviewed in the previous section, perception relies on activity endogenously produced by the nervous system, and not only on activity imposed by the sensory input alone. This corresponds to results on the effects of stimuli on the ongoing cortical activity. As has been shown by Arieli and colleagues (1996) using optical imaging of the visual cortex in cats, the ongoing cortical activity has a strong influence on the variability of stimulus evoked responses. Metaphorically speaking: "…the effect of a stimulus might be likened to the additional ripples caused by tossing a stone into a wavy sea." (Arieli, 1996). There is growing evidence that endogenous, ongoing activity in sensory cortices plays an important role in the meaningful interpretation of stimuli learnt by the subject. Thus, in the design of a proper functioning cortical neuroprosthesis the ongoing cortical activity has to be taken into account.

As has been repeatedly demonstrated by multichannel recordings of the electrocorticogram (ECoG)[6], complex aperiodic patterns exist in the ongoing cortical activity which cannot be discarded as noise (Lilly, 1954; DeMott, 1966; Livanov, 1977)[7]. However, no systematic relationship between these activity patterns and the sensory input could be found. Recording from 400 channels DeMott (1966) suggested that sensory input "is presented to the cortex not as a map, but as a very

---

[6] The ECoG is a field potential recorded directly from the cortical surface. Compared to the EEG recorded from the scalp, the ECoG provides a much higher spatial resolution. Both the ECoG and the EEG are basically generated by the same types of synaptic currents.
[7] Already 50 years ago, Lilly (1954) recorded cortical activity from 25 surface electrodes and displayed the recorded potentials by an array of light bulbs. Using photographs taken at high speed from these arrays, he described recurring "figures" in the cortical activity.

complex spatial-temporal sequence, in which every part of the cortex participates in displaying information from every part of the [sensory] field" (DeMott, 1966, p. 29).

Due to inadequate spatial sampling, the functional role of the cortical activity patterns remained unclear in these early experiments. By training rabbits to discriminate olfactory, somatosensory, visual or auditory stimuli and concurrently recording multichannel ECoGs at high spatial resolution from the corresponding sensory cortices, Freeman and colleagues were able to demonstrate that these complex spatial patterns are related to perception and learning (Barrie et al., 1996; Freeman & Barrie, 2000). In the β- and γ- frequency range of the ECoG (15 Hz to 80 Hz) they found that a common aperiodic waveform was shared by all recording channels over distances of up to 1 cm. Within short time segments of about 0.1 s, the amplitude of the common aperiodic oscillation was modulated across channels. By using a multivariate classification procedure, Barrie and colleagues (1996) identified patterns in the spatial amplitude modulation carried by the aperiodic oscillation. The patterns occurred at unpredictable points in time between 0.3 and 2 seconds after stimulus presentation and contained information about the behaviorally relevant stimulus classes. New cortical activity patterns emerged with discrimination learning of novel pairs of stimuli, but patterns remained stable as long as the behavioral context was not changed. Interestingly, the learning induced cortical activity patterns showed a lack of invariance with respect to the physical stimulus properties. For example, when the same pair of stimuli was presented to an animal again after intervening training with another pair of stimuli, the former activity pattern did not recur. Instead, a new pattern emerged with the same pair of stimuli. The patterns always changed when the behavioral context and, this way, the meaning of the stimuli changed, e.g. in intervening blocks of training with new stimuli or with a contingency reversal. Freeman therefore hypothesized that the patterns did not encode the physical stimulus properties, but referred to the meaning of the stimuli for the animal. Ohl et al. (2001) were able to directly test this hypothesis by objectifying the subjective states of an animal in a category learning experiment. In their experiment Mongolian gerbils learnt in sequential blocks of training to abstract the categories 'upward' and 'downward' from pairs of rising and falling frequency modulated (FM) tones largely varying in their spectro-temporal properties. The formation of a category manifested in a sudden transition from discrimination behavior to categorization behavior occurring at an individual point of time in each animal's learning history. In the

discrimination phase, learning induced patterns identified in the ECoG recorded from the auditory cortex changed whenever a new pair of stimuli was introduced to the animal. After the transition from discrimination to categorization behavior, the patterns stabilized and became invariant with the categories. Thus, the patterns reflected the perceptual sorting of stimuli into only subjectively meaningful categories in a manner that abstracted from the precise physical composition of the stimuli.

The analysis of spatial phase distributions in the ECoG (Freeman & Barrie, 2000) indicated that the activity patterns were not imposed by external input, but emerged from the intrinsic cortical dynamics. By extensive theoretical modelling based on nonlinear systems theory Freeman (2000b) proposed that the observed cortical activity patterns are self-organized by the cooperate action of large sets of cortical neurons. According to these models, ongoing cortical dynamics is destabilized upon sensory input caused by a stimulus. This perturbation is thought to lead to a state transition (Freeman, 1994) from a background "chaotic" state to an ordered state which manifests as a cortical activity pattern, which is unique for each class of stimuli that have the same meaning to the animal. Thus, the patterns are neither simple effects caused by the stimuli, nor representations of stimulus properties. Rather, the patterns reflect the individual history, the present context, and the expectancy of the subject which provides external input with meaning.

In this neurodynamic view perception is active, which goes well along with the theoretical framework of embodied cognition described in the previous section. According to Freeman (2000c), perception starts with action patterns initiated in the limbic structures underlying the emotional state of a subject expecting sensory input. Via the motor system, the emotional state can become overt as intentional behavior like taking appropriate postural stance in attention and orienting responses (Bischof et al., 2001), or mobilizing the cardiovascular, respiratory and endocrine systems. Preafferent input transmitted from the limbic system to the sensory cortices biases the ongoing cortical dynamics towards the sensory input, which is anticipated as a consequence of the motor actions of the animal (Freeman, 2000c; Kay et al., 1996; Kay & Freeman, 1998). Sensory input perturbs this sensitized stated of the cortex leading to the emergence of cortical activity patterns as described above.

In the models of Freeman (2000b), pattern formation relies on the intrinsic synaptic connectivity of the cortex. After multisensory integration, the limbic activity is updated (Freeman, 2000c) promoting plastic synaptic reorganization in the cortex, whenever the subject learns to attribute a new meaning to a stimulus as a consequence of its intentional actions. This results in a global change of the dynamics of the cortical system. Therefore, not only new patterns are formed with new discriminable stimuli, but all existing patterns change, too. Instead of storing static information about past events, such a memory system can dynamically integrate previous and new knowledge in a context sensitive way.

As indicated by the rapid succession of characteristic phase patterns in the ECoG, cortical state transitions occur at a rate of 3 to 7 per second (Freeman & Barrie, 2000). From this it was inferred that the circular process of intentional action, pattern formation, and update is iterated within about 0.2 s, which lies in the range of theta activity that can be recorded most prominently from the hippocampus, and which is thought to be related to cognitive processing (Buzsaki, 2002; Kahana et al., 2001; Basar et al., 2000).

Further evidence for such a view on cortical dynamics stems from studies on the level of single neurons. For example by analyzing spike activity recorded from multiple single neurons, Abeles and colleagues (1995) found that cortical activity flips among well-separated states of activity within which the firing rates were approximately stationary. Another study by Villa and colleagues (1999) demonstrated that particular spatiotemporal spike patterns, recorded from rat auditory cortex in the time when the animal is waiting for an acoustic stimulus to solve a GO/NO-GO task, can predict future behavioral responses.

In order to be useful, artificial sensory input delivered by patterned multi-site electrical stimulation via a sensory cortical neuroprosthesis must be interpreted in a way meaningful to the subject. However, electrical stimulation directly interferes with the iterative dynamics of the cortico-limbic system which underlies its meaningful interpretation. Ongoing cortical dynamics persists in cortical areas deprived from their sensory input due to their embedding in the cortico-cortical network. This is highlighted by the fact that sensory deprived cortical areas, e.g. the visual cortex in blind subjects or the auditory cortex in deaf subjects, can play a functional role with

tasks involving undeprived modalities (Bavelier & Neville, 2002). Therefore, the proper functioning of a neuroprosthesis implanted into deprived sensory cortical areas will rely on the proper interaction between electrical stimulation and the ongoing cortical dynamics. The optimization of electrical stimulus parameters for encoding stimulus features is important in this respect, although it is illusory to assume that the spatio-temporal fine structure of the physiological sensory input to the cortex can be mimicked one day with a cortical neuroprosthesis. Electrical stimulation imposes highly synchronous activity on a large population of both excitatory and inhibitory neurons within the cortex, which does not occur under normal physiological conditions. But even more important, in bypassing the afferent sensory pathways, electrical stimulation is not properly timed with respect to the ongoing cortical state transitions. Therefore, the development of a cortical neuroprosthesis must draw on the capacity of the cortex for neuroplastic reorganization, by which a neuroprosthetic device possibly integrates into cortical functioning. With a better understanding of how perception and learning with a cortical neuroprosthesis arises from the interaction between electrical cortical stimulation and the ongoing cortical dynamics, training and stimulation protocols could be designed that promote such a functional neuroplastic reorganization and that permit the cortical dynamics to unfold giving rise to meaningfully structured perception.

1.5. Motivations and aims of the work

The critical step in the development of a sensory cortical neuroprosthesis will be the generation of perception of meaningful objects and scenes in response to patterned multi-site electrical stimulation, which can guide the action of blind or deaf persons in their everyday life. In this respect, previous attempts in the development of sensory cortex prostheses focusing on the encoding of environmental stimuli into patterns of electrical cortical stimulation have been largely unsuccessful (Brindley & Lewin, 1968; Schmidt et al., 1996). This is probably due to the fact that the question of how subjects perceive and learn to interpret electrical stimuli applied to the cortex in a meaningful way has been neglected. The work presented here tries to make a step beyond the coding approach by explicitly addressing this question.

The general aim of this work was to investigate the interaction between ongoing cortical dynamics and neuroprosthetic stimulation. As has been already proposed earlier in the introduction, a meaningful interpretation of electrical stimuli applied to the cortex arises from this interaction through learning. Even in the simple case of electrical stimulation at single cortical sites, not much is known about physiological processes underlying the perceptual and behavioral effects. Thus, single-site electrical stimulation was chosen as a starting point, in order to find principles of interaction also relevant for the meaningful interpretation of patterned multi-site electrical stimulation.

For the characterization of the ongoing cortical dynamics a detailed physiological analysis is needed, which can be carried out best in animal experiments. Therefore, the first step of this work was to develop a suitable animal model, in which cortical activity could be recorded concurrently with electrical stimulation of the cortex in freely behaving learning animals. Although animals cannot verbally report their subjective perceptual states like humans, such states can be referred to by behavioral training and testing. Mongolian gerbils (Meriones unguiculatus) were chosen for the experiments, because their auditory cortex has been well characterized by a number of anatomical (Budinger et al., 2000a, b) and physiological studies (Thomas et al., 1993; Scheich et al., 1993; Hess & Scheich, 1996; Ohl & Scheich, 1996; Ohl et al., 2000a, b; Schulze et al., 2002). For example, mapping studies using electrophysiological recording techniques (Thomas et al., 1993), 2-deoxyglucose autoradiographic labeling (Scheich et al., 1993) and optical imaging (Hess & Scheich, 1996) have shown that the core fields of the auditory cortex, the primary field AI and the anterior auditory field AAF, have a mirror-imaged tonotopic organization about a common high-frequency border. In AI, the represented frequencies increased along the rostrocaudal axis, whereas they decreased in AAF (figure 6). Altogether, these studies revealed that the auditory cortex of the Mongolian gerbil is a functionally well organized structure, which permits to administer electrical stimulation to functionally circumscribed parts of it. Also, Mongolian gerbils have in contrast to other rodents a good hearing capability in the low frequency range of their audible spectrum comparable to that of humans (Ryan, 1976). Because in humans this low frequency range is involved in the processing of speech, the auditory systems of the Mongolian gerbil can serve as a good model for investigating sensory aspects of speech processing (Ohl & Scheich, 1997), which is

also an important facet in the development of an auditory cortical neuroprosthesis. Most importantly, these animals have a great learning ability, especially with auditory tasks (Scheich et al., 1997). For example using a shuttle-box GO/NO-GO avoidance paradigm, Mongolian gerbils can be quickly trained to detect acoustic stimuli (Stark et al., 2000), to discriminate between acoustic stimuli varying along different stimulus dimensions (Wetzel et al., 1998b; Schulze & Scheich, 1999; Ohl et al., 1999) and to even categorize stimuli largely varying in their physical properties (Wetzel et al., 1998a).

Using Mongolian gerbils, Breindl and Scheich (Breindl, 2001; Scheich & Breindl, 2002) have developed an animal model for a simple unidirectional cortical neuroprosthesis based on intracortical microstimulation (ICMS) of the thalamic input layer of AI. ICMS was chosen instead of cortical surface stimulation, in order to achieve spatially specific activation of different closely spaced cortical sites. Employing different coding strategies, they showed that the animals were able to gain behaviorally relevant percepts from ICMS by learning to extract spatial, temporal and spatiotemporal cues from the intracortical electrical stimuli. The animal model developed in the work presented here extended this model by combining discrimination learning of intracortical electrical stimuli with a concurrent recording of the electrocorticogram (ECoG) from AI at high spatial resolution. Recently, it has been shown by Ohl and colleagues (Ohl et al., 2001; Ohl et al., 2003a, b) that discernable spatial activity pattern emerge from the ongoing ECoG in the auditory cortex of the Mongolian gerbil with auditory discrimination and categorization learning of acoustic stimuli. These patterns rather referred to subjective perceptual states of the animal in the context of learning than to the physical properties of the presented stimuli.

The major aim of the present work was to determine whether such learning induced cortical activity patterns also emerge by the interaction of intracortical microstimulation and the ongoing cortical dynamics and, in case they do, compare them to the patterns found with acoustic training. This involved the following steps:

(1) Spatial and temporal characterization of the transsynaptically evoked cortical activity in order to specify the artificial sensory input imposed on the ongoing cortical activity by ICMS.

(2) Investigation of discrimination learning of intracortical electrical stimuli with a detailed analysis of the associated learning dynamics.

(3) Identification and characterization of spatial patterns in the ongoing cortical activity in relation to the meaningful interpretation of the intracortical electrical stimuli through learning.

It should be noted, that the work presented here was focused on basic principles of the interaction between a cortical neuroprosthetic device and the ongoing cortical dynamics leaving aside the technical problems that have to be solved in the development of such an interface. Accordingly, an unidirectional prosthetic device with only two channels was chosen for the experiments, which was rather simple compared to devices currently developed by other groups (Normann et al., 1999). While the interaction with a neuroprosthetic device was explored only in the auditory cortex, the derived principles would presumably pertain to the construction of neuroprostheses for the visual and other sensory cortices, too.

2. Materials and Methods

Data were obtained from six adult male Mongolian gerbils. They had an age of about 6 months and weighed between 85 and 100 g. Animals were housed under a light-dark cycle of 12:12 hours with free access to water and food (rodent food pellets and sunflower seeds). All animal experiments were surveyed and approved by the animal care committee of the Land Sachsen-Anhalt (No. 43.2-42502/2-325; IfN MD).

2.1. Design of electrode arrays for stimulation and recording

2.1.1. Depth electrode array (2×1) for intracortical microstimulation

For the application of intracortical microstimulation (ICMS), a 2×1 depth electrode array was built from teflon-insulated platinum-iridium microwire having a bare wire diameter of 51 µm and an insulation 32 µm in thickness giving a total diameter of 115 µm (AM-Systems, Carlsberg, USA). Two pieces of about 2 cm length were cut off the wire. The wire pieces were then crimped with one end to the first two contacts of a male 4-pin connector having a pitch of 1.25 mm (Molex Inc., Lisle, USA). Afterwards, the free endings of the wire pieces were carefully cut to expose their cross-sectional surface areas. Then the wire pieces were aligned in parallel at a distance of about 0.7 mm by passing them perpendicularly through two prepared electron microscopy object-holder grids (0.165 mm pitch, EMS GmbH, Munich, Germany). The circular grids had been previously cut into small rectangles and folded with the vertical parts arranged in parallel behind each other providing a guiding system for the wires pieces (Kruger, 1982). The cut wires were fixed to the grids by dental acrylic about 4 mm above their endings. An insect pin was cemented to the array for later attachment to a 3D-micromanipulator set. This resulted in a 2×1 array of stimulation electrodes with an interelectrode distance of about 700 µm (figure 3A).

For each stimulation electrode, a reference electrode was built from teflon-insulated platinum-iridium microwire with a bare wire diameter of 128 µm and an insulation 77 µm in thickness giving a total diameter of 205 µm (AM-Systems, Carlsberg, USA). The wire was cut into pieces of about 2 cm length. At one end of each wire piece the last millimeter of insulation was stripped off and bent into a small loop. The other ends were crimped to free male connector pins (Molex Inc., Lisle, USA).
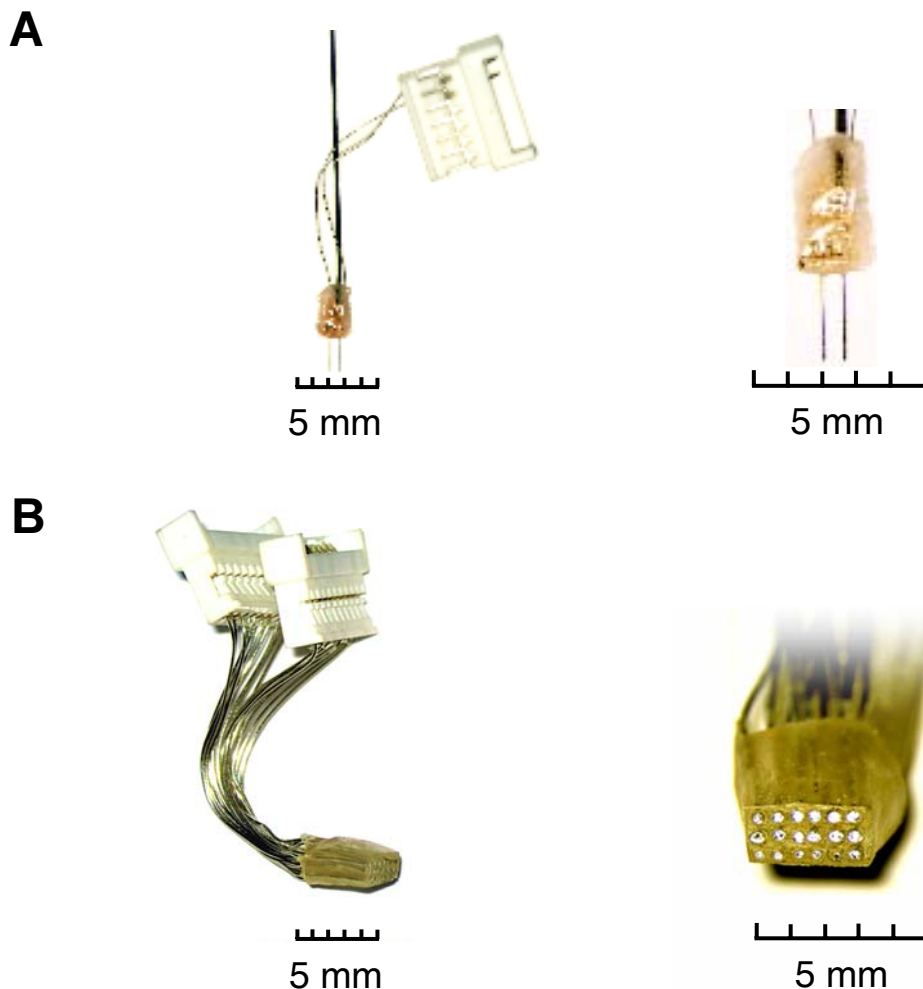
Figure 3: Photomicrographs of electrode arrays.
(A) Depth array (2x1) for intracortical microstimulation (ICMS) at two different sites in the depth of the cortex. Electrodes were made from platinum-iridium microwire (Ø 51µm) and were arranged at an interelectrode distance of ~ 700 µm.
(B) Epidural surface array (3x6) for the recording of the electrocorticogram (ECoG) at high spatial resolution. Electrodes were made from stainless steel wire (Ø 256 µm) arranged in a 3x6 matrix with an interelectrode distance of ~ 600 µm.

2.1.2. Epidural surface electrode array (6×3) for recording of the electrocorticogram at high spatial resolution

For recording a high resolution multichannel electrocorticogram (ECoG), a 6×3 epidural electrode array was built from teflon-insulated stainless steel microwire with a bare wire diameter of 256 µm, an insulation of 77 µm and thus a total diameter of 333 µm. (AM-Systems, Carlsberg, USA). The wire was cut into 18 pieces of about 2 cm length. Each wire piece was crimped to one of two male 10-pin connectors, having a pitch of 1.25 mm (Molex Inc., Lisle, USA). The free ends of the 18 wire pieces were guided through the holes 2 mm aluminum plate, which were arranged in a 6×3 matrix with 0.6 mm rectangular inter-hole distance (center to center). The first 5 mm of this 6×3 wire arrangement was embedded in dental acrylic and grinded to a little block after hardening using a grinding disk. The front plane of the block was polished, until a regular 3x6 matrix of bared cross-sectional wire surfaces was clearly visible. The final result was a 3x6 surface electrode array with an interelectrode distance of 600 µm (figure 3B). The interelectrode distances had been previously optimized by spatial spectral analysis of the ECoG (Barrie et al., 1996). Just before implantation (see subsection 2.2), the surface of the array was grinded to concave shape, to match the convexity of a given individual's cortical surface.

Reference and ground electrodes for the recording were built from the same stainless steel microwire. The wire was cut into pieces of about 2 cm length. At one end the last millimeter of insulation was stripped off, and the bared wire was bent into a small loop. The other ends were crimped to free male connector pins (Molex Inc., Lisle, USA).

2.2. Surgical preparation

Each of the six animals was surgically prepared for implantation of the two electrode arrays (see subsections 2.1.1. and 2.1.2.). Animals were anesthetized with Halothane (Höchst AG, Frankfurt a.M., Germany). Anesthesia was induced with 4 percent by volume for 8 minutes and maintained with 2 to 1.5 percent by volume. The top of the animal's head was shaved. Cranial skin was disinfected with iodine solution and removed from the interoccipital, parietal, and frontal bones with a

scissor. After spraying a local anesthetics (Gingicain, Höchst AG, Frankfurt a.M., Germany) on the wound, the remaining adipose tissue and the periosteum were also removed with a scalpel. The skin was further opened over the right temporal muscle. The dorsal part of the temporal muscle was carefully cut off and retracted from the squamous part of the temporal bone. A craniotomy over the right temporal cortex about 4 mm in diameter was cut with a drill. Thereby, the right process of the occipital bone and the right retrotympanic process of the temporal bone served as anatomical landmarks for positioning the craniotomy opening over the primary auditory fields, as shown in figure 4A. The dorsal edge of the craniotomy followed the occipital process. It was tried to expand the opening ventrally enough to give access to the ventral parts of auditory cortex. However, caudally a large venous blood vessel running within the temporal bone precluded the direct exposure of ventral aspects of the auditory cortex beyond the retrotympanic process. In the rostral part, the craniotomy could be expanded ventrally beyond the retrotympanic process exposing also ventral parts of auditory cortex. Rostrocaudally, the craniotomy extended from the caudal edge of the temporal muscle to about 1 millimeter beyond the point where the occipital and the retrotympanic process converge.

Small holes were drilled in the parietal and frontal bones. Four screws with a diameter of about 1 mm were inserted in the holes. Furthermore, a hole was drilled into the dorsal part of the bulla, and a small bent metal tie was inserted. A small aluminum bar of about 1 cm length was attached medially over the frontal bones. The bar was used for fixating the animal while plugging the recording cables to its head connectors before starting an experiment. The screws and the tie were later embedded in dental acrylic, in order to fix the implanted arrays, the connectors, and the aluminum bar to the skull.

2.3. Electrode implantation

Stimulation electrodes of the 2x1 depth arrays were implanted with the aim of stimulating two different sites located along the rostrocaudal tonotopic gradient of primary auditory field AI close to its input layer IV (figure 5). The 3x6 epidural surface array was implanted in order to obtain a high spatial resolution recording of the electrocorticogram (ECoG) right above primary auditory cortex (figure 5 and 6).
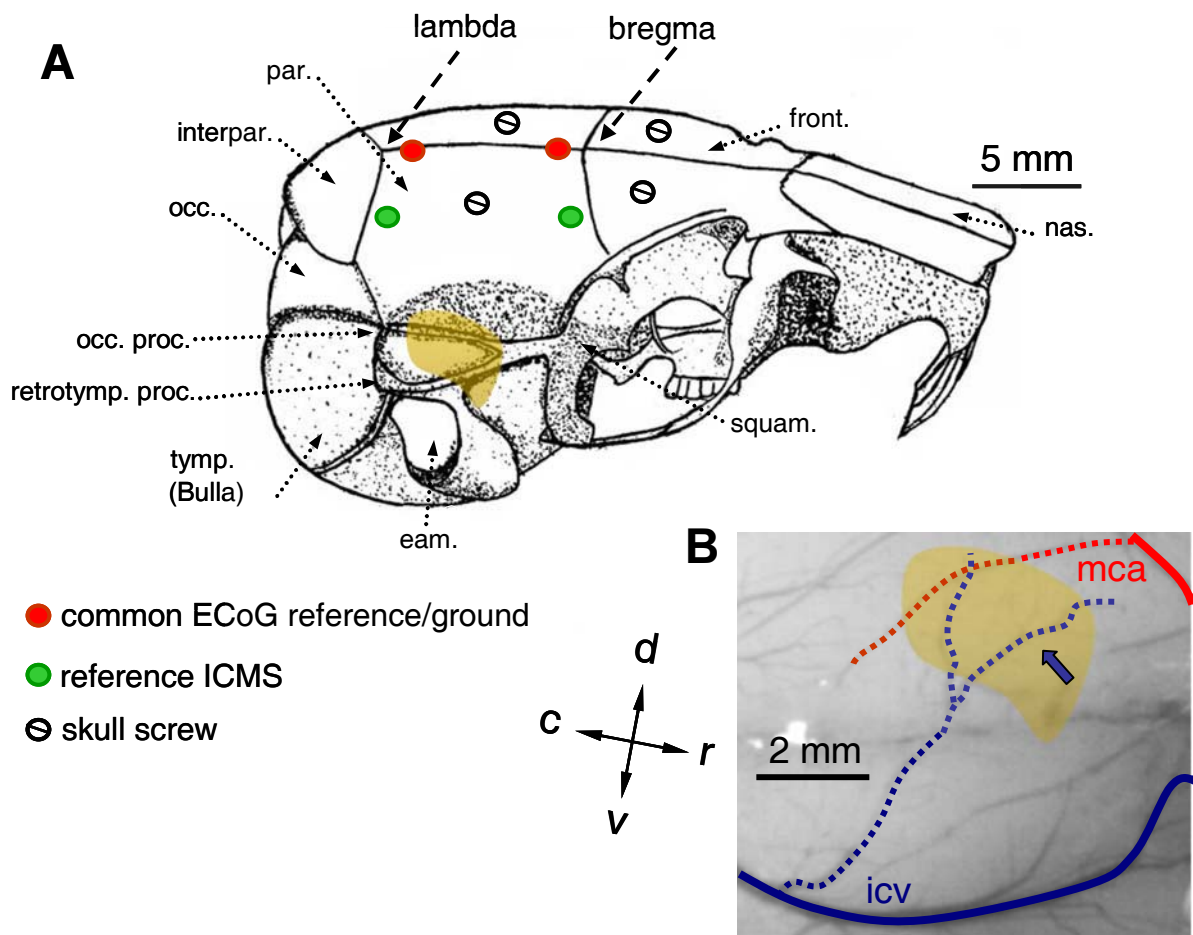
Figure 4: Surgical preparation.

(A) Positions of the craniotomy (yellow area), the anatomical landmarks (dashed arrows), the reference electrodes (red, and green circles), and the screws (black circle) on the skull (eam. = external auditory meatus, front. = frontal bone, interpar. = interparietal bone, nas. = nasal bone, occ. = occipital bone, occ. proc. = occipital process, par. = parietal bone, retrotymp. proc. = retrotympanic process, squam. = squamous part of the temporal bone, tymp. = tympanic part of the temporal bone).

(B) Schematic view of the cortical vascularization pattern formed by branches (dotted lines) of the middle cerebral artery (mca, red line) and the inferior cerebral vein (icv, blue line), as seen through the craniotomy opening (yellow area). The rostrocaudal border between auditory fields AI and AAF is typically found along the rostral ascending branch of the icv (blue arrow).

First, the electrodes serving as reference and ground were implanted. Reference electrodes for the caudal and the rostral stimulation sites were placed on the dura by inserting their bared and looped endings through small wholes drilled close to the caudal and rostral edge of the dorsal part of the parietal bone, respectively (green

circles, figure 4). Two electrodes optionally serving as common reference or ground for the ECoG recording were placed on the superior sagittal sinus by inserting their bared and looped endings through small wholes drilled along the median line between the parietal bones close to the anatomical landmarks lambda and bregma (red circles, figure 4). The free connector pins of the altogether four reference/ground electrodes were pushed in a 4-pin connector housing (Molex Inc., Lisle, USA). The assembled connector was then cemented to the left parietal bone. The parietal and frontal bones were covered with dental acrylic embedding the electrode wires, screws, and the metal tie. After implantation, the electrode arrays and connectors were cemented to this cap of dental acrylic yielding a stable conjunction between bone and electrode arrays.

Implantation of the electrode arrays was guided by visual inspection of the cortical vascularization pattern and by stereotactic measurements relative to the anatomical landmarks (figure 4) (Budinger et al., 2000a). After placing the reference electrodes, the electrode array for intracortical microstimulation (ICMS) was mounted on a set of 3D-micromanipulators and implanted with the electrode tips along the rostrocaudal axis of primary auditory cortex at a radial depth of about 0.6 mm close to cortical layer IV. Implantation depth was approximated by a medial offset to the plane tangentially to the temporal surface of the lissencephalic cortex. In order to target the primary auditory fields, the rostral electrode was positioned by visual inspection of the characteristic cortical vascularization pattern formed by the ascending branches of the inferior cerebral vein (icv) and the descending branches of the middle cerebral artery (figure 4B). Typically, the high-frequency border between the primary auditory field AI and the anterior auditory field AAF is located at a characteristic ascending branch of the icv. The rostral electrode was placed about 0.2 mm caudal to that branch. This position was about 3.2 mm rostral to the anatomical landmark lambda, corresponding to the high frequency range of primary auditory field AI (Scheich et al., 1993; Thomas et al., 1993). According to the interelectrode distance, the second stimulation electrode was located about 0.7 mm caudally to the first targeting the mid to low frequency range of AI. The dura was punctuated at the sites where the electrodes penetrated the cortex. Then the electrode array was slowly advanced in dorsal-to-ventral direction approximately tangential to the temporal cortical surface, until they reached the lower half of the craniotomy at about 1.3 mm.
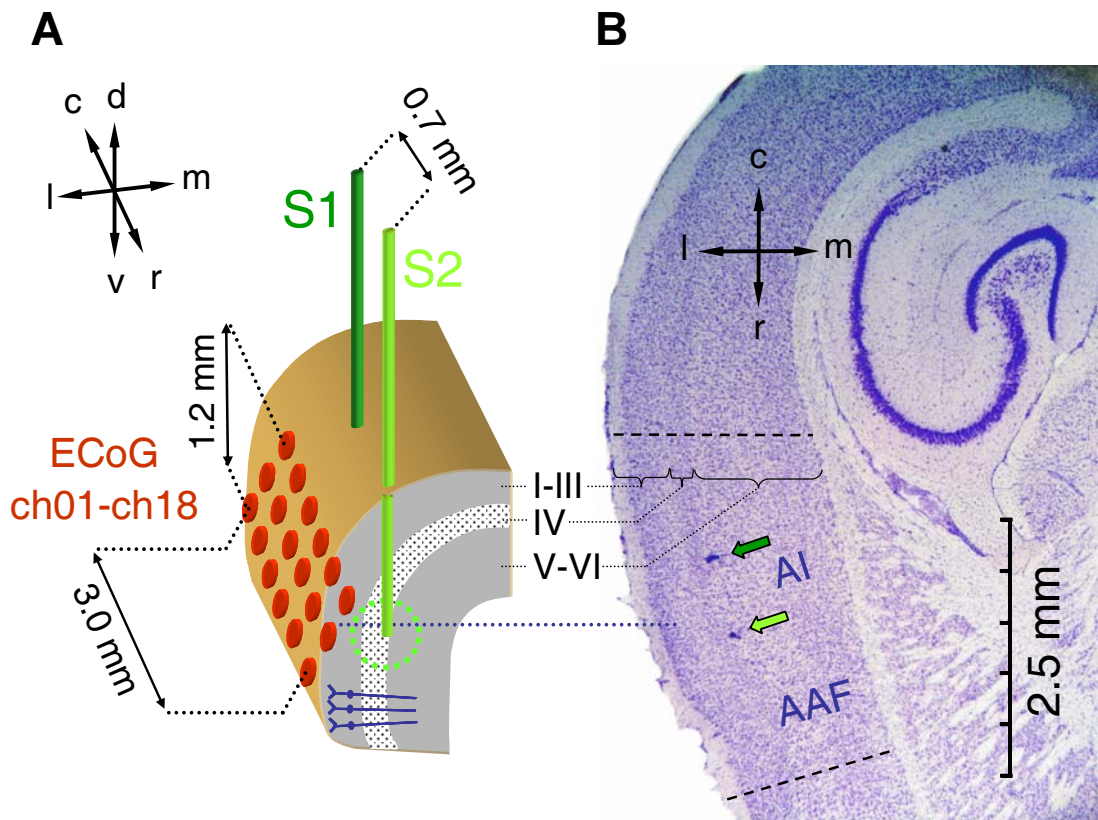
Figure 5: Positions of the implanted electrode arrays for stimulation and recording in a schematic view of cross sections of the temporal cortex.

(A) A pair of stimulation electrodes S1 (dark green) and S2 (light green) was implanted into the depth of the right primary auditory field AI close to its input layer IV. Electrode tips were positioned along the rostrocaudal axis (caudal electrode S1, rostral electrode S2) with an interelectrode distance of ~ 0.7 mm. The 3x6 ECoG recording array (ch01-ch18 in dark red, 0.6 mm interelectrode distance) was centered epidurally over the right AI. The length axis of the array was rostrally inclined into ventral direction about 10° from the horizontal plane (see also figure 6).

(B) Nissl stained horizontal section showing two small lesions (green arrows), which were caused by the tips of the two implanted stimulation electrodes indicating their location within temporal cortex. The rostrocaudal extent of the auditory core fields, AI and AAF, are marked by dashed lines. The cortical layering is shown by the curly brackets.
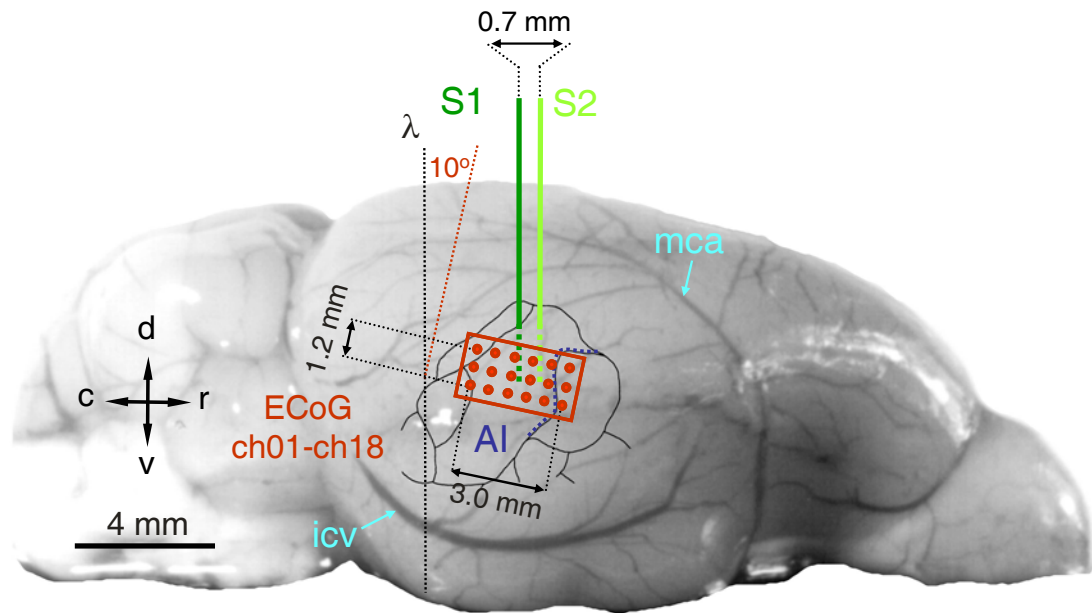
Figure 6: Positions of the implanted electrode arrays for stimulation and recording in a schematic view from the right lateral side of the brain (see legend figure 5; icv = inferior cerebral vein, mca = middle cerebral artery).

The ECoG array was positioned on the temporal surface of the cortex (figure 5 and 6). To achieve an orientation of the electrode tips parallel to the tonotopic gradient, the length axis of the array was rostrally inclined into ventral direction about 10˚ from the horizontal plane (Ohl et al., 2000a). It centered laterally over the stimulation electrodes with caudal recording electrodes about 1.5 mm rostral to lambda.

The exposed cortical surface was covered with an antiseptic lubricant (KY-jelly, Johnson & Johnson, New Brunswick, USA) and the craniotomy was closed with dental acrylic fixating the arrays to the preformed dental acrylic cap on the head of the animal. Finally, the three connectors of the arrays were cemented onto the left side of the dental acrylic cap on the head. After implantation, animals were allowed to recover for three to five days before the start of the training procedure.

2.4. Intracortical microstimulation (ICMS)

ICMS[8] of grey matter was applied by current pulses generated with an isolated pulse stimulator (Model 2100, A-M Systems Inc., Carlsorg, USA). The current pulses were delivered through the stimulation electrodes of the 2x1 depth array. Animals were stimulated with single current pulses during test measurements and with trains of current pulses during training (figure 7).
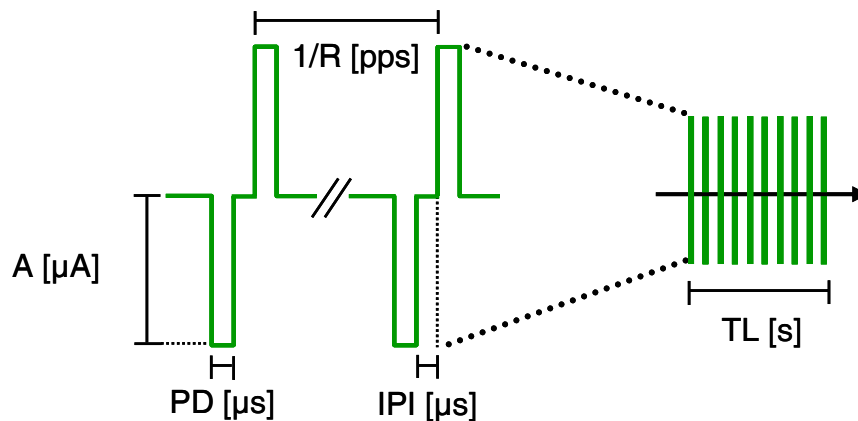
Figure 7: Stimulus parameters of single and trains of electrical current pulses used for intracortical microstimulation (ICMS). The first phase of the biphasic pulses always had a negative amplitude (cathodal first), whereas the second phase was always positive. The amount of current (A) per phase was measured in µA and was equal for both phases. The inter-phase interval (IPI) was measured in µs, the phase duration (PD) in microseconds (µs), the pulse rate (R) in parts per second (pps), and the train length (TL) in seconds (s).

Current pulses used were biphasic, in order to avoid tissue damage by chemical reactions due to electrode polarization (Lilly et al., 1955). To keep the charge balanced, the amount of current and the phase duration were the same for both phases, which differed only in the sign of their amplitudes. Being more effective in exciting neurons, the cathodal phase, i.e. the phase with the negative current amplitude, was leading. A phase duration of 200 µs/phase was chosen, which is

---

[8] ICMS directly excites local populations neurons by passing an extracellular current through the tissue, which leads to an extracellular voltage gradient across the neurons. Due to their membrane capacities and their transmembrane resistances, the intracellular voltage gradients differ from the extracellular gradient across the cells. This changes the transmembrane potentials of the cells resulting in a depolarisation of parts of the neurons and the generation of action potential at axonal elements (Ranck, 1975).

close to the chronaxie of neocortical pyramidal cells[9] (Stoney et al., 1968; Nowak & Bullier, 1998a). No inter-phase interval was inserted between the two phases, because the stimulators used did not allow for.

To become perceptually and behaviorally relevant, electrical stimulation of sensory cortex has to be extended in time for a few hundreds of milliseconds (Libet et al., 1964). Therefore, pulse trains consisting of 61 single charge-balanced biphasic current pulses (0.6004 s train length) were used in the training procedure (Rousche & Normann, 1999). The pulse rates were all set to 100 pps with the corresponding inter-pulse interval of 10 ms exceeding the refractory periods of neocortical pyramidal cells.

For each animal, the amount of current used both for single electrical current pulse stimulation as well as for the electrical current pulses of the trains applied during the training procedure was adjusted at each stimulation electrode in a test measurement one day before the start of the training procedure (see subsection 2.5.1.). Single pulse electrically evoked potentials (EEPs) were measured in response to ICMS with single electrical current pulses (for parameters see above). Single pulse EEPs of all 18 recording-channels were inspected after each single stimulus repetition. For each animal and for each stimulation electrode, the amount of current was set to a value resulting in a single pulse EEP with an amplitude of about two or three times the background activity at the recording channel showing the maximum response. The values were then adjusted to yield single pulse EEPs of about the same size and shape at the site of maximum response for both stimulation electrodes (figure 20 and 21). The amounts of current found by this procedure varied between 50 µA and 70 µA across animals and electrodes. With a phase duration of 200 µs this corresponded to a charge transfer between 10 nC and 14 nC per phase. As the stimulation electrodes had a diameter of 51 µm, and thus an exposed cross-sectional surface area of 0.002 mm^2, charge densities at the electrode tips ranged between 4895 nC/mm^2 and 6853 nC/mm^2 per phase (table 1). Charge-density thresholds for producing histological damage were found to be equal or greater than 16000 nC/mm^2

---

[2] The chronaxie of neural elements can be determined by a strength-duration curve, which displays the amount of current needed to evoke a neural response as a function of the phase duration of the pulse. The time on the strength-duration curve for twice the rheobase current, which is the current required for evoking a response with a very long pulse, defines the chronaxie. Stimulation with phase durations close to the chronaxie guarantees for optimal stimulation in terms of minimized charge transfer.

per phase, when using train durations of several hours with a pulse rate of 20 pps delivered through depth electrodes made of platinum combined with iridium with a tip size of 0.002 mm^2 (Agnew et al., 1986; McCreery et al., 1986; Tehovnik, 1996). Therefore, by using the parameters specified above, ICMS with single or trains of electrical current pulses was considered as save.

	current amplitude [µA]		charge per phase [nC]		charge density [nC/mm^2]		eff. current spread min. [mm]		eff. current spread max. [mm]	
animal	S1	S2	S1	S2	S1	S2	S1	S2	S1	S2
035	70	70	14	14	6853	6853	0.14	0.14	0.51	0.51
036	70	70	14	14	6853	6853	0.14	0.14	0.51	0.51
037	70	70	14	14	6853	6853	0.14	0.14	0.51	0.51
038	60	60	12	12	5874	5874	0.13	0.13	0.47	0.47
046	50	50	10	10	4895	4895	0.12	0.12	0.43	0.43
047	70	50	14	10	6853	4895	0.14	0.12	0.51	0.43

Table 1: Measures characterizing the biphasic electrical current pulses applied for intracortical microstimulation. Values are shown for the six animals used in the experiment and for each stimulation electrode (S1 and S2), separately. The first phase of the biphasic pulses had always a negative amplitude (cathodal first). Amount of current (equal for both phases) is given in microampere (µA), charge per phase in nano-coulomb (nC), minimum and maximum effective current spread in millimeter (mm), and charge density in nC/mm2.

2.5. Recording

During all recordings the animal was sitting in a shuttle-box, which was acoustically and electrically shielded. All 18-channel electrocorticograms (ECoGs) were recorded monopolarly from the electrodes of the 6×3 epidural surface array against one of the common reference electrodes and a second common ground electrode. The signals recorded from the 18 electrodes of the 6×3 surface array were fed into a preamplifier by a harness of thin, flexible cables with receptacles plugged into the connectors on

the head of the animal. The cable harness still permitted the animal to move freely and to turn around in the shuttle-box. The signals were then amplified either 5000 or 10 000 times and band-pass filtered between 3 dB cutoff frequencies of 0.1 Hz and 100 Hz using five 4-channel high-impedance amplifiers (Xcell-3×4, FHC, Bowdoinham, USA).

2.5.1. Recordings of responses to stimulation with single electrical current pulses in a test measurement before the start of the training procedure

The day before the start of the training procedure, 18-channel electrocorticograms (ECoGs) were recorded in response to intracortical microstimulation (ICMS) with single electrical current pulses (biphasic, cathodal-first, 200 µs/phase) (figure 7) in a test measurement. During the measurement the animals resided in one of the two compartments of the shuttle-box, which were separated by an inserted wall (for the setting of the parameters of the ICMS see section 2.4.). At each stimulation electrode, amount of current was varied between 10 µA and 120 µA, and finally set to a value (table 1) according to a procedure described in 2.4. In each animal, single pulse ICMS was repeated 80 times at each stimulation electrode with an inter-stimulus interval of 2.3 s. For each stimulus repetition, sweeps from 1.0 s pre- to 1.0 s post-stimulus time were recorded, sampled at 1 kHz, and stored to disk by a digital data acquisition system (DataWave Technologies, USA). Analysis of the single pulse electrically evoked potential is detailed below.

2.5.2. Recording of the electrocorticogram (ECoG) during the training procedure

During each training session 18-channel electrocorticograms (ECoGs) were recorded from the 120 trials with an intertrial interval varying randomly between 15 s and 19 s. Within each trial, a conditioned stimulus (see section 2.6.) was presented consisting of a train of current pulses delivered through one of the two stimulation electrodes (see section 2.4.). For each trial, sweeps from 2.0 s pre- to 3.0 s post-stimulus time

were recorded, sampled at 1 kHz, and stored to disk by a digital data acquisition system (DataWave Technologies, USA). Data were analyzed offline, as described in detail below.

2.6. Training

After implantation, animals were given a rest for three to five days. After further one or two days of test measurements and adaptation to the setup, animals were trained in a shuttle-box by using a GO/NO-GO avoidance paradigm carried out in 7 consecutive sessions (figure 8). The sessions succeeded in intervals of one to three days (Wetzel et al., 1998b; Ohl et al., 1999). The task for the animals was to discriminate intracortical microstimulation (ICMS) of two different sites located along the tonotopic gradient of the primary auditory cortex. The positive conditioned stimulus (CS+) was an electrical stimulus applied to one of the two sites, which was paired with an aversive unconditioned stimulus (US) consisting of a mild electrical shock delivered through the grid-floor of the shuttle-box. The CS+ predicted the occurrence of the US following the CS+ after a delay. The animals always had the chance to escape the US by changing the compartment of the shuttle-box, i.e. jumping across the hurdle separating the two compartments. The change of compartment defined the conditioned response (CR). Resembling the natural flight response of the Mongolian gerbils, the animals learnt the CR in relation to the onset of the US often within the first session, allowing the animal to escape the aversive US.

The negative conditioned stimulus (CS-) was not paired with an US and consisted of an electrical stimulus delivered through the electrode at the other site. Whenever the animal showed a CR within a delay after the onset of the CS-, it received a mild electrical error shock (ES) through the grid-floor. The amplitudes and delays of the ES were set equal to those of the US. The CS- predicted the ES but not the US.

According to learning theory (Wasserman & Miller, 1997) it was expected, that the animals change from the initial escape to an avoidance strategy using the CS+ as a predictor for the US. If the animals were able to discriminate the CS+ from the CS-, they should be able learn to anticipate the US by the CS+ only, showing a CR to the CS+ but not to the CS-, thus avoiding the ES (Stark et al., 2004).
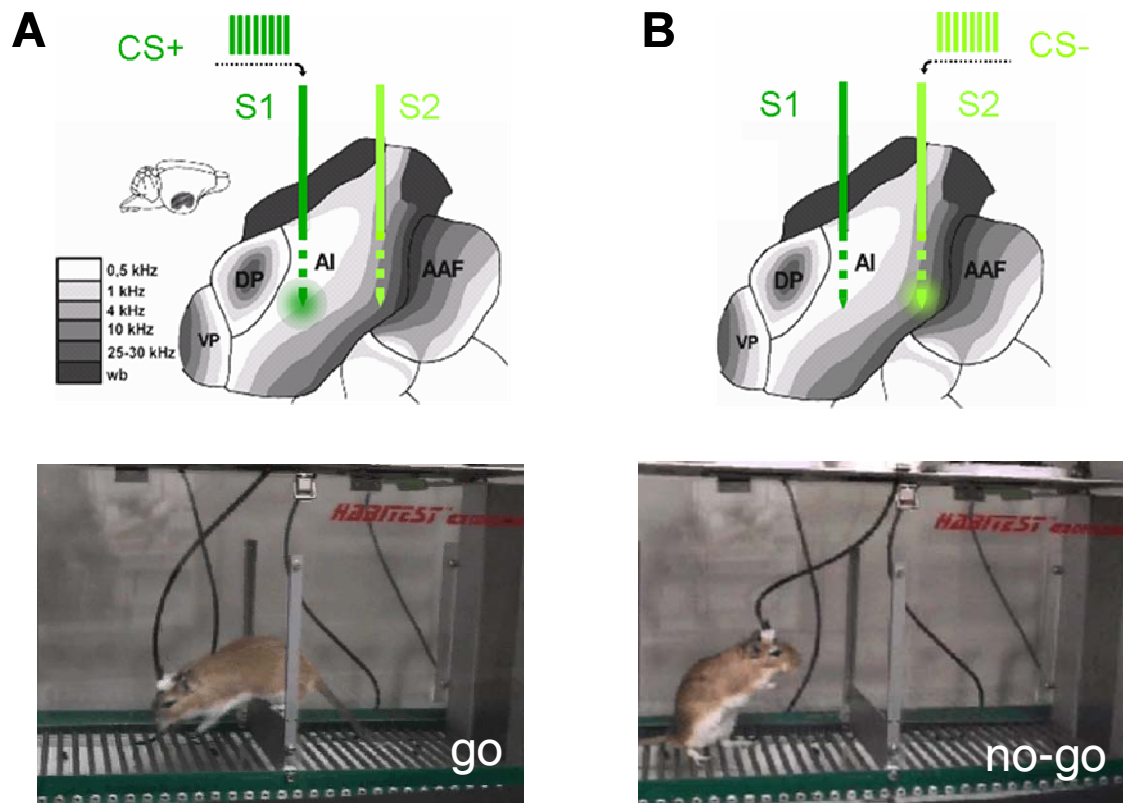
Figure 8: Intracortical microstimulation (ICMS) and training in the shuttle-box. According to the rostrocaudal tonotopic gradient of primary auditory field AI, the caudal stimulation electrode S1 was positioned in the low- to mid-frequency part (0.5 kHz to 4 kHz) of AI and the rostral electrode S2 in the mid- to high-frequency part (4 kHz to 30 kHz) of AI. Animals were trained in a shuttle-box with a GO/NO-GO avoidance paradigm, to discriminate low- from high-frequency sites of electric stimulation. In order to avoid a mild electric foot shock through the grid floor, the animals had to make a GO response (A) to the positive conditioned stimulus CS+ (changing the compartment by jumping across the hurdle of the shuttle-box) and a NO-GO response (B) to the negative conditioned CS- (staying in the compartment). Stimuli consisted of trains of charge-balanced biphasic current pulses (0.6 s train length, amount of current ranging between 50 μA and 70 μA). The CS+ (A) was a pulse train delivered either through the stimulation electrode within the low- (S1) or within the high-frequency part (S2) of the tonotopic representation of AI. The CS- (B) was a train delivered by the other electrode, respectively (see table 2).

The US-amplitude was adapted to the animal's behavior by keeping it below the pain-threshold with the animal showing no vocalization or freezing on the shock, but setting it high enough to make the animal change the compartment. This was achieved by US-amplitudes between 200 µA and 400 µA. The delay between CS and US was selected randomly from three fixed values, i.e. 3.5 s, 4.5 s, and 5.5 s, so that the animal couldn't predict the exact time of occurrence of the US. This kept the animals from retaining an escape strategy by a prepared reaction to the onset of the US without making differential use of the conditioned stimuli.

animal	naive		after contingency reversal	
	S1	S2	S1	S2
035	-	+	+	-
036	-	+	nf	nf
037	+	-	nf	nf
038	-	+	no	no
046	+	-	no	no
047	+	-	-	+

Table 2: Contingencies for all six animals; (+) indicates the stimulation electrode used for delivering the train of electrical current pulses serving as CS+; (-) indicates the electrode delivering the pulse train serving as CS-; (nf) means that the training could not be finished after the contingency reversal; (no) means that no contingency reversal was carried in that animal.

In three animals the CS+ was a train of biphasic current pulses (200 µs/phase, cathodal phase leading, 100 pps pulse rate, 0.6004 s train-length) delivered through the caudal stimulation electrode, which was located in the low- to mid-frequency part of AI. The CS- was a train with the same parameters delivered through the rostral electrode to the mid-to high-frequency part of AI (table 2). In the other three animals the pulse train was delivered through the rostral electrode (mid- to high-frequency part of AI) as a CS+ and through the caudal electrode (low- to mid-frequency part of

AI) as a CS-. Parameters for stimulation with trains of current pulse were set according to section 2.4 (figure 7). Resulting amounts of current for each stimulation electrode and each animal are listed in table 1.

Before the start of each session, the animals were allowed to explore the shuttle-box for 3 minutes, not to confound the explorative compartment changes at the beginning of each session with changes related to the conditioned and unconditioned stimuli. A session consisted of 60 CS+ and 60 CS- trials presented in a pseudo-random sequence with an inter-trial interval varying randomly between 15 and 19 s. Reaction times for the CR were recorded after the stimulus relative to its onset and stored to disk by the shuttle-box system.

After the first block of training, when all animals had reached a significant discrimination performance over at least three consecutive sessions, a contingency reversal was carried out in four of the animals with the former CS+ becoming the CS- and the former CS- becoming the CS+. This way, it was tested whether the animals discriminated between CS+ and CS- in contrast to simply detecting the CS+.

2.7. Histology

In order to analyze the effects of chronic implantation and chronic intracortical microstimulation (ICMS), Nissl stained sections were prepared from five of the six animals (035, 036, 037, 038, and 047). About one week after finishing the training, the animals were killed by pulmonary injection of T61 (Höchst AG, Frankfurt a.M., Germany) and decapitated. The dental acrylic cap was lifted from the skull, and the electrode arrays were carefully explanted. The brain was removed and frozen in 2-methylbutane cooled to -70° in liquid nitrogen. Horizontal sections of 40 μm were cut on a Leica cryostat and stained with cresyl violet. In one animal (036), the Nissl preparation failed. In the remaining animal (046), a newly developed technique for mapping neural activity was explored (Goldschmidt et al., 2004). The technique is based on the activity dependent cellular uptake of the potassium-analog thallium (Tl^+). After injection of thallium, ICMS was applied for 15 minutes. Then, the animal was injected with a high dose of anesthetics and transcardially perfused with glutaraldehyde for fixation and a sulfide for Tl^+-precipitation. After the perfusion, the

electrode arrays were explanted, the brain was removed, and frozen in 2-methylbutane cooled to -70° in liquid nitrogen. Horizontal sections of 25 µm thickness were made on a Leica cryostat followed by further steps thallium staining. A detailed analysis of the activity dependent thallium uptake is beyond the scope of this work. However, the layering of the cortex, and the position and the size of the lesions induced at the sites of the implanted electrodes could be well determined from the histological sections. Also, the positions of the two stimulation electrodes relative to the 3x6 epidural array were visually inspected after their explantation.

3. Data Analysis

All computations were executed using own programs which were developed in Matlab v. 6.1 (© MathWorks) on a standard PC.

3.1. Histological analysis of lesions and electrode positioning

Consecutive horizontal sections were microscopically analyzed and surveyed for effects of electrode implantation and chronic intracortical microstimulation (ICMS) by visual inspection of consecutive sections proceeding from dorsal to ventral ones. Together with a scale bar projected on to the microscopic picture, regions of interest were digitally photographed using a Fujii FinePix S2 Pro digital camera on a Leica DMR microscope system. Measurements within the digitally photographed sections were carried out with reference to the scale bar by using line segments drawn on the photomicrographs with the Adobe Photoshop software running on a Macintosh computer. The scale bars had a length of 2.5 cm corresponding to an actual length of 2.5 mm within the microscopic image at the lowest, 1.0 mm at the medium, and 0.5 mm at the highest level of magnification used for the analysis. The length of the line segments could be measured with a precision of at least 0.05 cm, which corresponded to an actual precision of 0.05 mm for the lowest, 0.02 mm at the medium, and 0.01 mm for the highest level of magnification. For all measurements in the thallium stained sections of animal 046, a shrinkage factor of 10% was taken into account due to tissue fixation.

Within Nissl stained sections, glial cells can be distinguished from neurons by their small intensively stained nuclei and their barely visible cell body. In neurons, on the other hand, the cell bodies are clearly visible by the large amounts of Nissl substance in the cytoplasm surrounding the less intensively stained larger nuclei[10] (Ahrens et al., 1990). Furthermore, astrocytes and microglial cells can be differentiated by the

---

[10] Cresyl violet particularly stains the nuclei, the nucleoli, and the rough endoplasmatic reticulum (rER) of cells, also called Nissl substance. In neurons, the rER in the cytoplasm surrounding the nuclei is clearly visible and can be separated from the nuclei, whereas in the smaller glial cells, the rER can be hardly separated from the dominating nuclei.

shape of their nuclei. Astrocytes have oval shaped nuclei, whereas microglial cells have rather square shaped nuclei. Additionally, the nuclei of microglial cells are smaller and are stained more intensively.

Types, size, and packing densities of neurons were used for determining the layering of the cortex. Glial reactions, e.g. glial proliferation and scar formation by astrocytes and microglia, as reaction to the traumatic lesion induced by the implantation, were determined by local increases of the density of glial cells around the implantation sites (figure 5B). In order to identify possible inflammatory processes, the histological sections were surveyed for large phagocytotic cells and wide spread increases of the densities of glial cells, especially of microglial cells.

Nissl stained sections were examined for neuronal injury and cell death, as it can be caused by traumatic lesions induced during electrode implantation, as well as by the toxicity of electrode materials, or by hyper-excitation due to electrical stimulation. Therefore, the Nissl stained section were surveyed for regions of nuclear debris, neuronal chromatolysis, shrinkage of neurons, and reduced neuronal densities[11] (Agnew et al., 1983; Agnew et al., 1986). In the thallium stained sections of animal 046, lesions were identified by the lumina marking the electrode tracks.

In each of the five animals, from which histological sections were obtained, pairs of local lesions found in the sections served as markers for locating the two stimulation electrodes in relation to the cortical layering and to anatomical landmarks used as references for the measurements.

The dorsoventral position of the stimulation electrode array was determined relative to the dorsal roof of the caudate putamen, which was used as a dorsoventral reference (Scheich et al., 1993). Section-thicknesses of 40 µm (25 µm for animal 046) were summed up from the most dorsal section containing the dorsal roof of the caudate putamen to the most ventral section containing pairs of local lesions, which marked the location the two stimulation electrode tips. The values were compared to the dorsoventral positions of auditory fields AI and AAF, as have been previously reported with injections of the anterograde tracer biocytin into AI and AAF (Budinger et al., 2000a).

One of the three most ventral sections containing pairs of local lesions within the right temporal cortex, which presumably indicated the positions of the electrode tips, was selected for further analysis. In these sections, the size of the local lesions was evaluated by drawing circles around the centers of the lesions. The radius of the smallest circle around the whole region affected by the lesion, i.e. showing increased glial cell densities or reduced neuronal densities, defined the size of the lesion. Interelectrode distances were determined from the distances between the centers of the lesions indicating the positions of the two electrode tips. Furthermore, the cortical depth of the electrode tips was measured perpendicular to the cortical surface and compared to the depths of the lateral and medial boundaries of layer IV with layer III and V, respectively. Finally, the rostrocaudal position of each stimulation electrode was determined with reference to the rostral pole of the ventral hippocampus. It has been previously shown by functional autoradiographic labeling (Scheich et al., 1993) that a line drawn through the rostral hippocampal pole perpendicularly to the cortical surface coincides with the 1.5 kHz isofrequency contour within layer IV of field AI with a standard deviation of 0.2 mm. Therefore, two lines were drawn perpendicularly to the cortical layering, one crossing the hippocampal reference and the other crossing the center of the lesion induced by the electrode tip. The rostrocaudal position of each stimulation electrode relative to the hippocampal reference was determined by measuring the distance between the two points where the hippocampal reference line and the line crossing the lesion center intersected the center of layer IV, respectively. For each stimulation electrode, this rostrocaudal position was compared with the rostrocaudal positions of the borders of fields AI and AAF, as determined from isofrequency contours labeled in 2-Fluorodeoxyglucose autoradiographs at layer IV (Scheich et al., 1993; Budinger et al., 2000a).

3.2. Effective current spread of ICMS

The amount of electrical current needed to directly activate a certain neuron by intracortical microstimulation (ICMS), i.e. its axon or its cell body, is generally assumed to be proportional to the square of the distance between the neuron and the

---

[11] Injury of neurons leads to a loss of Nissl substance, so called chromatolysis. If the injury results in cell death, the whole cell is degraded leaving nuclear debris, which can be identified by the Nissl staining.

electrode tip (Stoney et al., 1968; Tehovnik, 1996). With r being the distance between electrode tip and neuron in mm, I the amount of current in μA, and K the so called current-distance constant measured in μA/mm^2, this relation can be expressed as:

$$I = K \cdot r^2 \qquad (1)$$

K depends on the phase duration of the current pulse and on the properties of the neuron. The current-distance constant of a neuronal element is positively correlated the threshold for electrical stimulation[12] with large values of K corresponding to high-threshold neurons and small values of K corresponding to low-threshold neurons.

In contrast to white matter, grey matter can be regarded as being isotropic, i.e. having equal resistivity in all spatial directions. Given a certain amount of current, a minimal sphere around the stimulation site can be determined which contains all directly activated neurons of a certain threshold. The radius r of this sphere is called effective current spread and can be calculated by rewriting equation (1):

$$r = \sqrt{\left(I \Big/ K \right)} \qquad (2)$$

Accordingly, the effective current spread r is large for low-threshold neurons, which have small values of K, and it is small for high-threshold neurons, which have large values of K. In the motor cortex of the cat, Stoney and coworkers (1968) found that the values of K range from a minimum of 272 μA/mm^2 to a maximum of 3460 μA/mm^2 when using a 200 μs cathodal current pulse.

In order to estimate the spatial extent of direct electrical excitation, the minimum and the maximum effective current spread for single current pulses was calculated at each stimulation site by using the current-distance constants determined by Stoney

---

[12] The current-distance constant can be related to the threshold of electrical excitation of a neuron via its length constant. It has been shown that the current-distance constant is negatively correlated with the conduction velocity of a neuron's axon (Hentall et al., 1984). Accordingly, the current-distance constant decreases with increasing axon size and is smaller for myelinated than for non-myelinated axons. As the length constant increases with the radius of the fibre and decreases with cytoplasmatic resistivity, it increases with axon size and conduction velocity. Also, the length constant increases with the specific membrane resistance and thus with increasing degree of myelinisation. Therefore, the current-distance constant is inversely proportional to the length constant of the excited neural element. According to Ranck (1975), the longer the length constant the lower is the threshold for extracellular electrical stimulation of the excited neural element. Hence, the current-distance constant is large for high-threshold neurons and small for low-threshold neurons.

and coworkers (1968). It was assumed for auditory cortex of the Mongolian gerbil that the maximum and the minimum effective current spread for a single cathodal-first biphasic current pulse with 200 µs phase duration can be calculated by equation (2), and that the range of current-distance constants is approximately the same as in the motor cortex of the cat. Then, the maximum effective current spread was approximated by introducing the minimum current-distance constant of 272 µA/mm^2 for K in equation (2). For approximating the minimum effective current spread, the maximum current-distance constant of 3460 µA/mm^2 was used for K.

However, it should be noted that with the pulse-trains applied during training, the effective current spread will depend on temporal summation and nonlinearities according to the excitability cycles of the stimulated cells (Butovas & Schwarz, 2003). Equation (2) does not exactly hold in this case. Therefore, the minimum and maximum current spread for single pulses, as calculated above, was only used as a first approximation for the spatial extent of the direct electrical excitation.

3.3. Analysis of discrimination behavior

3.3.1. Response classes and learning curves

If the animal showed a conditioned response (CR) in the critical interval between a minimum reaction time of 0.3 s and the shortest CS-US-delay plus the minimum reaction time, i.e. 3.7 s after stimulus onset, this response was classified as a GO-response. An omitted CR or a CR outside this critical interval was classified as NO-GO-response. With the two different stimuli CS+ and CS-, behavioral responses were further divided into four different response classes. GO-responses to the CS+ were classified as hits and NO-GO-responses to the CS+ as misses. GO-responses to the CS- were classified as false alarms and NO-GO-responses to the CS- as correct rejections.

Analysis was carried out for the sessions before and after the contingency reversal, separately. Response rates were expressed session-wise as relative frequencies for every response class by dividing the counts of hits and the counts of misses from a session by the number of CS+ presented in the session. The counts of correct

rejections and the counts of false alarms were divided by the number of CS- presented in the session. For evaluating the differential response of the animals to the CS+ and the CS-, hit-rates and false-alarm-rates were plotted over sessions giving so called learning curves. The significance of differences between responses to CS+ and CS- was tested in single sessions and animals by constructing a fourfold table from the response counts derived from the four different response classes. The fourfold table was then submitted to a two-sided χ^2-test on a significance level of $p < 0.05$.

Mean learning curves were calculated by averaging session-wise across the six animals. Hit-rates were tested for differing from false-alarm rates by using a Wilcoxon test on a significance level of $p < 0.05$ against the null hypothesis of equality of medians of hit and false-alarm rates.

3.3.2. Discrimination performance measured by the discriminability index d' according to signal detection theory

Discrimination performance was quantified by the discriminability index d', which is defined in signal detection theory (Green & Swets, 1966; MacMillan & Creelman, 1991). Discriminability index d' is independent from the criteria used by the subject to make a decision, i.e. the animal's internal bias towards one of the responses. In its general form, signal detection theory states the existence of an internal response space, which can be interpreted as a multidimensional perceptual space with its dimensions reflecting the different perceived attributes of a stimulus. Assuming that a stimulus presentation leads to a percept which can be scaled along the axes of this space, the percept is represented as a point within this space. However, due to external and internal uncertainties, the position of this point in the perceptual space varies from presentation to presentation of the same stimulus. External uncertainties are due to the noise of the physical stimulus itself. Internal uncertainties can emerge from sensory, but also from cognitive processes. This leads to a distribution of percepts over a region of the perceptual space that can be described by a probability

density function (figure 9A). Assuming that stimuli are easier to discriminate, if they are perceptually further apart, discriminability can be measured as a distance between two probability densities within the perceptual space, independent of the decision criteria used by the subject in the decision process.
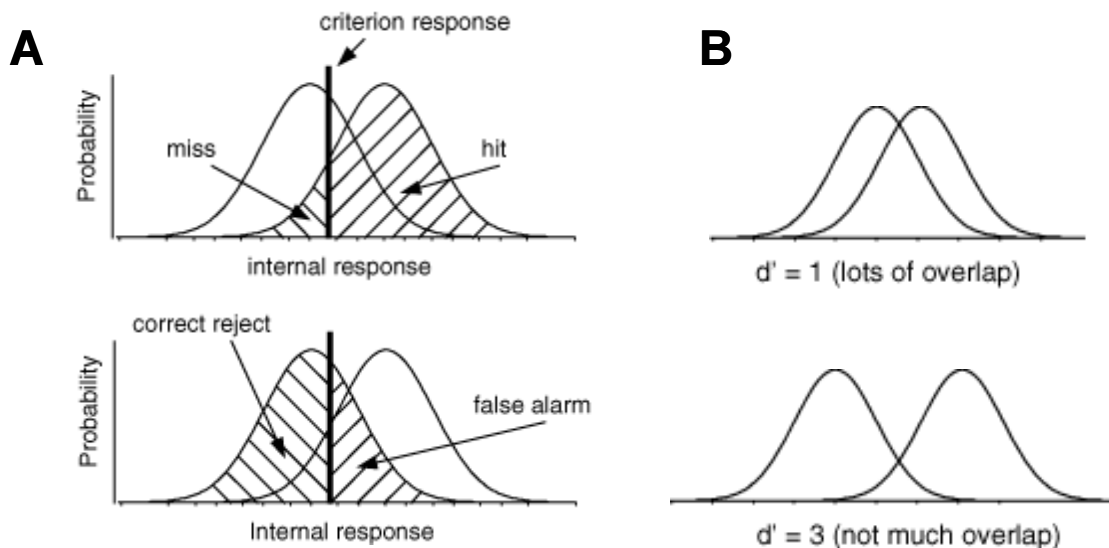
Figure 9: Behavioral discrimination performance measured by the discriminability index d', defined in signal detection theory (adapted from Heeger, 2003).

(A) Due to external and internal uncertainties, CS+ and CS- both lead to a distribution of percepts across stimulus presentations along the perceptual dimension relevant for discrimination. It is assumed that the distributions related to the CS+ and the CS- can be described by two gaussian probability density functions (pdfs), which differ in their mean, but have the same variance. Discriminability index d' is defined as distance between the two pdfs and can then be determined as z-score (difference of the two means divided by the standard deviation). The actual decision process is modeled by introducing a criterion level (vertical line). Percepts scaled below the criterion level result in a GO- and above the level in a NOGO-response. Hit- and miss-rates can be calculated by integrating the pdf corresponding to the CS+ on the right and left side of the criterion level, respectively (upper panel). False- alarm- and correct-rejection-rates can be calculated in the same way from the pdf corresponding to the CS-.

(B) Discriminability index d' increases with decreasing overlap between the two probability density functions (pdfs). Measured by a z-score, the overlap is reduced with increasing difference between the means, but also with decreasing variance of the pdfs.

For the GO/NO-GO-paradigm used here, it was assumed that the animal discriminated CS+ and CS- on the basis of a single attribute, namely the site of intracortical microstimulation (ICMS) within the tonotopic gradient of the auditory fields leading to different percepts. Then each of the two stimuli of the paradigm can be represented by a distribution of percepts which is described by a one-dimensional probability density function (pdf). Assuming that the pdf is approximately gaussian (figure 9A), a straight forward measure for d', i.e. the distance between the two Gaussian pdfs, is the difference between their means expressed as standard deviations. These so called z-scores can be calculated, if both Gaussian probability densities have the same variance. Thus d' increases both with the difference between the means of the two Gaussian pdfs, but also with decreasing variance (figure 9B). As a distance measure, d' has true ratio scaling properties, which means that the ratio of d' values obtained from different stimulus conditions amounts to the relative discriminability of the stimuli under these conditions and allows comparison of discriminability across conditions. This is one of the main advantages of the measure d'.

The actual decision process can be modeled in terms of a criterion level dividing the perceptual axis into two parts. If a percept induced by a single stimulus presentation is scaled below the criterion level, it will result in a NO-GO-response, whereas lying above this level, it will initiate a GO-response. This allows for telling apart the two probability densities emerging from the two stimuli in an optimal way.

As the pdfs of the two stimuli are both extending from plus to minus infinity and thus are overlapping, the probability for a GO- or a NO-GO-response can be derived from integrating the probability densities from the criterion level to plus infinity and from minus infinity to the criterion level, respectively. Hence hit- and miss-rates can be directly calculated from the probability density related to the CS+ and false-alarm- and correct-rejection-rates from that related to the CS- (figure 9A)[13]. The discriminability index d' is independent of the criterion level and hence independent from the actual decision process.

---

[13] With a low criterion level, the animal has a bias towards the GO-response, i.e. the animal prefers to make a GO- response rather than a NO-GO-response. In contrast to this liberal strategy, the animal can set a high criterion level biased towards a NO-GO-response. This is called a conservative strategy.

The discriminability index d' can be calculated from the z-scores of the actually measured hit-rate H and false-alarm-rate F derived from the inverses of a standardized normal distribution function as

$$d'=z(H)-z(F) \qquad (3)$$

For every animal and every session, d' values were calculated by this equation. However, the z-scores cannot be calculated analytically and thus were approximated numerically (Odeh & Evans, 1965). In order to avoid infinite values of d' for H = 1 and F = 0, these rates were converted to H = 1-1/(2N+) and F = 1/(2N-), with N+ and N- being the number of presented CS+ and CS-, respectively.

Mean d' values were calculated by averaging across the six animals. Differences between sessions were tested by the Kruskal-Wallis H test on a significance level of p < 0.05 against the null hypothesis of discrimination performances being equal across sessions. Significance of increases from one session to the next were tested by using the Mann-Whitney U test on a significance level of p < 0.05 against the null hypothesis of equal performance with alpha being Bonferroni corrected for multiple testing (Bortz,.1999, p.260-263).

3.4. Analysis of the electrocorticogram (ECoG)

3.4.1. Artifact rejection, removal of power line interference, and signal preconditioning

All recordings were surveyed for recording artifacts in every channel. Intracortical microstimulation (ICMS) caused characteristic stimulus artifacts in the recording both with single electrical current pulses and with trains of current pulses. Stimulus artifacts were investigated in detail from temporal ensemble averages across ECoG sweeps recorded in response to single current pulses (see subsection 3.4.2.) during a test measurement before the start of the training procedure and in response to pulse trains (see subsection 3.4.3.) presented as CS+ and CS- during training. Stimulus artifacts did not last for more than 10 ms after the end of electrical

stimulation. Therefore, the maximum interval affected by the stimulus artifact was assumed to be 10 ms after stimulus onset for single pulses and 610 ms after stimulus onset for pulse trains.

Amplifier clippings, as they occurred with movements of the animal, and large fast oscillations in the recording associated with muscle artifacts were identified by visual inspection. Sweeps containing artifacts besides the electrical stimulus artifact at more than two channels were excluded from analysis. In sweeps with no more than two channels affected by the artifact, the signals from the bad channels were replaced by averages built from the signals of their direct neighbors. From the 80 stimulus repetitions with single-pulse stimulation at each electrode between 75 and 80 artifact-free repetitions were left after artifact-rejection. From the ECoG recording during training, between 43 and 60 of the 60 CS+ trials (54 on average) and between 46 and 60 of the 60 CS- trials (56 on average) remained artifact-free for each animal and each session. In some animals the recording quality in the first two sessions was very low. In session 1 of animal 035 less than 10 trials remained after artifact rejection for the CS+ and the CS-, respectively. Therefore this session had to be omitted from analysis.

The 50 Hz power line interference was removed by reconstructing it from the ECoG signal. For each channel of a recorded sweep the signal was filtered between 48 and 52 Hz and afterwards divided into consecutive intervals of 20 ms corresponding to the length of one period of a 50 Hz sine wave. Signal segments were then averaged across the segment index. Assuming that the power line interference has stable amplitude and phase over the length of the sweep, the mean across the signal segments was used as an estimator for one period of the power line interference. The estimated period was extended to the length of the entire signal and then subtracted from it. Power line interference was so removed from the time before, during and after the interval affected by the stimulus artifact, separately.

Digital filtering of ECoG signals prior to further analysis was performed by using a FIR-filter of order 300, with a symmetric impulse response truncated by a Hamming window. Accordingly, the applied filter kernel had a length of 300 ms and was anti-causal having zero phase distortion. Using this filter kernel the time affected by the electrical stimulus artifact was extended 150 ms before and after the raw stimulus

artifact after digital filtering. Thus, an interval between 150 ms before and 760 ms after the onset of the train of current pulses was possibly influenced by the electrical stimulus artifact.

3.4.2. Analysis of evoked potentials in response to single current pulses

Electrically evoked potentials were analyzed in response to single current pulse stimulation (biphasic, 200 μs/phase, cathodal phase leading, for amounts of current see table 1) by calculating temporal ensemble averages across stimulus repetitions either channel-wise (TEAs) or after spatial ensemble averaging across channels (TSEA). For each animal and for each stimulation electrode, the ECoG signals recorded from the 80 stimulus repetitions (see subsection 2.5.1.) were digitally high-pass filtered at a cut off frequency of 3 Hz from 1.0 s pre- to 1.0 s post-stimulus time. Afterwards the signals were z-standardized channel-wise by subtracting the mean and dividing by the standard deviation of values derived from a pre-stimulus baseline not affected by the electrical stimulus artifact (1.0 s to 0.15 s pre-stimulus time). TEAs were calculated for each of the 18 channels across all artifact-free stimulus repetitions in reference to stimulus onset from 0.05 s pre- and 0.17 s post-stimulus time. SEAs were calculated across the 18 channels for each stimulus repetition. TSEAs were calculated from the SEAs across all artifact-free stimulus repetitions in reference to stimulus onset from 0.05 s pre- and 0.17 s post-stimulus time.

3.4.3. Analysis of evoked potentials in response to trains of current pulses applied during training

For each training session, electrically evoked potentials were analyzed in response to trains of current pulses (biphasic, 200 μs/phase, cathodal phase leading, pulse rate 100 pps, train length 0.6004 s) applied as CS+ and CS- during training (see subsection 2.6.) by calculating temporal ensemble averages across stimulus repetitions either channel-wise (TEAs) or after spatial ensemble averaging across channels (TSEA).

For each animal and for each session, the ECoG signals recorded from the CS+ and CS- trials were digitally high-pass filtered from 2.0 s pre- to 3.0 s post-stimulus time at a cut off frequency of 3 Hz. Afterwards the signals were z-standardized channel-wise by subtracting the mean and dividing by the standard deviation of the values derived from a pre-stimulus baseline (2.0 s to 1.0 s pre-stimulus time). TEAs were calculated for each of the 18 channels in reference to stimulus onset from 1.0 s pre- and 2.0 s post-stimulus time across artifact-free CS+ and CS- trials, separately. SEAs were calculated across the 18 channels for each trial. TSEAs were calculated from the SEAs in reference to stimulus onset across artifact-free CS+ and CS- trials, separately.

3.4.4. Spatial pattern classification in the ongoing ECoG

Analysis of the multichannel ongoing ECoG aimed for identifying stimulus induced spatial patterns of activity in the β- and γ-band (15 to 80 Hz) which were related to the behavioral discrimination between CS+ and CS-. This was achieved by a previously introduced multivariate classification procedure (Barrie et al., 1996). Parameters like window lengths and filter bands were used according to this study, where they have been optimized for yielding best classification results.

The two sets of artifact-free CS+ and CS- trials were each split into two disjunctive subsets A and B by dividing them into even and uneven set indices. This resulted in altogether four subsets, namely CS+$_A$ and CS+$_B$ from the CS+ trials, and CS-$_A$ and CS-$_B$ from CS- trials. The size of the subsets n_s ranged between 20 and 30 trials.

ECoG signals were digitally bandpass filtered between 10 and 80 Hz restricting the signal to the β- and γ-band of the ongoing ECoG (see subsection 3.4.1.). Spatial activity distributions were obtained for every single trial of each subset by determining the mean power within 180 ms time windows stepped in 20 ms steps through the bandpass filtered ECoG signal of each channel from 2 s pre- to 3 s post-stimulus time (figure 10). Note that the sampling period for the ECoG signals was 1 ms. Mean power in the the β- and γ-band was determined by the root mean

squared (RMS) amplitude $R_{k,l}^{(s)}(i)$ calculated across 180 bandpass filtered ECoG samples $V_{k,l}^{(s)}(t_j)$ at t_j within time window i for each channel k and for each trial l of a subset with running index s (equation (4)).

$$R_{k,l}^{(s)}(i) = \sqrt{\sum_{j=1}^{180}(V_{k,l}^{(s)}(t_j))^2} \qquad \forall\ s \in \{1,2,3,4\}, \qquad (4)$$
$$l \in \{1,...,n_s\},$$
$$i \in \{1,...,n_w\},$$
$$k \in \{1,...,18\}$$

where s = 1 indicates subset CS+$_A$, s = 2 subset CS+$_B$, s = 3 subset CS-$_A$, and s = 4 subset CS-$_B$. The number of time steps i is given by n_w, and n_s is the number of trials of the subset with index s.

The RMS amplitudes of the 18 channels were summarized into an 18-dimensional state vector characterizing the spatial distribution of activity in the time window i of trial l in subset s. To remove activity common to the channels, each state vector was z-standardized across channels by subtracting its mean and dividing by its standard deviation resulting in the z-standardized state vector $\bar{R}_l^{(s)}(i)$. The left panel of figure 12 displays for each channel k the waveform $V_{k,l}^{(s)}(t_j)$ of a representative 180 ms segment of the bandpass filtered ECoG signal. In the right panel, the corresponding spatial distribution of z-standardized RMS amplitudes $\bar{R}_l^{(s)}(i)$ at that time is shown. With the time windows i stepped along the time axis of a single trial (figure 10), the temporal development of the spatial activity distribution described by $\bar{R}_l^{(s)}(i)$ follows a trajectory in an 18-dimensional state space.
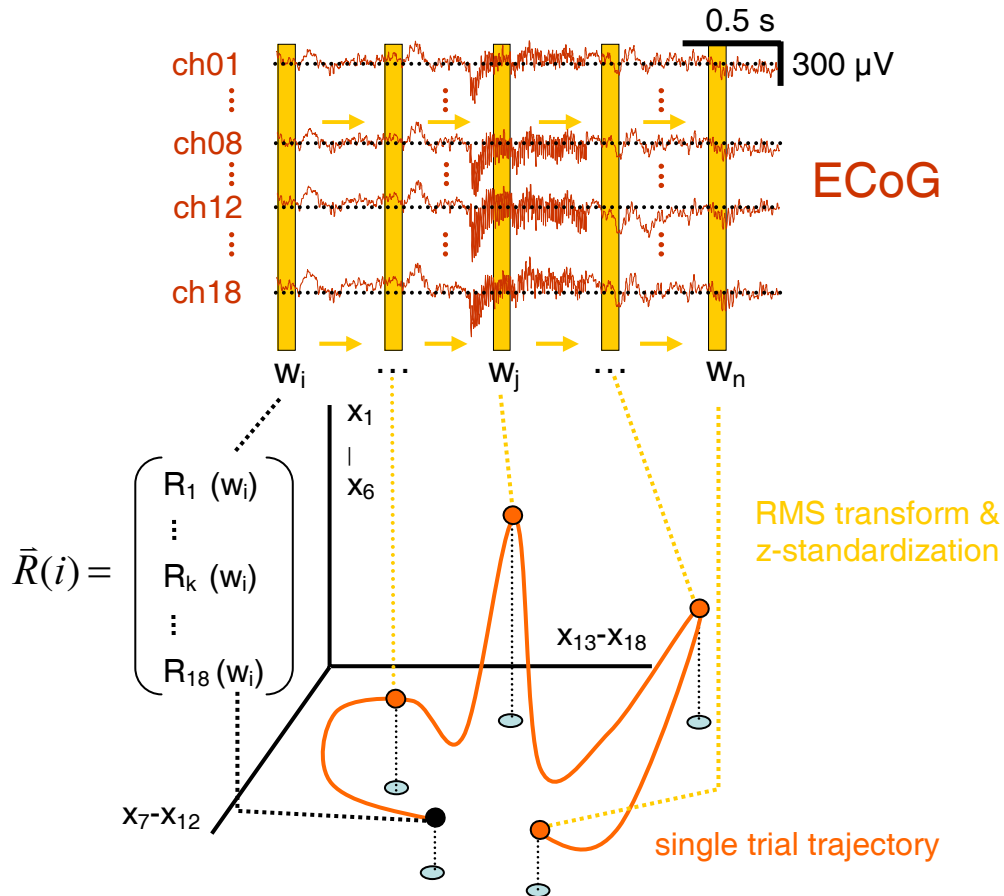
Figure 10: Schematic diagram illustrating the calculation of the spatial distribution of cortical β- and γ-band activity as a function of time in a single trial. Time windows of 180 ms (yellow boxes) were stepped through the digitally bandpass filtered (15 Hz to 80 Hz) ECoG signals (red traces) in 20 ms intervals. The spatial distribution of the mean power of the filtered ECoG signal within each time window wi was obtained from the channel-wise calculation of root mean square (RMS) amplitudes Rk(wi) across each wi. RMS amplitudes were z-standardized across channels and summarized into a state vector, which can be represented as a point in the 18-dimensional (x1-18) signal space. For each trial, describes the relative spatial distribution of signal power developing along a trajectory (orange line) as a function of the 20 ms time steps i.
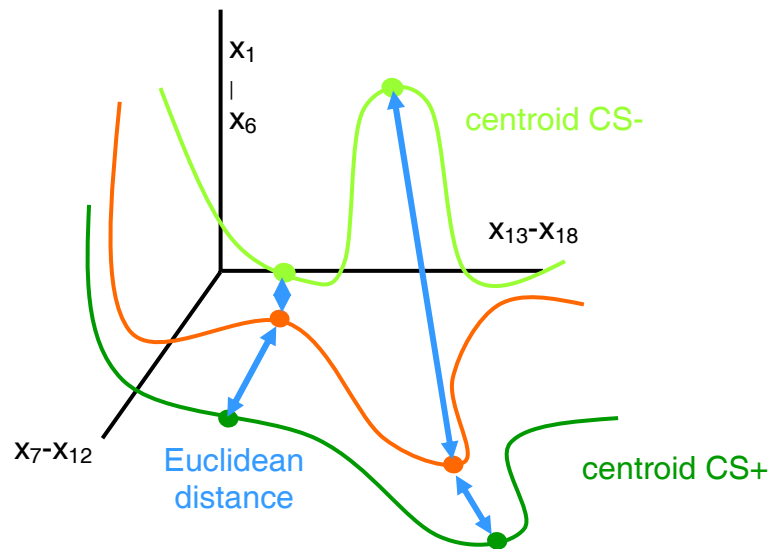
Figure 11: Multivariate classification procedure for sorting spatial cortical activity distributions in the β- and γ-band into the behaviorally relevant stimulus classes (CS+ and CS-) as a function of time. For each single trial, the cortical activity distribution is described as a state vector (see figure 10) developing in time along a trajectory (orange line) in the 18-dimensional signal space (x_{1-18}). A CS+ and a CS- centroid (light and dark green lines) was built from averaging across sets of single trial trajectories taken from each of the corresponding stimulus classes. For each instant in time, state vectors were classified according to the stimulus class of the centroid they were closer to in terms of their Euclidean distance (light blue arrows). Numbers of correctly classified trials were counted for each instant in time across trials and evaluated by a binomial statistics.

For each time step i in a subset of trials s, a series of centroids $\vec{C}^{(s)}(i)$ of the spatial activity distributions was calculated by averaging the trajectories described by the state vectors $\vec{R}_l^{(s)}(i)$ across all trials l belonging to subset s:

$$\vec{C}^{(s)}(i) = \frac{\sum_l^{n_s} \vec{R}_l^{(s)}(i)}{n_s} \qquad \forall\ s \in \{1,2,3,4\}, \quad (5)$$
$$l \in \{1,...,n_s\},$$
$$i \in \{1,...,n_w\},$$

For every time window, Euclidean distances were calculated trial by trial of all state vectors $\vec{R}_l^{(s_a)}(i)$ in the two subsets A to each of the two centroids derived from the subsets CS+$_B$ and CS-$_B$, respectively:

$$D(\vec{C}^{(s_b)}(i), \vec{R}_l^{(s_a)}(i)) = \sqrt{\sum_{k=1}^{18} (C_k^{(s_b)}(i) - R_{k,l}^{(s_a)}(i))^2} \qquad \forall\ s_a \in \{1,3\}, \quad (6)$$
$$s_b \in \{2,4\},$$
$$l \in \{1,...,n_{s_a}\},$$
$$i \in \{1,...,n_w\}$$

with s_a = 1,3 being the running indices of subsets CS+$_A$ and CS-$_A$, s_b = 2,4 the running indices of CS+$_B$ and CS-$_B$, and n_{sa} being the number of trials in the two subsets A.

Based on the Euclidean distances, a state vector $\vec{R}_l^{(s_a)}(i)$ taken from the subsets A was classified as CS+ if it was closer to the centroid CS+$_B$ and as CS- if it was closer to the centroid of CS-$_B$ (figure 11). This classification procedure was repeated by cross-classifying all state vectors from the subsets B with the centroids of the subsets CS+$_A$ and CS-$_A$.

A state vector was classified correctly if it was assigned to the stimulus class actually presented in the trial. After classifying the state vectors of every trial in this way, the number of correctly classified state vectors was summed up over all subsets for each time window i, separately. This resulted in a temporal sequence of numbers of

correctly classified trials. Classification performance was measured as percent correct classification by dividing the number of correctly classified trials by the total number of classified artifact-free trials, which ranged between 94 and 117 of the total number of 120 trials (see subsection 3.4.1.).

Significance of classification was tested against the null hypothesis of randomly sorting the state vectors into the stimulus classes. The probability $p_n(i)$ for obtaining at least the observed number of correctly classified trials $N(i)$ from a total number of trials n by chance ($p = 0.5$) was determined for each time window i using a cumulative binomial distribution:

$$p_n(i) = \sum_{n=N(i)}^{n_0} \binom{n_0}{N(i)} p^n (1-p)^{n_0-n} \qquad \forall\ i \in \{1,...,n_w\} \qquad (7)$$

$$n_0 = \sum_{s=1}^{4} n_s$$

Significant pattern classification was achieved in a time window i, if $p_n(i) < \alpha$ with the significance level α set to 0.05. As no significant classification should occur before stimulus onset, only the time windows after stimulus onset were tested for significant classification. Due to multiple testing, α had to be corrected. As the time windows overlapped, tests were not independent from each other. Therefore, a modified Bonferroni correction (Bortz, 1999, p.260-263) was applied as shown in equation (8).

$$\alpha' = \alpha \Big/ \left(n_t - k_s + 1\right) \qquad (8)$$

with α' being the corrected significance level, n_t the number of time windows used for testing ($n_t = 150$) and k_s the number of time windows from which significant pattern classification was obtained with $\alpha = 0.05$. Spatial cortical activity patterns related to the stimulus classes CS+ and CS- were identified in a time window i by a significant number of correctly classifying spatial activity distributions at that time.
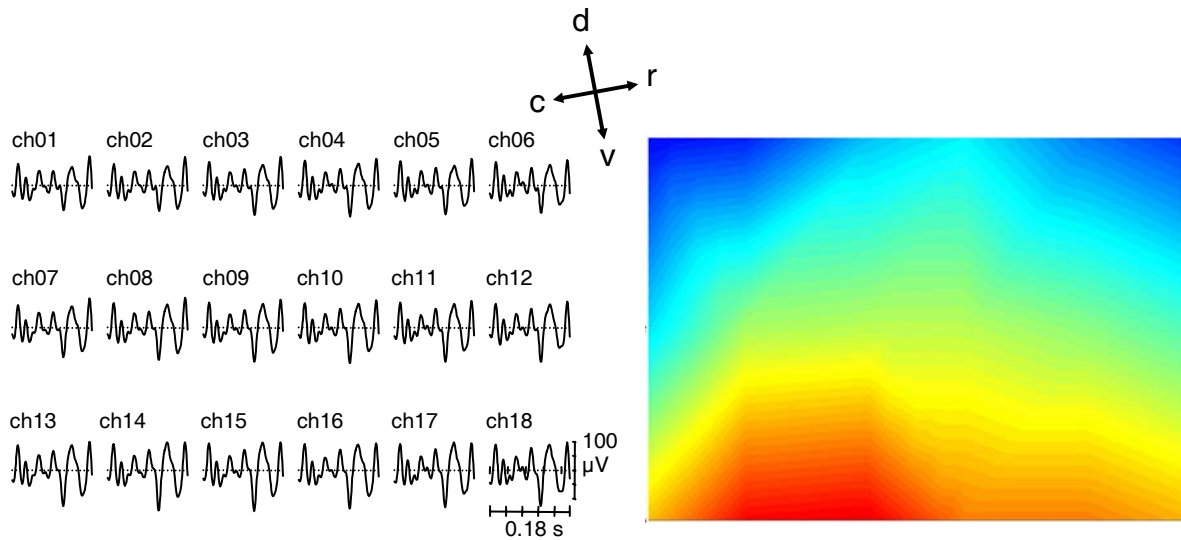
Figure 12: Waveforms and spatial activity distribution of a representative 180 ms segment in the β- and γ-band of the ongoing ECoG (animal 047, session 7, trial 60, 1.14 s to 1.32 s post-stimulus time). ECoG signals were digitally band-pass filtered between 15 Hz and 80 Hz. Signals of the 18 recording channels (ch01 to ch18) are plotted according to the positions of their recording electrodes within the 3x6 epidural surface array (left panel). The spatial distribution of cortical β- and γ-band power was obtained from a root mean square (RMS) transform of the segment followed by a z-standardization across channels (right panel). After interpolation between electrode positions, the spatial distribution of z-standardized RMS amplitudes is displayed in a color plot (high signal power in red, low signal power in blue). Anatomical directions dorsal (d), ventral (v), rostral (r), and caudal (c) are indicated by the orientation cross on top of the figure in reference to the animal.

3.4.5. Correlation analysis of behavioral discrimination performance and ECoG pattern classification performance

To investigate, how the emergence of spatial patterns in the ongoing ECoG relates to the discrimination behavior of the animals, correlation analysis was carried out between behavioral discrimination performance and ECoG pattern classification performance. Discrimination performance was quantified by the discriminability index d' (see subsection 3.3.2.) and classification performance was measured as percent correct classification (see subsection 3.4.4.). Correlation coefficients were calculated over sessions between d' values and maximum percent correct classification values derived from the time between the end of the electrical stimulus and the behavioral response, which was taken as the median of the hit reaction times. This time interval had a length about 1 s on average. In sessions where the animals showed less than

six hit responses, maximum percent correct classification values were selected from a 2 s interval after the end of the electrical stimulus. Only classification time windows in which interference with the stimulus artifact could be excluded were taken into account. As a control for classification at chance level, correlation coefficients were also calculated with maximum correct classification values taken from pre-stimulus time intervals of a length corresponding to the post-stimulus time intervals. Correlation coefficients were averaged across animals by the use of Fisher's z-transform. For every animal, each of the two correlation coefficients was transformed into Fisher's z-values and corrected for the small sample size (n<50) (Sachs, 1992, p.541-542). By this, the distribution of correlation coefficients was approximated to a normal distribution. Correlation coefficients across animals were tested for homogeneity by the use of Fisher's z-values and a χ^2-statistics (Sachs, 1992, p.545-546). As the null hypothesis of homogeneity couldn't be rejected on a significance level of $p < 0.05$, Fisher's z-values were averaged across animals. The two averages were then transformed back to yield a common correlation coefficient for pre- and post-stimulus time intervals, respectively. Limits of significant positive and negative correlation were calculated on a significance level of $\alpha = 0.05$. For this the standard deviation for the Fisher's z-values was estimated (Sachs, 1992, p.541-543) and the range including 95% of the variance around zero was calculated. The upper and lower limit of this range was transformed back into limits of significant positive and negative correlation.

3.4.6. Analysis of the spatial organization of ECoG patterns

The spatial organization of the patterns identified by the classification procedure was analyzed in terms of the spatial location of information relevant for the classification described above. Classification behavior was investigated after removing single recording channels or combinations of channels (vector components) from the state vector (Barrie et al., 1996; Ohl et al., 2003a). For each animal, the fourth consecutive training session, in which the animal showed significant stimulus discrimination (figure 16), was selected for the analysis. The animal had then reached a characteristic phase in its learning history entering the plateau phase its individual learning curve. After removing combinations of $n_r = \{0, 1, 2, \ldots, 17\}$ recording

channels, changes in the ECoG pattern classification performance were studied in the time window from which maximum classification performance after the end of the electrical stimulus was obtained for the complete pattern. For each number of removed channels $n_r = \{2, 3, \ldots, 16\}$, channel removal was repeated 200 times with different combinations of n_r channels drawn randomly out of all the 18 available. Each combination of n_r channels was used only once. For each combination of removed channels, percent correct classification values were determined. The median, the minimum, and the maximum of the 200 percent correct classification values were calculated for each number of removed channels n_r and stored to disk. To identify the vector components, i.e. the electrodes in the recording array, which contributed maximally to a spatial activity pattern identified by the classification procedure, the channel combinations yielding the minimum value of percent correct classification among the 200 removed combinations was determined for each animal and for each number of removed electrodes n_r. For $n_r = \{0, 17\}$, the same analysis was performed using all possible 18 combinations of channel removal.

4. Results

4.1. Effects of electrode implantation and chronic intracortical microstimulation on the histological morphology

By visual inspection of the Nissl stained sections, local agglomerates of cells with small, oval shaped nuclei and barely visible cell bodies were found at the sites of implantation of the stimulation electrodes within right temporal cortex (figure 13, 14, and 15). Sometimes, "fingers" of increased cell density protruded about 200 µm from the agglomerates into the surrounding tissue giving them a star-like appearance (figure 13, stimulation electrodes S1 and S2). These agglomerates of cells were often surrounded by a thin rim of reduced neuronal cell density, about 50 µm in thickness (figure 13, stimulation electrode S1). Often, the density of small, oval shaped cells was also slightly increased in the tissue surrounding the agglomerates. However, normal appearing neurons were always found close to the agglomerates. In some cases, a small lumen was found at the center of the agglomerate (figure 14, stimulation electrode S2).

Two of these local histological patterns lying between 0.60 mm and 1.00 mm apart, were found within each right temporal cortex of all four animals analyzed with Nissl staining. In three animals the agglomerates of cells could be traced over consecutive sections extending between 0.72 mm and 1.40 mm in dorsoventral direction. Proceeding from dorsal to ventral sections the observed histological pattern became more pronounced, i.e. the agglomerates grew larger, and their cell densities increased, and then vanished abruptly. In one animal (047), local agglomerates of cells could be identified clearly in only one section. In the 3 or 4 most ventral sections, in which local agglomerates of cells were found, their position corresponded well to the sites where the tips of the stimulation electrodes were expectedly located due to the implantation procedure (see section 2.3.). Taking all these observations together, the described histological pattern can be attributed to lesions induced at the sites of the implanted electrodes becoming more pronounced at the electrode tips.
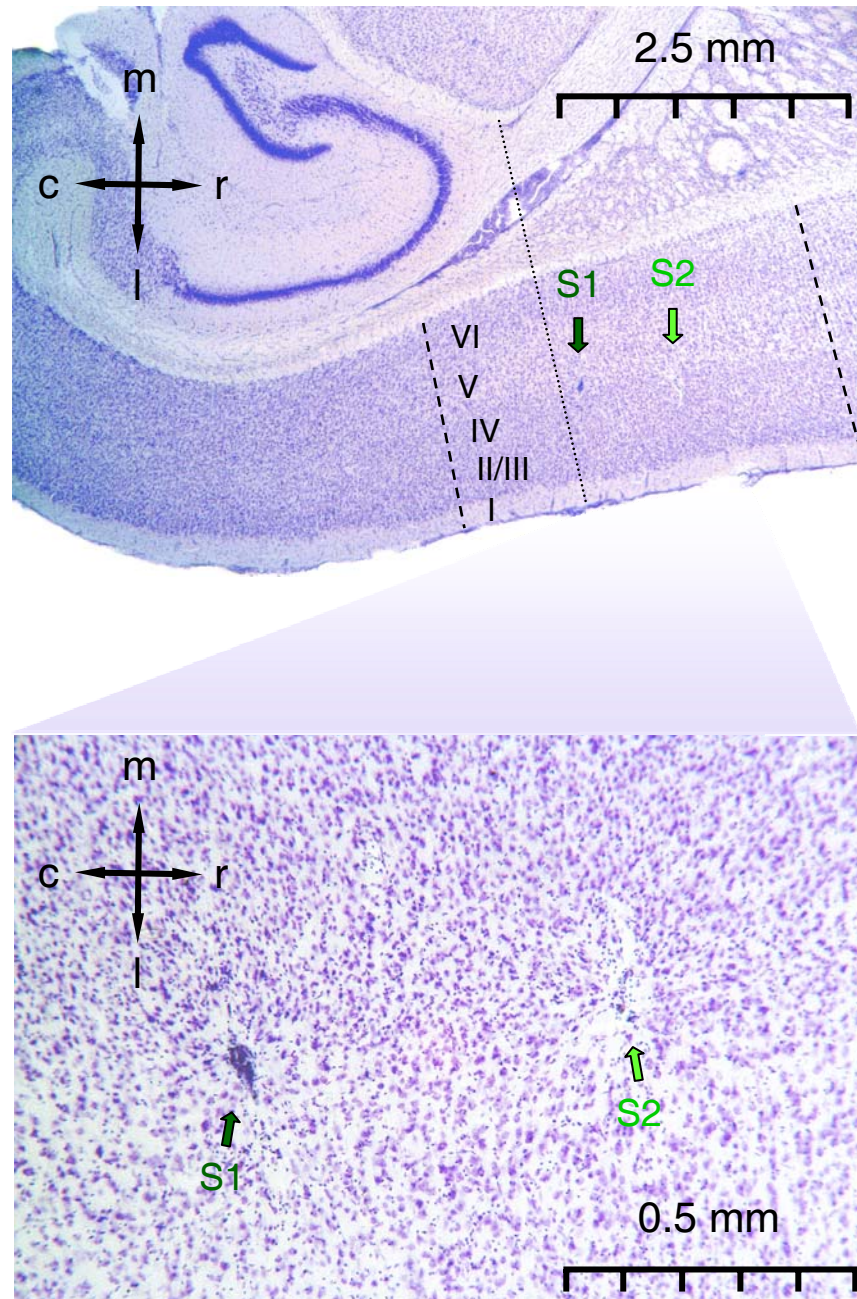
Figure 13: Digital photographs of a Nissl stained horizontal 40µm-section from right temporal cortex of animal 035 taken at a low (upper panel) and a high (lower panel) level of magnification (see scale bar). Lesions at the tips of the implanted stimulation electrodes S1 and S2 are marked by the green arrows. Positions of the tips of the stimulation electrodes were determined by the centers of the lesions relative to the cortical surface, the cortical layering (I to VI) and a hippocampal reference line (dotted line) indicating the 1kHz isofrequency contour in AI. The rostrocaudal extent of the auditory core fields AI and AAF, which were determined by their pronounced layer IV, are marked by dashed lines.
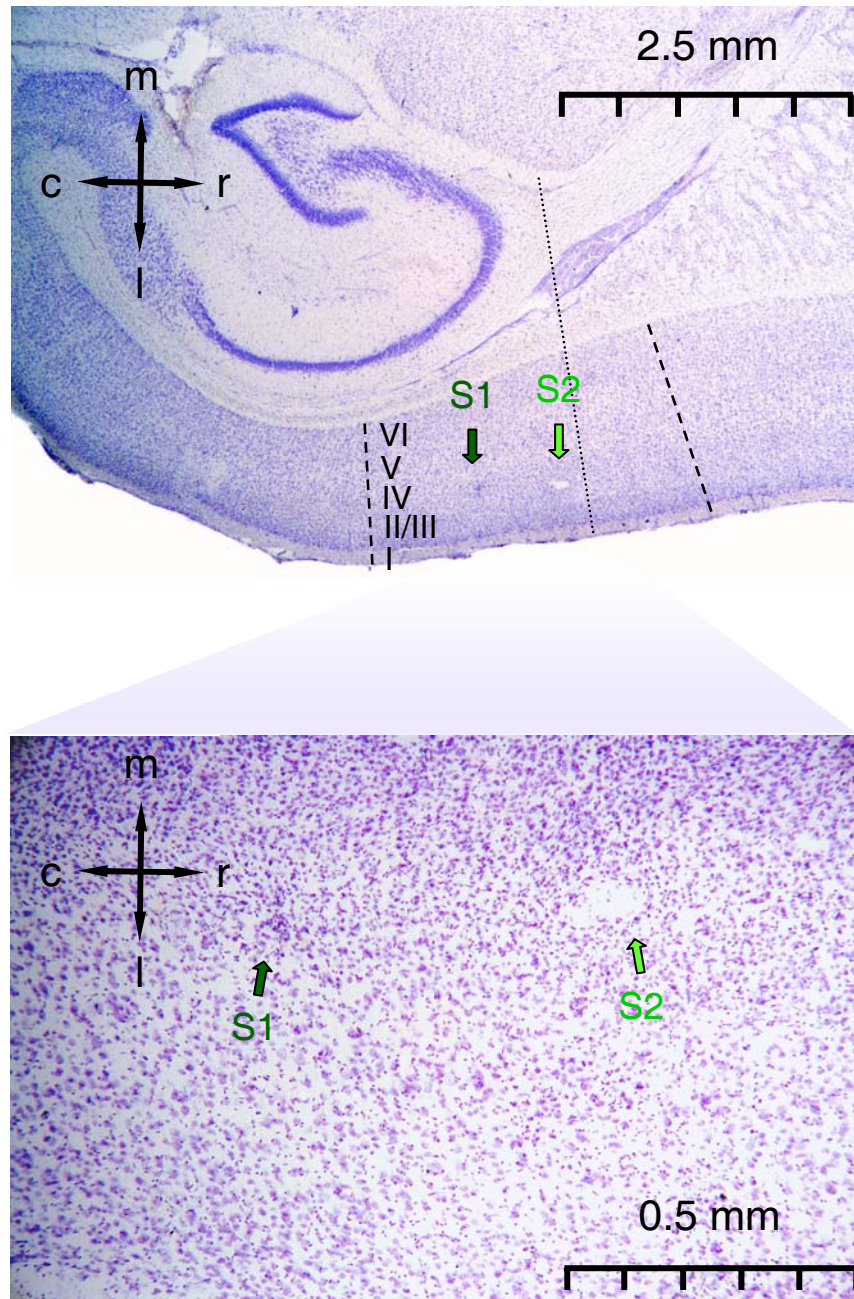
Figure 14: Digital photographs of a Nissl stained horizontal 40µm-section from right temporal cortex of animal 047 taken at a low (upper panel) and a high (lower panel) level of magnification (see scale bar). Lesions at the tips of the implanted stimulation electrodes S1 and S2 are marked by the green arrows. Positions of the tips of the stimulation electrodes were determined by the centers of the lesions relative to the cortical surface, the cortical layering (I to VI) and a hippocampal reference line (dotted line) indicating the 1kHz isofrequency contour in AI. The rostrocaudal extent of the auditory core fields AI and AAF, which were determined by their pronounced layer IV, are marked by dashed lines.

Due to their morphology, the cells making up the histological pattern appeared to be glial cells, most likely astrocytes according to the oval shape of their nuclei. It is well known that glial cells form a local sheath around foreign material implanted into grey cortical matter, a so called glial scar. The central lumen, sometimes observed at the lesion site, probably marked the electrode track. As the brain tissue was not fixated with glutaraldehyde prior to electrode explantation, the electrode track probably collapsed with the removal of the stimulation electrodes in most of the Nissl stained sections.

In the thallium stained sections of animal 046, which was perfused with glutaraldehyde prior to electrode explantation, the electrode tracks could be easily identified. The central lumina found at each lesion site were similar to the shape and size of the implanted microwire and could be dorsoventrally aligned over several consecutive sections (figure 15, animal 046).

At some implantation sites the tissue was slightly ruptured (figure 13, stimulation electrode S2). The tissue rupturing could have occurred either with implantation or, as it is well known that cells can adhere to the electrode material, with electrode explantation. The thin rim of reduced neuronal cell density around the lesion probably indicates local cell death, as it can be caused by a traumatic lesion or intensive electrical stimulation close to the tip of the stimulation electrode.

Lesion size defined as the radius of the smallest circle which could be drawn around the region affected by the lesion (table 3) varied between 0.10 and 0.21 mm. Though not investigated systematically, no relationship between lesion size and the amount of current used for the electrical pulses (table 1), the time during which the implant was carried, and the amount of electrical stimulation expressed by the number of training sessions during which ICMS was applied could be determined (table 3). At distances more than 0.21 mm away from the centers of the lesions, no abnormalities in the Nissl stained sections could be found. As far as it could be determined from Nissl staining, there were no histological signs of generalized inflammation or toxicity like increased densities of microglial cells or the appearance of large phagocytotic cells. In conclusion, histology showed only local effects of lesioning like glial scar formation and local cell death. These effects were more pronounced at the electrode tips.

In animal 035 and 047, right temporal cortex seemed to be slightly flattened (figure 13 and 14). This could be eventually due to the pressure imposed on the cortex by the chronically implanted 3x6 epidural surface array. However no histological abnormalities were found within the cortex beneath this flattened region.

	max. lesion radius [mm]		implantation time [days]	amount of electrical stimulation [# of sessions]
animal	S1	S2	S1 & S2	S1 & S2
035	0.19	0.17	43	19
036	n.a.	n.a.	22	9
037	0.14	0.13	30	10
038	0.21	0.19	25	7
046	0.17	0.13	65	19
047	0.11	0.10	20	7

Table 3: Size of lesions induced by electrode implantation and/or intracortical microstimulation (ICMS). Lesion size around the tip of each stimulation electrode (S1 and S2), implantation time from the day of surgical preparation to the day of histological preparation, and amount of electrical stimulation expressed by the number of training sessions during which ICMS was applied are listed for the animals which were histologically analyzed. Lesion size was defined as the radius of the smallest circle which could be drawn around the region affected by the lesion. Data are not available (n.a.) for animal 036 due to a failure of histological processing.

4.2. Electrode positioning

The centers of each of the two lesions found in one of the three most ventral sections were taken as markers for the location of the tips of the stimulation electrodes. All lesions marking electrode tips were located in the depth of the right temporal cortex (figure 13 and 14). In four animals (035, 037, 038, and 047), they were all close in radial proximity to a continuous band of densely packed cells in the upper third of the lateromedial extent of the temporal cortex. This band of densely packed cells

corresponded well to a coniocortical pattern with its distinctive layer IV found in the core fields of the auditory cortex of the Mongolian gerbil, AI and AAF (Budinger et al., 2000a). The band of densely packed cells in layer IV extended about 4 mm in rostrocaudal direction. In all analyzed animals, lesions marking the electrode tips were positioned centrally or in the caudal half along the rostrocaudal axis of this band. Thus, the electrode tips were apparently located in vicinity of layer IV within the core fields of auditory cortex. In animal 046, which was analyzed with the thallium imaging technique (Goldschmidt et al., 2004), lesions marking electrode tips were found at a greater radial depth below layer IV, close to the border of layer V and VI. Due to their rostrocaudal position they located within central coniocortex.

In order to determine the electrode positions more precisely, quantitative measurements were made referring the locations of lesions at the electrode tips to cortical structures and anatomical landmarks. The cortical depth of the centers of each lesion was measured relative to the cortical surface. According to the values in table 4 all the lesions at the electrode tips were found at depths between 0.40 mm and 1.07 mm relative to the cortical surface. The lateral border of layer IV with layer V was found at depths between 0.27 mm and 0.60 mm and the medial border with layer V at depths between 0.50 mm and 0.81 mm. Comparing the depths of the lesions with the depths of the lateral and medial borders of layer IV at every lesion site, all lesions were located within a range between 0.02 mm lateral and 0.04 mm medial to layer IV (table 4), except in animal 046 where the lesions were found at a greater depth, 0.32 mm and 0.42 mm medial to layer IV, approximately at the border between layer V and VI.

With the exception of animal 037, the distance between the electrode tips was always between 0.6 mm and 0.7 mm, as it was expected from the design of the stimulation electrode array. In animal 037 the distance amounted to 1 mm and thus was larger than expected (table 4).

The dorsoventral positions of the electrode tips were quantified relative to the dorsal roof of the caudate putamen (Scheich et al., 1993; Budinger et al., 2000a). In three animals (035, 037 and 047), lesions at the electrode tips were found between 0.72 mm and 0.88 mm ventral to that landmark. In the other two analyzed animals (038 and 046), lesions were found much more ventral at 1.49 mm and 2.04 mm relative to the dorsal roof of the caudate putamen.

animal	inter-elec.-dist. [mm]	d.-v.-pos. [mm]	r.-c.-pos. [mm]		cortical depth [mm]		layer IV lateral depth [mm]		layer IV medial depth [mm]	
			S1	S2	S1	S2	S1	S2	S1	S2
035	0.70	0.72	0.24	1.02	0.83	0.71	0.60	0.54	0.80	0.81
036	n.a.	n.a.	n.a.	n.a.	n.a.	n.a.	n.a.	n.a.	n.a.	n.a.
037	1.01	0.88	-0.13	0.96	0.76	0.36	0.58	0.37	0.80	0.56
038	0.64	2.04	0.23	0.95	0.67	0.63	0.47	0.42	0.63	0.59
046	0.63	1.49	-0.1	0.76	1.00	1.07	0.38	0.40	0.68	0.65
047	0.61	0.72	-0.78	-0.16	0.40	0.40	0.36	0.42	0.50	0.58

Table 4: Positioning of stimulation electrodes S1 and S2 within temporal cortex determined from lesions found in the histological sections. Dorsoventral positions (d.-v.-pos.) were measured relative to the roof of the caudate putamen. Rostrocaudal positions were measured relative to a hippocampal reference line corresponding to the 1 kHz isofrequency contour in primary auditory cortex AI (Scheich et al., 1993). Lateromedial positions (cortical depth) were determined perpendicular to the cortical surface and compared to the depth of the lateral and medial borders of cortical layer IV. Data are not available (n.a.) for animal 036 due to a failure of histological processing.

The rostrocaudal positions of the electrode tips were determined relative to the rostral pole of the ventral hippocampus. As has been previously reported, the dorsal part of field AI extends from about 1 mm caudal to about 1 mm rostral to the hippocampal reference with a progression of the frequency representation from caudal to rostral. According to these studies, the field AAF extends from about 1 mm rostral to about 3 mm rostral to the hippocampal reference with the tonotopic gradient in rostral-to-caudal direction with a common high-frequency border between AI and AAF.

In four animals (035, 037, 038 and 046), the caudal electrodes S1 were located close to the hippocampal reference line functionally corresponding to the mid-frequency region of AI around the 1.5 kHz isofrequency contour (Scheich et al., 1993). The

rostral electrode tips in these animals were located between 0.76 mm and 1.02 mm rostral to the hippocampal reference close to the high-frequency border between AI and AAF. In animal 047 the caudal electrode tip was located 0.78 mm caudal and the rostral electrode tip 0.16 mm caudal to the hippocampal reference line. The caudal stimulation electrode was therefore positioned in the low- and the rostral electrode in the mid-frequency range around 1.5 kHz of AI.

Thus, in three animal (035, 037, and 047), the stimulation electrodes were located within AI, close to the input layer IV. Rostral stimulation electrodes were often positioned near the common high frequency border of AI and AAF. In the two other analyzed animals (038 and 046), lesions marking the tips of the stimulation electrodes were found at a greater ventral offset along the dorsoventral axis and in one of the two animal (046) also at a greater radial depth close to the border of layer V and VI.

It was not possible to determine the position of the 3x6 epidural surface array from histological analysis, but the relative positioning of the stimulation electrodes to the epidural surface array was visually inspected after explantation showing that most of the stimulation electrodes were located about 0.5 mm medial to the surface array beneath its rostral part and close to its ventral edge.

4.3. Effective current spread of ICMS

According to the amount of current used for ICMS, the effective current spread, i.e. the radius of a sphere around the stimulation site containing neurons of a certain threshold being activated by a single electrical current pulse (cathodal first, 200 µs/phase), was calculated for each stimulation electrode for high- and low-threshold cortical neurons, respectively (see section 3.2.). As can be taken from table 1, effective current-spread ranged from 0.12 to 0.14 mm for high- and from 0.43 to 0.51 mm for low-threshold neurons (figure 15). On the basis of an approximated mean distance between stimulation electrodes of about 0.7 mm in the present study, a spatial overlap resulted between the two populations of low-threshold neurons activated by a single current pulse delivered either through stimulation electrodes S1 or S2. No such overlap resulted for high-threshold neuron populations.
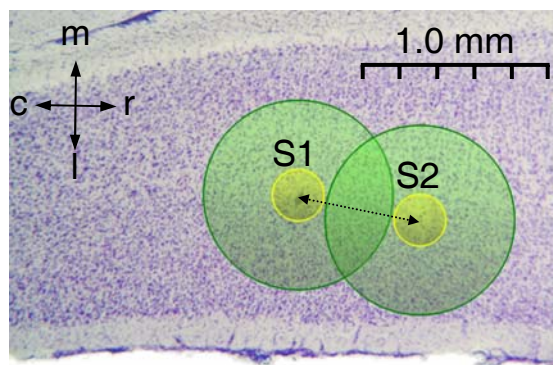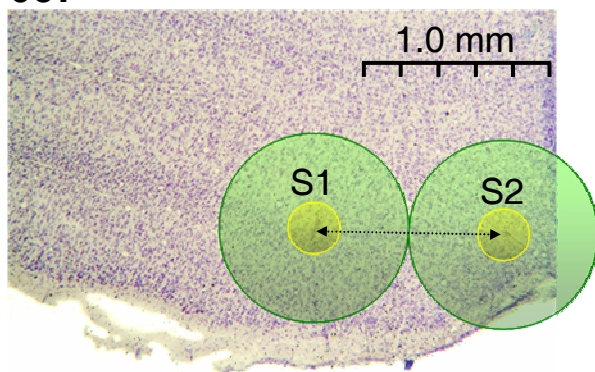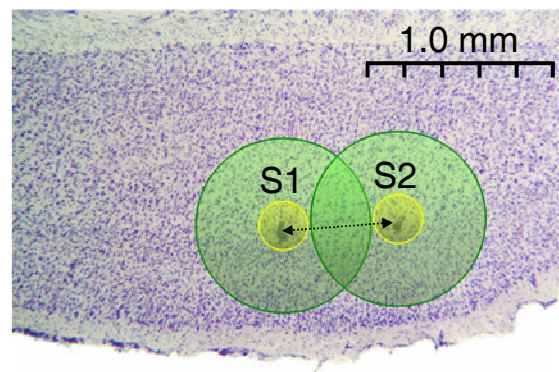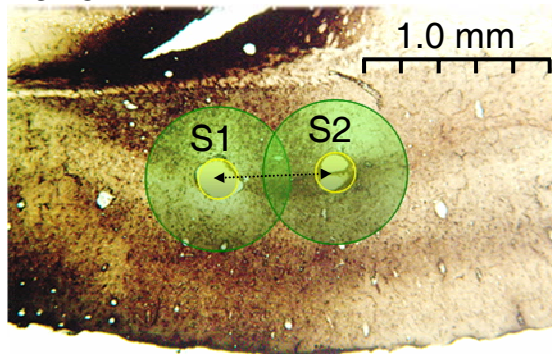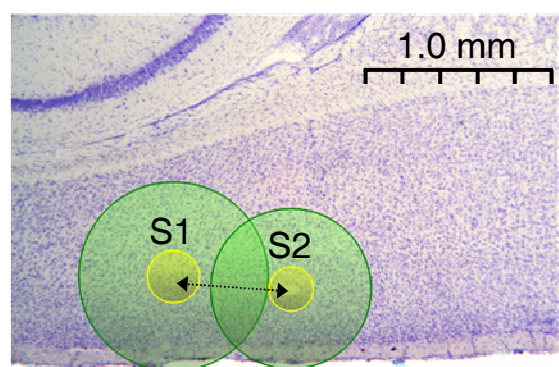
Figure 15: Minimum (yellow disks) and maximum (green disks) effective current spread of ICMS at each of the stimulation electrodes S1 and S2 illustrated within digital photographs of Nissl (035, 037, 038 and 047) or Thallium (046) stained sections showing lesions which indicate the positions of the tips of the stimulation electrodes in the depth of primary auditory cortex (AI). Histological processing failed in animal 036.

4.4. Discrimination learning

Figure 16 shows individual learning curves for all animals. In the four animals 035, 036, 037, and 047, hit-rates were below 0.2 in the first sessions of the training and increased to values above 0.5 within one or two sessions beginning with the third or fourth session. After the steepest increase, the increment of the hit-rates became smaller finally reaching levels around 0.8 as the learning curves entered a plateau phase. Sometimes a small drop of the hit-rate was observed in later sessions, for example at session 6 in animals 035 and 036. However, already within the next session, the hit-rate returned to or even exceeded its former value. In the other two animals (038 and 046) the steepest increase of the hit response curve was found between the fourth and the fifth session, with hit-rates increasing from below 0.2 to above 0.5 within one session. False-alarm-rates, on the other hand, either stayed below 0.2 (animals 038, 046 and 047) or followed a biphasic rise-fall time course (animals 035, 036 and 037) reaching a maximum between 0.2 and 0.4 in the fifth or sixth session. Significant discrimination performance, i.e. hit-rates becoming significantly different from false-alarm-rates (χ^2, p < 0.05), was achieved by the animals 035, 036, 037, and 047 from the fourth session on. After the animals had shown significant discrimination performance in four consecutive sessions, their learning curves entered a plateau phase.

In the other two animals (038 and 046), significant discrimination performance was reached from the fifth session on. Altogether, animals 038 and 046 showed a slightly different learning dynamics. The increase of hit-rates was delayed in these two animals compared to the four other animals, and continuing significant discrimination performance was reached at later training sessions.

The mean learning curve averaged across all six animals (figure 18A) showed a steep, monotonic increase of the hit-rate above 0.6 between the third and the fifth session. The mean false-alarm-rate follows a biphasic rise-fall time course always staying below 0.2. It increased slightly from the third session on, reached its maximum at the fifth session, and then decreased again towards zero. Standard errors of the mean ranged between 0.01 and 0.1. From the fourth session on, hit-rates clearly exceeded the false-alarm-rates both differing significantly from each other (Wilcoxon, p < 0.05).
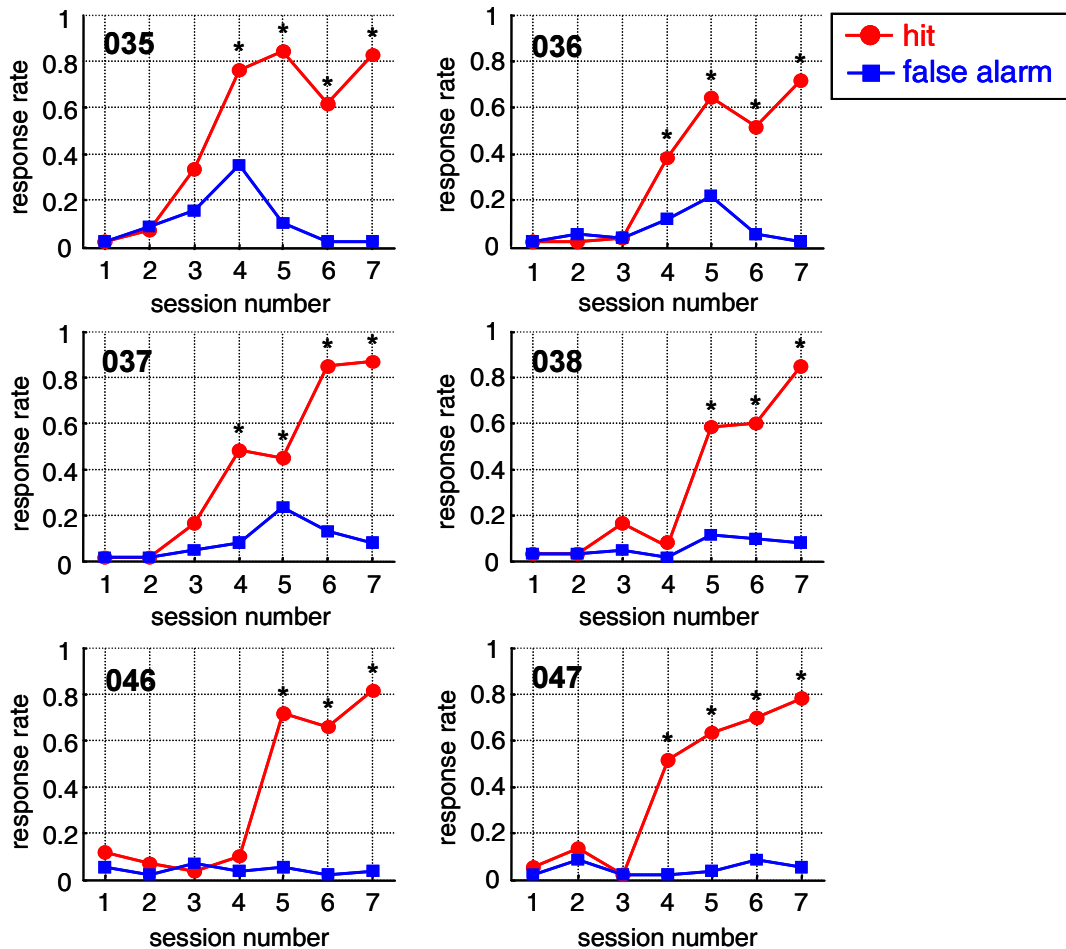
Figure 16: Individual learning curves for all six animals. Hit-rates (red circles) and false-alarm-rates (blue squares) are plotted over training sessions. Significant differences between hit- and false-alarm-rates (two-sided χ^2-statistics, P < 0.05) are marked by asterisks (*).

Discrimination performance was quantified by the discriminability index d' (see subsection 3.3.2.), which is plotted over sessions for each animal in figure 17. In all six animals d' was smaller than 1.0 for the first three sessions and sometimes even negative, e.g. in session two of animal 036. Discriminability index d' increased from the second (animals 035, 036, and 037), the third (animals 046 and 047), and the fourth session (animals 038) on, finally reaching values above 2 in all animals. Occasionally d' dropped about 1.0 for a single session, but reached or even exceeded its prior levels within the next session (animal 036, session 6). In two animals (046 and 047) the curve of d' over session had a sigmoid shape approaching an asymptote of about 2.5 within the last three sessions. In the other four animals d' further increased monotonically over the last sessions reaching values between 2.4 and 3.4.
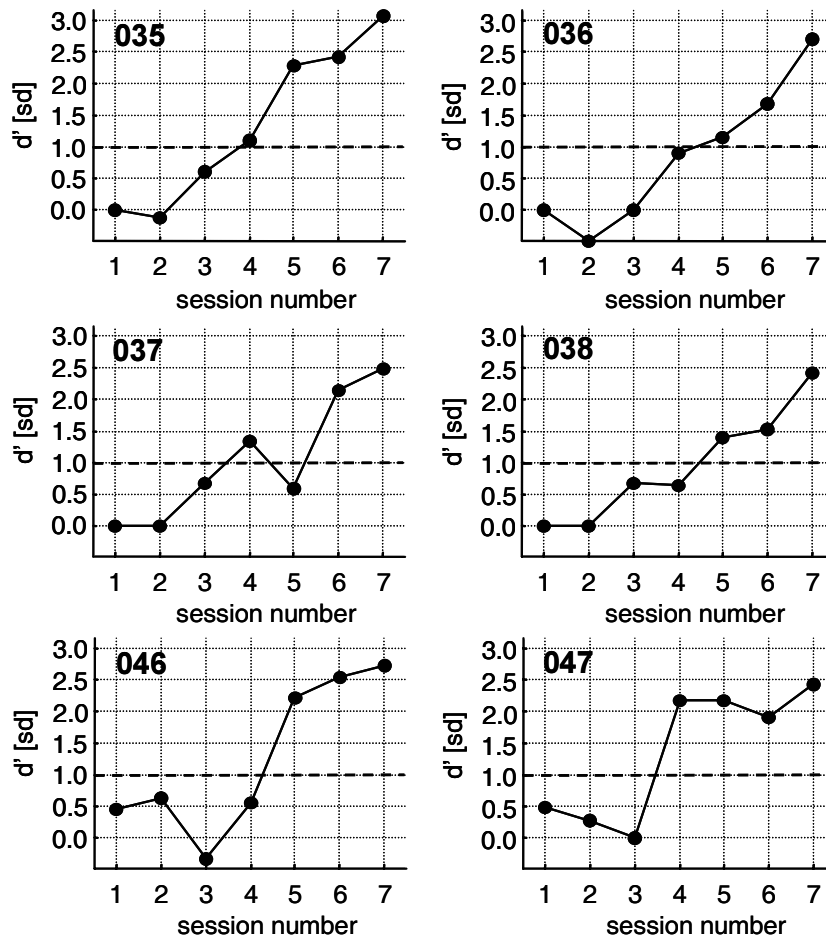
Figure 17: Discrimination performance quantified by the discriminability index d'
plotted over training sessions for each animal. Values of d' larger than one indicate a
significant discrimination performance.

In figure 18B d' values averaged across animals (n=6) are plotted over sessions. The
mean d' curve appeared to be sigmoid, although it terminated before approaching its
upper horizontal asymptote. For the first three sessions, mean d' values stayed
below 0.5. Then d' increased monotonically towards 2.7 with its steepest part
between the third and the fourth session. Significant differences over sessions were
found by testing with the Kruskall-Wallis H test (p<0.05). Post hoc testing revealed
that differences were significant between each one of the first two and each one of
the last two sessions and between the third and the seventh session. This indicates
that the steepest increase of d' occurred between the third and the sixth session.

As shown in figure 19 (upper panel), in animal 035 the hit-rate slightly increased from
0.5 to about 0.7 over sessions. The false-alarm-rate of about 0.8 dropped quickly
towards zero from the second session on. From the third session on, the hit-rate was
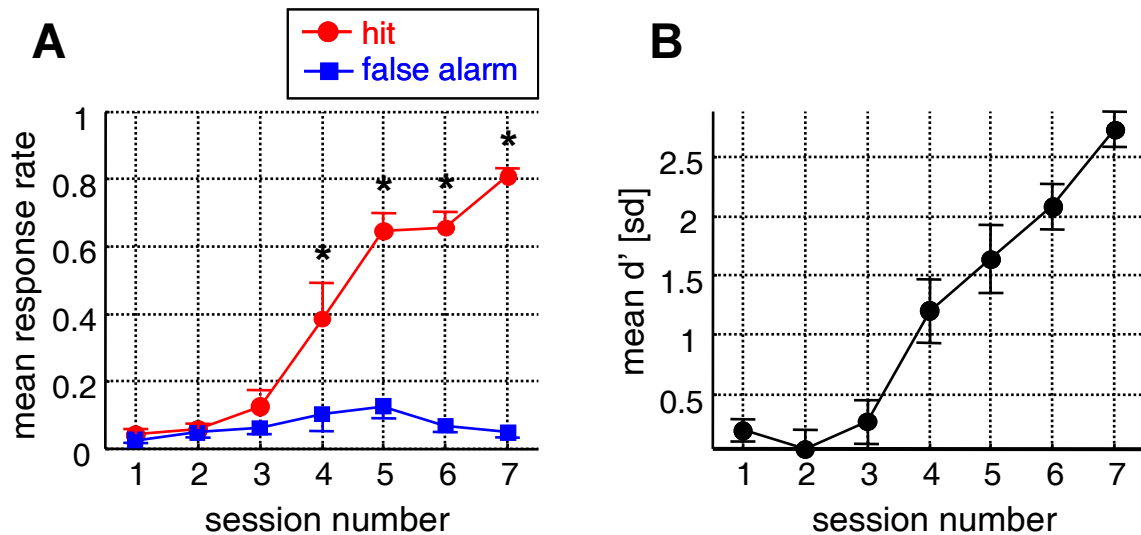
Figure 18: Mean discrimination performance over training sessions averaged across animals (n=6).

(A) Mean and standard errors of learning curves across animals. Significant differences (two-sided Wilcoxon signed rank test, p <0.05) between hit-rates (red circles) and false-alarm-rates (blue squares) are marked by asterisks (*).

(B) Mean and standard errors of discrimination performance over sessions measured as discriminability index d' across animals. Values of d' larger than one indicate a significant discrimination performance.

larger than the false-alarm-rate, and both differed significantly from each other (χ^2, p<0.05). In animal 047 (figure 19, lower panel) the hit-rate increased monotonically from below 0.1 in the first session after the reversal reaching a level around 0.7 from the seventh session on. From the first to the fifth session the false-alarm-rate fell from 0.4 towards zero. Afterwards, it increased again reaching the level of the hit-rates. It covaried with the hit-rate over sessions 7 to 9. Then it dropped towards zero again. Hit- and false-alarm-rates differed significantly (χ^2, p<0.05) in session 4 and 5 and from session 10 to 12 with hit-rates being larger than false-alarm rates. Thus, both animals achieved significant discrimination performance over at least three consecutive sessions indicating that the animals could make use of both stimuli. This suggests that that animals discriminated between the two stimuli and did not simply solve the task by detecting one stimulus, but not the other.

Marked behavioral differences were found between the animals in the first two sessions after the contingency reversal. Animal 035 showed a high rate of GO-responses to both stimuli, whereas the response rates to CS+ and CS- were low in animal 046. By comparing the last session before contingency reversal (session 7

in figure 16) with the first session after the reversal (figure 19, session 1), one can see that animal 035 largely increased its response rate to the stimulus which changed its meaning from CS+ to CS- already in the first session without much further increase in the following sessions. At the same time, the response rate to the stimulus changing from CS+ to CS- remained at a high level for the first two sessions after the reversal decreasing monotonically afterwards. On the other hand, in animal 046, the response rate to the stimulus changing its meaning from CS+ to CS- largely decreased within the first session. The response rates to this stimulus were found about the same level in the last session before and the first session after the contingency reversal, then increasing monotonically over sessions.
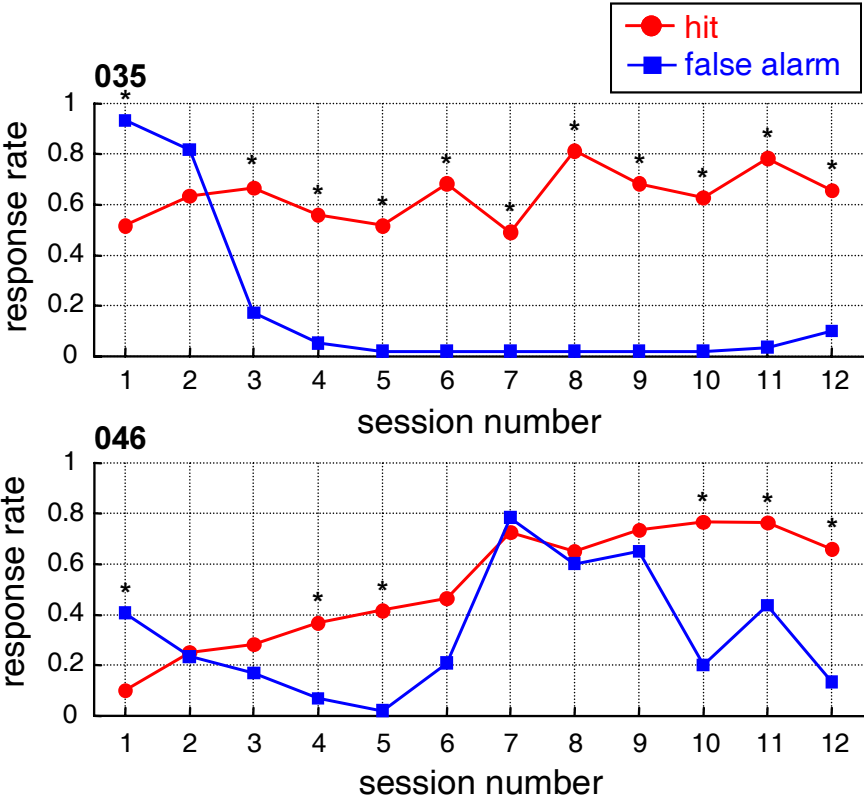
Figure 19: Individual learning curves from two animals (035 and 047) after a contingency reversal. Hit rates (red circles) and false alarm rates (blue squares) are ploted over training sessions. Here the CS- from the first block of training was presented as CS+ and the former CS+ as CS-. Significant differences between hit- and false-alarm rates (two-sided χ^2-statistics, $P < 0.05$) are marked by asterisks (*).

In summary, the results show that the animals learnt to discriminate intracortical microstimulation at two different sites along the tonotopic gradient of AI within four or five sessions of training. In two animals, discrimination learning seemed to be slightly delayed.

4.5. Electrically evoked potentials

For the investigation of the interaction between ongoing cortical dynamics and intracortical microstimulation (ICMS), it is also important to characterize the temporal and spatial specificity of input imposed onto the ongoing cortical activity by the electrical stimuli. Succeeding the direct excitation of neural elements within the spatial range of the effective current spread (see section 4.3.), neural populations are activated transsynaptically. This transsynaptic activation is reflected in the evoked potentials derived from the ECoG recordings by temporal averaging. Evoked potentials were analyzed in response to single current pulses during a test measurement preceding training and in response to trains of current pulses applied as CS+ and CS- during training. Temporal ensembles averages (TEAs) were calculated from high-pass filtered (3 Hz cutoff-frequency) and z-standardized ECoG signals channel-wise, which preserved spatial information from the recording electrodes (figure 21 and 27). Also, temporal ensemble averages were calculated after spatial ensemble averaging across channels, so called temporal and spatial ensemble averages (TSEAs, figure 20, 25, and 26). In particular, segments of the ECoG signals or the spatial ensemble averages were averaged across stimulus repetitions of the test measurement or separately across CS+ and CS- trials of a training session in reference to stimulus onset. Waveforms occurring in the TSEAs and the TEAs were characterized by their peaks in terms of amplitude, latency, and peak width at 50 % of the maximum amplitude. TSEAs and TEAs were also used to assess electrical stimulus artifacts seen with ICMS.

4.5.1. Electrical stimulus artifacts

Current pulses delivered through the stimulation electrodes caused stimulus artifacts in the recordings. In the TEAs and the TSEAs, electrical stimulus artifacts could not be separated from the physiological response on objective grounds. From the TSEAs and the TEAs in figure 20 and 21, a large negative peak can be seen at the time of the delivery of each current pulse (t=0). The negative peak had a width of about 2 ms and was invariantly followed by a slower and smaller positive deflection with a peak latency of about 5 ms and a peak width of about 5 ms returning to zero at about 7 ms after stimulus delivery. Already by its temporal characteristics (dominant spectral energy > 100 Hz), this waveform was considered as an electrical stimulus artifact, because it was assumed that contributions of the evoked potential are found only at frequencies lower than 100 Hz. Nevertheless, it cannot be excluded that unobservable early waves of the evoked potential have contributed to the the artifact peaks.

The same biphasic waveform was also seen with each electrical current pulse of the pulse trains presented during the training procedure (figure 25, 26, and 27). At each time when a current pulse was delivered this artifact waveform was superimposed onto a slower wave, which probably reflected evoked physiological activity. Although the amplitudes of the electrical stimulus artifact varied considerably between pulses, recording sessions, and animals, the artifact waveform itself was highly invariant in this respect. It neither changed with different amounts of currents used for ICMS, nor from pulse to pulse in a train. This invariance makes it rather unlikely that this waveform originated from physiological activity.

The time after the stimulus which must be considered affected by the artifact was always less then 10 ms with a single current pulse. The stimulus artifact caused by a train of current pulses consisted of a train of biphasic artifact-waveforms affecting the recording between 0.00 s and 0.61 s after stimulus onset. By digital filtering with an anti-causal filter kernel of order 300, the interval possibly affected by the artifact was extended to 0.15 s pre- and 0.76 s post-stimulus time. As expected, digital filtering, i.e. high-pass filtering at 3 Hz or bandpass filtering between 15 Hz and 80 Hz, introduced small ripples to the signals 0.15 s before the onset and 0.15 s after the offset of the current pulse train (figure 25, 26, and 27).

4.5.2. Potentials evoked by single electrical current pulses

Characteristic evoked potentials in response to stimulation with single current pulses were found in the TSEAs and TEAs at each stimulation electrode of five animals (035, 036, 037, 038, and 047), whereas in animal 046 electrically evoked potentials were small in amplitude and could be hardly separated from the background activity. As the electrical stimulus artifact lasted for about 10 ms, evoked potentials could not be analyzed for latencies much shorter than 10 ms. After the electrical stimulus artifact, a strong negative deflection occurred in all of the temporal ensemble averages of the five animals with a peak latency of about 12 ms (figure 20 and 21)[14]. The average peak amplitude of this short latency negative wave was between 2 and 4 standard deviations below the pre-stimulus baseline (see examples in figure 20). Temporal peak width was about 12 ms at 50 % of the maximum peak amplitude.

The peak amplitude of the short latency negative wave varied across electrodes in the 3x6 array. The maximum amplitudes were expectedly found around the site of electrical stimulation. For example, figure 21 shows that both the artifact and the negative wave evoked at the caudal stimulation electrode (S1) had their maximum peak values at more caudal positions compared to the artifact and the negative peak evoked at the rostral stimulation electrode (S2). Figure 22 and 23 display the topography of the short latency negative peak. The peak amplitude at each recording channel was expressed as percent of the maximum peak amplitude across recording channels for each animal and condition. Percent maximum amplitudes at the electrode positions corresponding to the recording channels were spatially interpolated.

In figure 22 and 23, the resulting spatial distributions of the normalized peak amplitude of the short latency negative wave are plotted as a color map over the area covered by the 3x6 epidural surface array. In most cases, a single focal maximum was found in the spatial distribution of the negative peak amplitude (figure 22 and 23). The position of the spatial peak maximum in these cases was in accordance with the position of the stimulating electrode relative to the position of 3x6 epidural surface array, as it was determined by visual inspection after explantation of the electrode arrays (see section 4.2.). Also, the distance between the spatial activity focus evoked

at stimulation electrode S1 and the activity focus evoked at S2 corresponded to the interelectrode distance of about 0.7 mm. The spatial extent of the focal activation was roughly determined by the radius of the 50 % isocontour in the spatial distribution of the normalized peak amplitude, which ranged between 0.6 mm and 1.8 mm and often exceeded the dimensions of the array. Accordingly, there often was a considerable spatial overlap between focal activity evoked at stimulation sites S1 and S2. In two cases (S2 in animal 036, S1 in animal 046) the topography of the short latency negative peak displayed two foci of activation distributed along the rostrocaudal axis at locations that could not be matched to the positions of the stimulation electrodes.
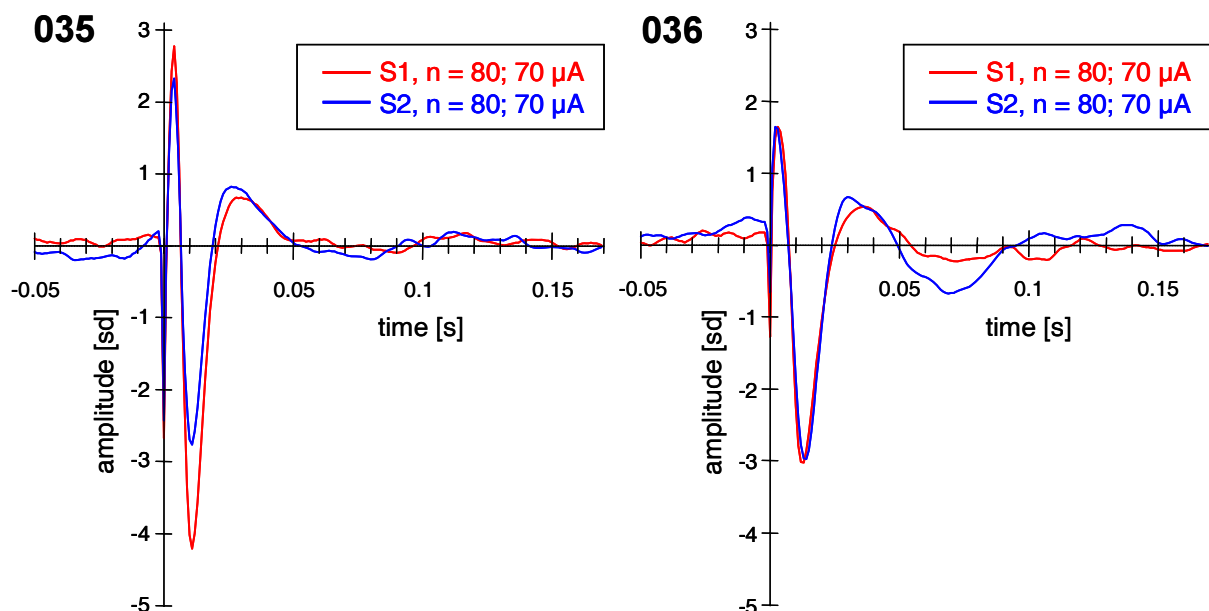
Figure 20: Typical examples of responses evoked by single electrical current pulses delivered through stimulation electrode S1 (red) and S2 (blue). Data are shown for two animals (035 and 036) from recordings during the test measurement before the start of the training procedure. Temporal ensemble averages of the spatial ensemble averages across the 18 channels of the ECoG recorded from the 3x6 epidural surface array (TSEAs) are plotted for stimulation through electrodes S1 and S2. TSEAs were calculated from the SEAs by averaging across artifact-free stimulus repetitions (n = 80). Prior to averaging, all signals had been digitally high-pass filtered at 3 Hz and z-standardized in reference to a pre-stimulus baseline of 1 s. Time is referenced to stimulus onset t = 0, and amplitude is given in standard deviations obtained across the 1 s pre-stimulus baseline. Amount of current of the single pulses (biphasic, cathodal first, 200µs/phase) was set to values between three and four times threshold of evoking a response (70 µA stimulation site in both animals). The same values were later used in the pulse trains applied as CS+ and CS- in the training procedure.

---

[14] Note that it cannot be excluded that later phases of the stimulus artifact have contributed to this peak.
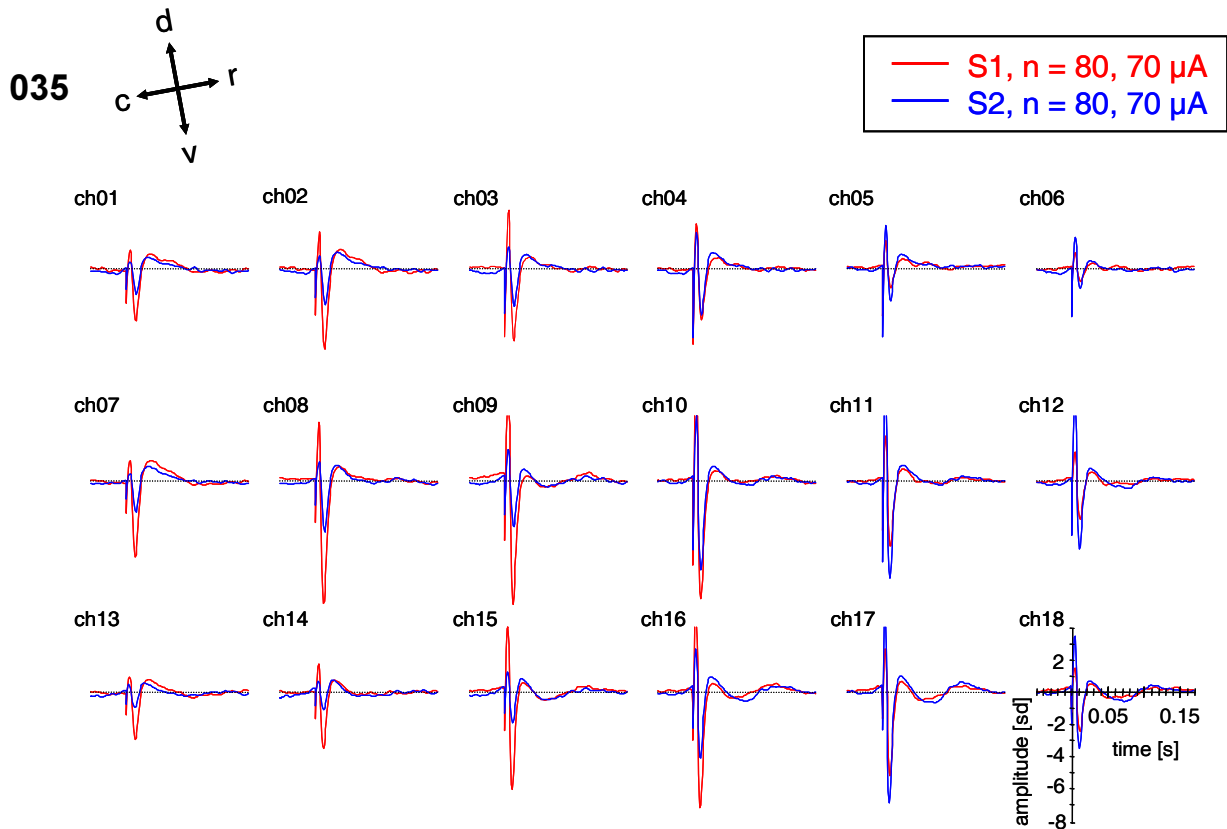
Figure 21: Spatial variation of responses evoked by single electrical current pulses delivered through stimulation electrode S1 (red) and S2 (blue). A typical result is shown for animal 035 from recordings during the test measurement before the start of the training procedure. Temporal ensemble averages (TEAs) of the ECoG are plotted channel-wise (ch01 to ch18) at the positions of the recording electrodes in the 3x6 array for stimulation through electrode S1 and S2. Anatomical directions dorsal (d), ventral (v), rostral (r) and caudal (c) are indicated by the orientation cross on top of the figure. TEAs were calculated channel-wise by averaging across artifact-free stimulus repetitions in reference to stimulus onset. Prior to averaging, signals had been digitally high-pass filtered at 3 Hz and z-standardized in reference to a pre-stimulus baseline of 1 s. Time is referenced to stimulus onset t = 0 and amplitude is given in standard deviations obtained across a 1 s pre-stimulus baseline. Amount of current of the pulses (biphasic, cathodal first, 200µs/phase) was set to values between three and four times threshold of evoking a response (70 µA for S1 and 70 µA for S2). The same values were later used in the pulse trains applied as CS+ and CS- in the training procedure.
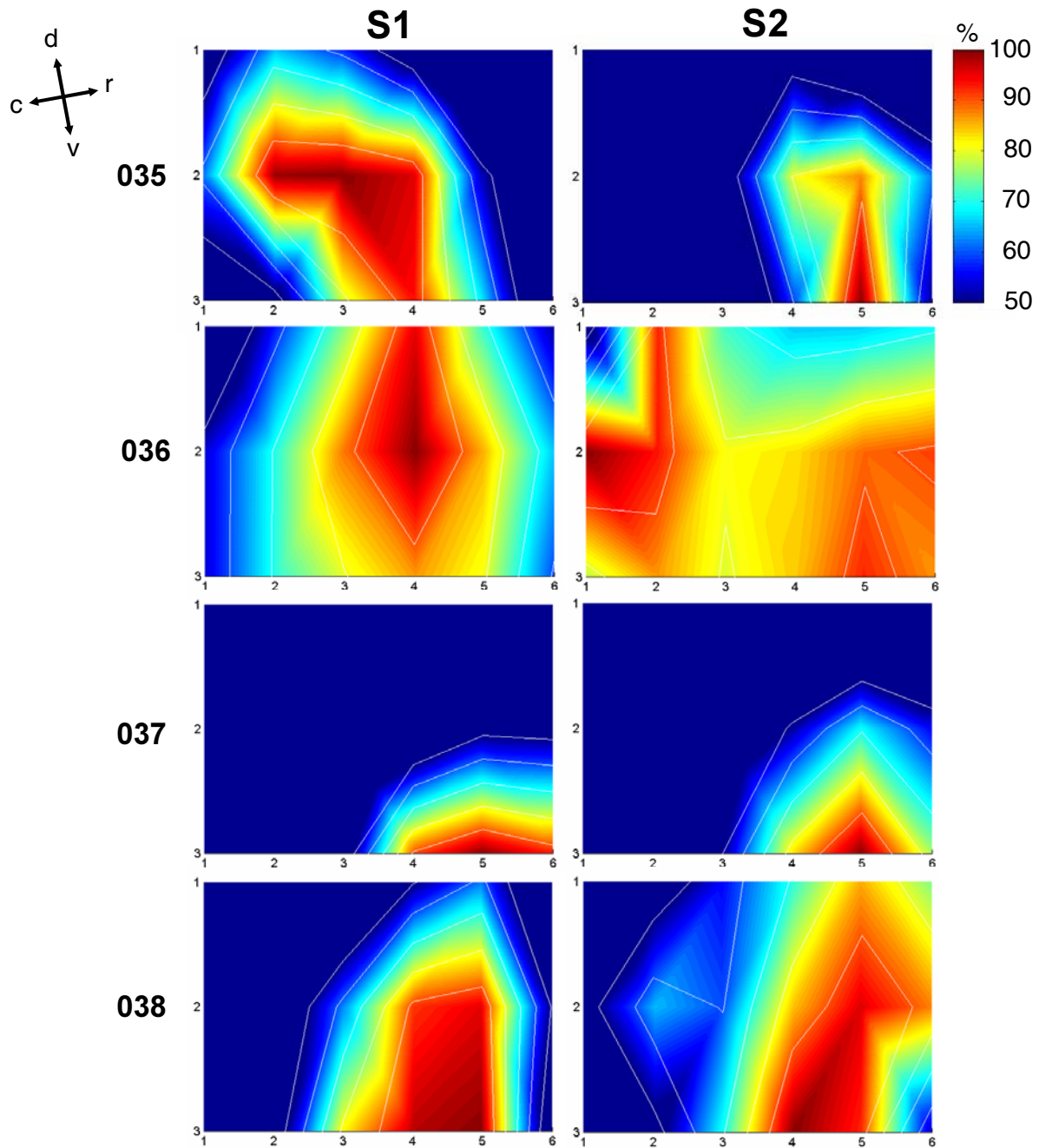
Figure 22: Topography of the short latency negative peak of the evoked potential occurring about 12 ms after the delivery of a single electrical current pulse through stimulation electrode S1 (left column) and S2 (right column). Results are shown for animals 035, 036, 037, and 038. Peak amplitudes were expressed as percent of the maximum peak amplitude across recording channels for each animal and condition. Percent maximum amplitudes at the positions of the recording electrodes corresponding to the recording channels were spatially interpolated. Each resulting spatial distribution of the normalized peak amplitude of the short latency negative wave is plotted as a color map (see colorbar at the right side of the upper row of plots) over the area covered by the 3x6 epidural surface array. Anatomical directions dorsal (d), ventral (v), rostral (r) and caudal (c) are indicated by the orientation cross at the upper left side of the figure.
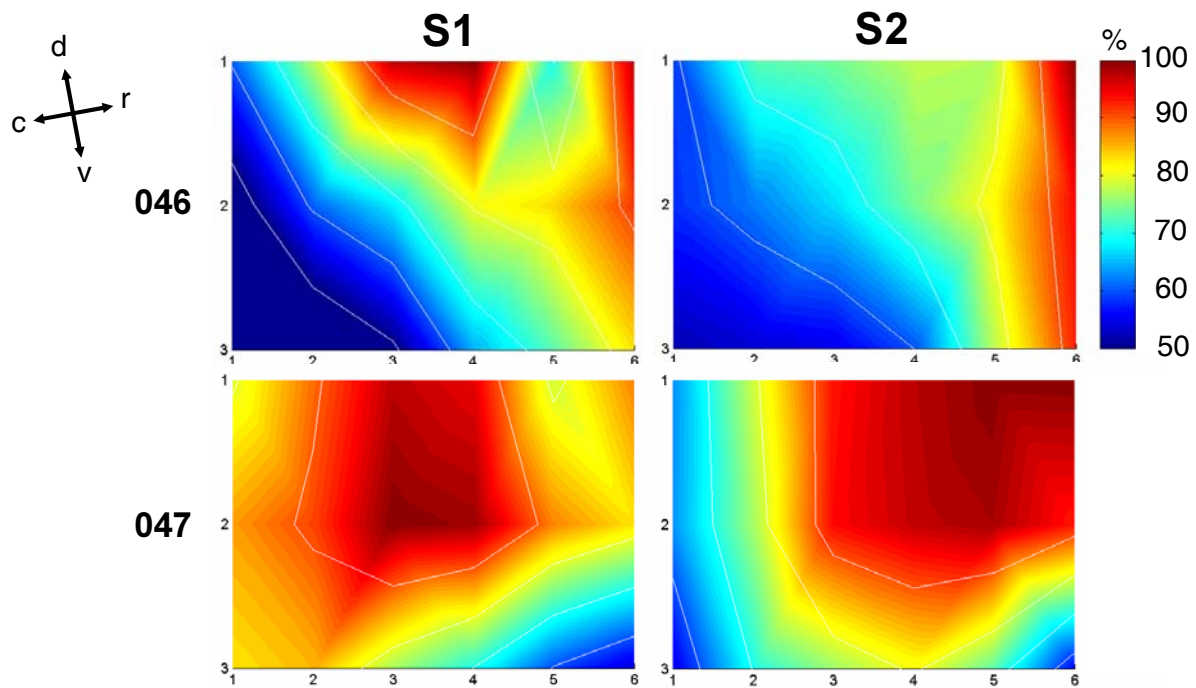
Figure 23: Topography of the short latency negative peak of the evoked potential occurring about 12 ms after the delivery of a single electrical current pulse through stimulation electrode S1 (left column) and S2 (right column). Results are shown for animals 046 and 047. Peak amplitudes were expressed as percent of the maximum peak amplitude across recording channels for each animal and condition. Percent maximum amplitudes at the positions of the recording electrodes corresponding to the recording channels were spatially interpolated. Each resulting spatial distribution of the normalized peak amplitude of the short latency negative wave is plotted as a color map (see colorbar at the right side of the upper row of plots) over the area covered by the 3x6 epidural surface array. Anatomical directions dorsal (d), ventral (v), rostral (r) and caudal (c) are indicated by the orientation cross on the upper left side of the figure.

The short latency negative wave was followed by a smaller positive wave, which had a peak amplitude of about 0.5 standard deviations above the pre-stimulus baseline, a peak latency of about 20 ms, and a peak width of about 25 ms at 50 % of the maximum peak amplitude. The peak amplitude was less dependent on the site of electrical stimulation than the preceding negative wave (figure 21), and the topographies of the positive peak were often difficult to interpret (figure 24). Both, single and multiple spatial maxima were found. No clear relationship could be determined between these maxima and the stimulation sites.

The positive wave was followed by two or three further negative and positive waves with decaying peak amplitude. Thus, the overall waveform of the single pulse electrically evoked potential resembled a frequency-modulated damped oscillation lasting for about 150 ms after the delivery of the current pulse with rapidly decaying amplitude and a frequency decreasing from about 80 Hz to about 20 Hz.
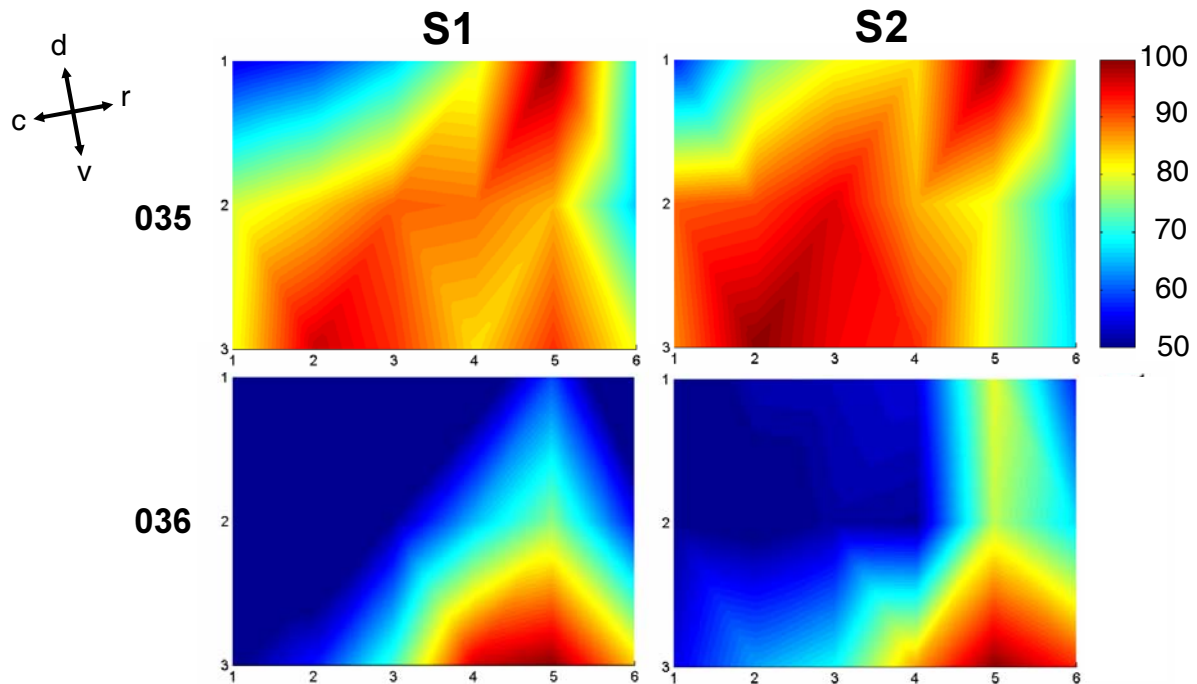
Figure 24: Topography of the second, positive peak of the evoked potential occurring about 25 ms after delivery of a single electrical current pulse either through stimulation electrode S1 (left column) or S2 (right column). Examples are shown from animals 046 and 047. Peak amplitudes were expressed as percent of the maximum peak amplitude across recording channels for each animal and condition. Percent maximum amplitudes at the positions of the recording electrodes corresponding to the recording channels were spatially interpolated. Each resulting spatial distribution of the normalized peak amplitude of the short latency negative wave is plotted as a color map (see colorbar at the right side of the upper row of plots) over the area covered by the 3x6 epidural surface array. Anatomical directions dorsal (d), ventral (v), rostral (r) and caudal (c) are indicated by the orientation cross on the upper left side of the figure.

4.5.3. Potentials evoked by trains of current pulses

During the presentation of trains of current pulses, the most prominent feature in the TEAs and TSEAs was a large electrical stimulus artifact as can be seen in figure 25 and 26. This artifact consisted of fast biphasic waveforms occurring with each pulse in the train, which were highly similar to the artifact waveform observed with single pulse stimulation (figure 20 and 21). In five animals (035, 036, 037, 038, and 047), these artifact waveforms were superimposed to a slower frequency-modulated damped oscillation, which in some cases outlasted the electrical stimulus (see for example animal 035 in figure 25 and 26). The frequency of this oscillation decreased from about 20 Hz to about 5 Hz. Its amplitude decayed within 0.5 s to 1.0 s after stimulus onset. The first negative wave of this oscillation had a large negative peak amplitude sometimes exceeding the input range of the amplifiers. It occurred at a peak latency of about 30 ms after the onset of the pulse train with a temporal peak width of about 50 ms at 50% of the maximum peak amplitude. A smaller positive peak followed this negative peak at a latency of about 100 ms relative to stimulus onset (figure 25 and 26). Although difficult to separate from the electrical stimulus artifact, the slow damped oscillation described above was considered as an electrically evoked potential. However, one cannot fully exclude that artifacts due to electrical stimulation largely contributed to this oscillation, e.g. by electrode polarization or temporal summation of single artifact waveforms. In animal 046, the overall amplitudes of these electrically evoked potentials were very small at both stimulation electrodes, about 5 times smaller than those found in the other animals.

With the same amount of current used for single and trains of electrical current pulses, the peak amplitudes of the potentials evoked by the pulse trains were much larger than those evoked by single pulses. The overall waveform of the potential evoked by a pulse train resembled that of a temporally dispersed single pulse evoked potential (figure 20 and 21). Spatial variations of the peak amplitudes were difficult to determine due to the electrical stimulus artifact (figure 27). However, the spatial maximum of the peak amplitudes of the first negative wave seemed to be located at the stimulation sites. No evoked activity was found in the TEAs and TSEAs at latencies longer than 1 second after stimulus onset.

Typical examples of TSEAs are shown for an early training session (session 3), when the animals had not yet reached significant discrimination performance, and for a late training session (session 7), when the animals had entered the plateau phase of their learning curves (figure 14). From these examples it can be seen that the peak amplitudes and overall duration of the evoked potentials in response to stimulation with trains of current pulses varied across animals, sessions and between the CS+ and CS-. A detailed analysis of this variability was, again, precluded by the large electrical stimulus artifact. However, a slight increase in the overall amplitude of the electrically evoked potentials over training in response to both, CS+ and CS-, was consistently found by visual inspection.

In summary, electrically evoked potentials were found in response to ICMS with single and trains of electrical current pulses. They had the shape of a damped frequency-modulated oscillation. The electrically evoked potentials in response to trains of electrical current pulses were slower than the single pulse electrically evoked potentials. Most often, the spatial maximum of the short latency negative peak of the electrically evoked potential was located at the site of ICMS. In the case of single pulse stimulation, evoked activity extended between 0.6 mm and 1.8 mm from the stimulation site. The overall amplitudes of the electrically evoked potentials in response to the CS+ and the CS- pulse trains applied during training both slightly increased over training sessions.
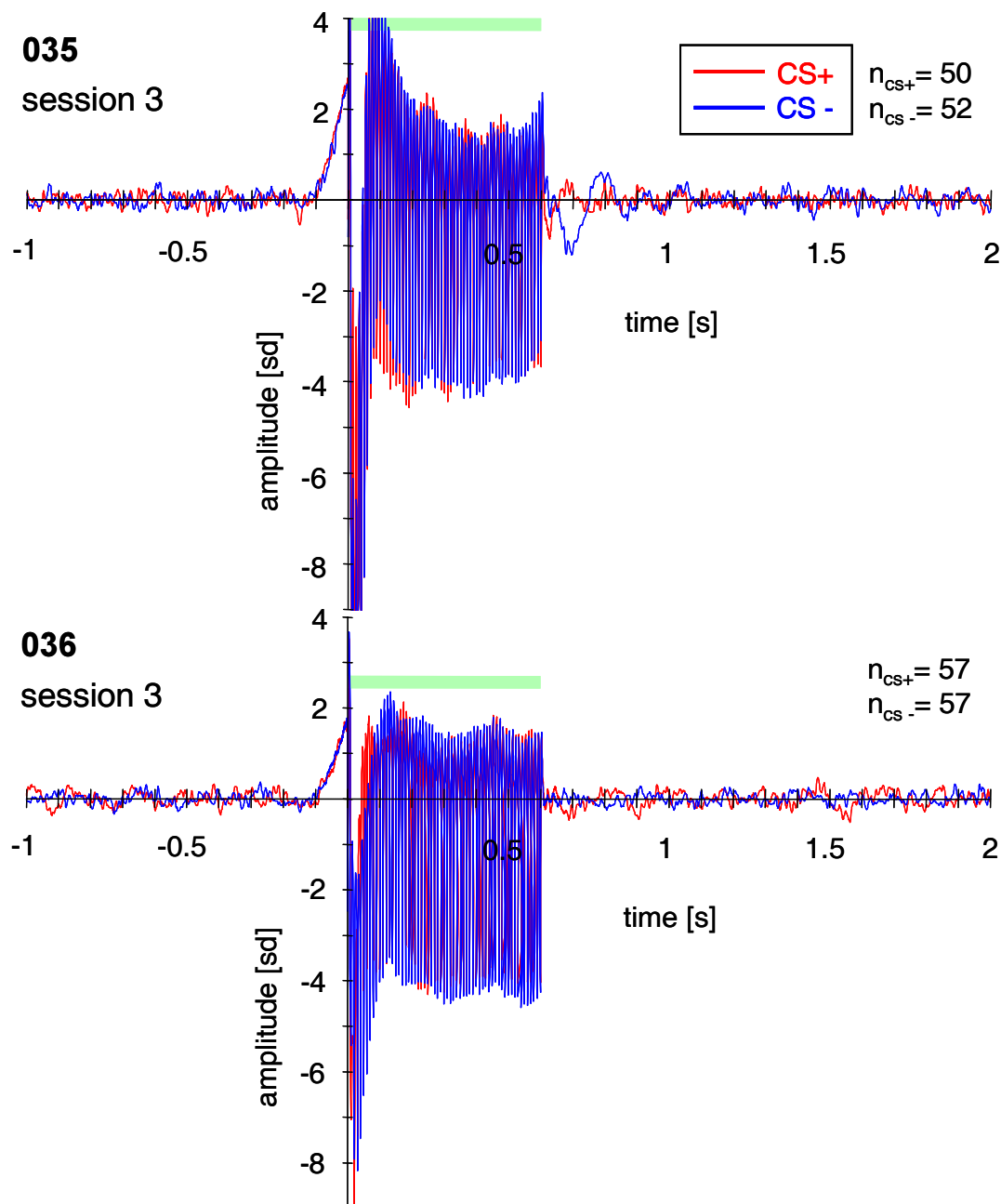
Figure 25: Typical examples of responses evoked by trains of electrical current pulses delivered as CS+ (red) and CS- (blue) during an early training session, when the animals did not yet reach significant discrimination performance (session 3). Data are shown from recordings of animals 035 and 036. For each of the CS there is shown a temporal ensemble average of the spatial ensemble averages across the 18-channels of the ECoG recorded from the 3x6 epidural surface array. These TSEAs were calculated by averaging separately across artifact-free CS+ and CS-trials in reference to stimulus onset (ensemble sizes are given by numbers n_{cs+} and n_{cs-} in the figure). Prior to averaging, all signals had been digitally high-pass filtered at 3 Hz and z-standardized in reference to a pre-stimulus baseline from 2 s to 1 s pre-stimulus time. Time is referenced to stimulus onset (t = 0) and amplitude is given in standard deviations obtained across the 1 s pre-stimulus baseline. Amount of current of the pulses (biphasic, cathodal first, 200µs/phase) was set to values between three and four times threshold of evoking a response (70 µA for S1 and 70 µA for S2). Train length was 0.6004 s as indicated by the green rectangle.

Figure 26: Typical examples of responses evoked by trains of electrical current pulses delivered either as CS+ (red) or CS- (blue) during a late training session, when the animals entered the plateau phase of their learning curves (session 7). Data are shown from recordings of animals 035 and 036. For each of the CS, there is shown a temporal ensemble average of the spatial ensemble averages across the 18-channels of the ECoG recorded from the 3x6 epidural surface array. These TSEAs were calculated by averaging separately across artifact-free CS+ and CS-trials in reference to stimulus onset (ensemble sizes are given by numbers n_{cs+} and n_{cs-} in the figure). Prior to averaging, all signals had been digitally high-pass filtered at 3 Hz and z-standardized in reference to a pre-stimulus baseline from 2 s to 1 s pre-stimulus time. Time is referenced to stimulus onset (t = 0) and amplitude is given in standard deviations obtained across the 1 s pre-stimulus baseline. Amount of current of the pulses (biphasic, cathodal first, 200µs/phase) was set to values between three and four times threshold of evoking a response (70 µA for S1 and 70 µA for S2). Train length was 0.6004 s as indicated by the green rectangle.

Figure 27: Spatial variation of responses evoked by trains of electrical current pulses delivered as CS+ (red) and CS- (blue) during a late training session, when the animal entered the plateau phase of its learning curves (session 7). A typical example is shown from the recording of animal 037. For each recording electrode in the 3x6 array (ch01 to ch18) the temporal ensemble averages (TEAs) for CS+ and CS- are plotted. Anatomical directions dorsal (d), ventral (v), rostral (r) and caudal (c) are indicated by the orientation cross on top of the figure. TEAs were calculated channel-wise by averaging separately across artifact-free CS+ and CS- trials in reference to stimulus onset (ensemble sizes are given by numbers n_{cs+} and n_{cs-} in the figure). Prior to averaging, all signals had been digitally high-pass filtered at 3 Hz and z-standardized in reference to a pre-stimulus baseline from 2 s to 1 s pre-stimulus time. Time is referenced to stimulus onset t = 0, and amplitude is given in standard deviations obtained across the 1 s pre-stimulus baseline. Amount of current of the pulses (biphasic, cathodal first, 200µs/phase) was set to values between three and four times threshold of evoking a response (70 µA for S1 and 70 µA for S2). Train length was 0.6004 s as indicated by the light green rectangle.

4.6. Spatial activity patterns in the ongoing electro-corticogram (ECoG) during training

From the visual inspection of single trial ECoG recordings, it became immediately apparent that the waveforms recorded from the electrodes of the 3x6 epidural surface array were highly similar across recording channels. This high degree of spatial coherence is illustrated by the left panel of figure 12, which displays for each recording channel a representative 180 ms segment of the ongoing ECoG digitally bandpass filtered in the β- and γ- frequency range (15 Hz to 80 Hz). All recording channels shared the same aperiodic oscillatory waveform, which is typical for ECoG recordings at high spatial resolution (Barrie et al., 1996; Freeman & Barrie, 2000). Whereas the waveform were highly similar within a spatial window of several millimeters (Freeman & Barrie, 2000), the overall amplitude of the common aperiodic oscillation within a short time segment varied across the channels, as illustrated by the distribution of signal power in the left panel of figure 12. Several studies have shown that in the sensory cortices these aperiodic oscillations can serve as a carrier wave for spatial amplitude modulations of the ECoG, which develop into stimulus induced discernable spatial patterns when an animal learns to perceptually sort stimuli into meaningful classes in the course of discrimination and categorization training (Barrie et al., 1996; Ohl et al., 2001; Ohl et al., 2003a; Ohl et al., 2003b). These patterns cannot be retrieved by temporal ensemble averages of the ECoG across trials, because at each time the pattern emerges from the ongoing activity the waveform carrying the pattern is different, e.g. varying in its phase from trial to trial.

In order to identify spatial activity patterns in relation to discrimination learning of the electrical stimuli, a multivariate classification procedure was employed, based on a method of cross-classification of spatial activity distributions in the β- and γ-band of the unaveraged ongoing ECoG. A spatial activity distribution was defined as the distribution of mean power in a 180 ms time window of the β- and γ-band ECoG across the 18 recording channels. The time window was stepped in 20 ms steps through the digitally bandpass filtered (15 Hz to 80 Hz) ECoG signals recorded from the 6x3 epidural surface array trial by trial. In each 180 ms time window, mean power in the the β- and γ-band was quantified as root mean squared (RMS) amplitude for each of the 18 recording channels. RMS amplitudes were z-standardize across

channels. Then, for each 180 ms time window of a 20 ms time step, the spatial activity distributions were classified trial by trial as closer to a CS- centroid or closer to a CS+ centroid on the basis of a Euclidean distance metric. Numbers of correctly classified trials of a session were summed across trials for each time step. Pattern classification performance was measured in percent of correctly classified trials (see subsection 3.4.4. for details).

4.6.1. Identification of spatial activity patterns in the ongoing ECoG

Spatial activity patterns in the ECoG related to the stimulus classes CS+ and CS- were identified by epochs of significant pattern classification. Significance of pattern classification was evaluated in 20 ms time steps against the probability p_n of finding at least the number of correctly classified spatial activity distributions across single trials by chance (null hypothesis under the assumption of a binomial distribution of correct and incorrect classifications as detailed in subsection 3.4.4.). Whenever a so determined p_n-value was found to be below a predetermined level of significance in a time step, the spatial activity distributions in the corresponding 180 ms time window must have contained information about the stimulus classes, by which they significantly contributed to the correct classification at that time. A "meaningful" spatial activity pattern was then defined as a spatial distribution of signal power in a 180 ms time window of the in the ongoing β- and γ-band ECoG, which contained information about the stimulus classes.

To evaluate the significance of pattern classification over time, the decadic logarithm of the p_n-values for obtaining the observed number of correctly classified trials in a training session by chance is plotted for each 20 ms time step of classification. In figure 28 and 29, results are shown from an early (session 3, left column of plots) and a late training session (session 7, right column of plots) representing characteristic phases of the learning history of an animal. Session 3 was the session, before the animals reached significant discrimination performance the first time. It characterized a phase in the learning history when the animals had learnt to react to the US by changing compartments in the shuttle-box, but did not yet show significant discrimination between CS+ and CS- (figure 16). Session 7 was the fourth of a set of consecutive sessions in which the animals showed significant stimulus

discrimination. It characterized a phase in the learning history when the animals had entered the plateau phase of their learning curves (figure 16). A significance level of $\alpha = 0.05$ was assumed for ECoG pattern classification and adjusted to multiple testing after stimulus onset by a modified Bonferroni correction (Bortz, 1999, p.260-263). For each animal and session, this resulted in a corrected α' value ranging between 0.001 and 0.0005. The decadic logarithm of the α' value is indicated in each plot by a dashed horizontal black line. For each animal, the timing of its behavioral response in session 7 was described by the mean and the median of the reaction times of the hit responses represented by a continuous and a dashed vertical red line, respectively. The standard deviation of the reaction times is shown by the continuous horizontal red line in each plot of session 7. The 180 ms time windows, from which significant ECoG pattern classification was obtained, i.e. having p_n-values below the significance level α', are marked by small red triangles in the plots of figure 28 and 29. Classification time windows interfering with the electrical stimulus artifact are highlighted by a green background area.

As shown by figure 28 and 29, the sequence of p_n-values over time displayed peaks below the significance level α'. In four of the six animals (035, 036, 037, and 047), peaks of significant p_n-values extending over several consecutive classification time windows (20 ms steps) marked epochs of significant pattern classification during and after the presentation of the electrical stimulus (figure 28). No significant pattern classification was found during pre-stimulus time in these animals.

In session 7, when the animals entered the plateau phase of their learning curves, late epochs of significant pattern classification were found after the end of the electrical stimulus, outside the time range affected by the electrical stimulus artifact (green background area). Most of these late epochs preceded the mean and the median of the hit reaction times (continuous and dashed vertical red lines) characterizing the time of the behavioral response. Also, the highest significant classification performance, i.e. the lowest significant p_n-value, was reached in the late epochs between the end of the electrical stimulus and the behavioral response.

The described late epochs of significant pattern classification were not found in early training sessions (figure 28, session 2). They emerged from the fourth or the fifth training session on, except in animal 036, where such epochs could be only obtained from session 7. The timing of the epochs varied considerably across sessions and animals. Thus, the late epochs seemed to be neither precisely time-locked to the stimulus, nor to the behavioral response.
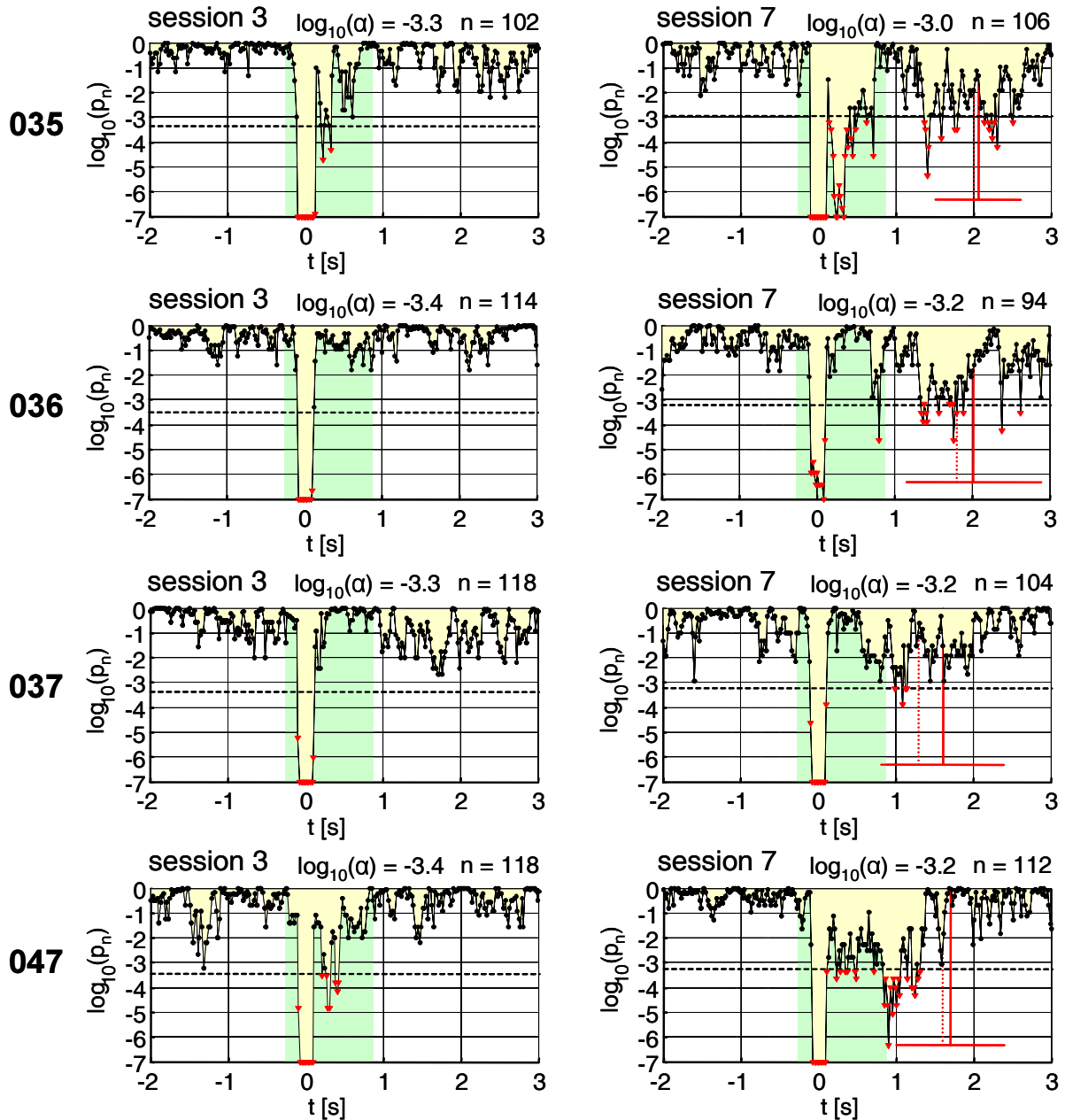
Figure 28: Significance of pattern classification as a function of time (20 ms time steps). The plots show the $\log_{10}$ of the probability p_n of finding at least the number of correctly classified spatial activity distributions in single trials by chance (null hypothesis). A spatial activity distribution was defined as the distribution of mean β- and γ-band power in a 180 ms time window of the ECoG across the 18 recording

channels. Distribution of mean power was quantified by root mean squared (RMS) amplitudes, which were z-standardized across channels. Time is referenced to stimulus onset (t = 0). Results from four animals (035, 036, 037 and 047) are shown for an early training session, one session before the animals reached significant discrimination performance (session 3), and a late session, when the animals entered the plateau phase of their learning curves (session 7). The number of classified trials in a session is given by the number n on top of each plot. Significance levels α' were obtained by a modified Bonferroni-correction for multiple testing in the time window after the end of the electrical stimulus. For each animal and session, the $\log_{10}(α')$ value is given on top of each plot and is indicated as a dashed line within each plot. Significant p_n-values below the α' level are marked by small red triangles. For the late session (session 7), mean, median, and standard deviation of the reaction times of the hit responses are indicated as continuous vertical red line, dashed vertical red line, and horizontal red line, respectively. The green area marks the time range in which pattern classification was possibly interfering with the electrical stimulus artifact.

Early epochs of significant pattern classification were found during the presentation of the electrical stimuli (figure 28). However, a contribution of the electrical stimulus artifact to classification performance during the delivery of the electrical stimuli could not be excluded for these epochs, especially after digital bandpass filtering between 15 and 80 Hz, which introduced a temporal dispersion of the artifact (see subsection 4.5.1.). Highly significant pattern classification (p_n-values < 10^{-12}) was obtained from classification time windows centered at the first 100 ms after stimulus onset in all sessions of the four animals. Classification performance was close to 90% correct at that time. These early epochs, which appeared to be precisely time-locked to the stimulus, can be seen in figure 28 directly after stimulus onset in both training sessions (2 and 7) of the four animals shown. Further significant peaks in the temporal sequence of p_n-values emerged over training sessions later during the delivery of the electrical current pulse trains.

As shown in figure 29, different results were obtained from animal 038 and 046. In animal 038, early epochs of significant pattern classification were found, similar to those of the four animals described above. Though, the late epochs of significant pattern classification were found always after the mean and the median of the hit reaction times (figure 29, animal 38, session 7) and thus occurred much later as in the four animals reported above. In animal 046, no late epochs of significant pattern classification were found at all. Significant pattern classification in this animal was obtained only from classification time windows during electrical stimulus presentation.

In the early epochs of significant classification around 100 ms post-stimulus time, pattern classification performance was much lower than in the other animals, as shown by the higher p_n-values of the early epochs in this animal compared to the other animals (p_n-values $> 10^{-5}$).
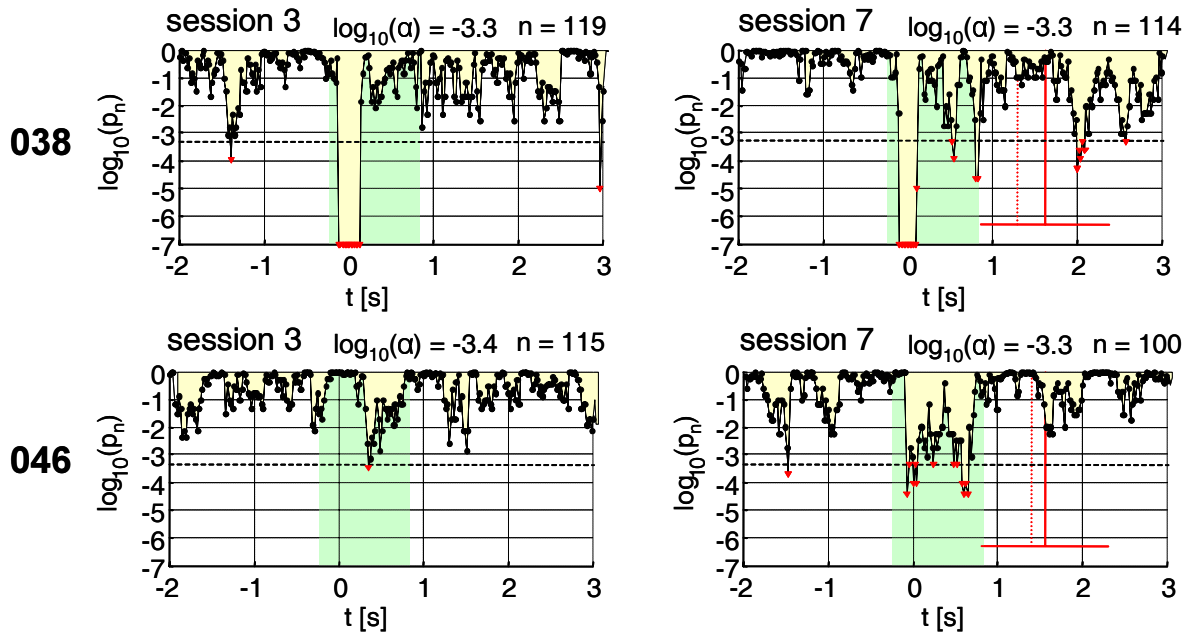
Figure 29: Significance of pattern classification as a function of time (20 ms time steps). The plots show the $\log_{10}$ of the probability p_n of finding at least the number of correctly classified spatial activity distributions in single trials by chance (null hypothesis). Results from two animals (038 and 046) are shown for the early training session 2 and the late training session 7. No peaks of significant pattern classification were found between the end of the electrical stimulus and the median or mean of the hit reaction times in these animals. The number of classified trials in a session is given by the number n on top of each plot. Significance levels α' were obtained by a modified Bonferroni-correction for multiple testing in the time window after the end of the electrical stimulus. For each animal and session, the $\log_{10}(α')$ value is given on top of each plot and is indicated as a dashed line within each plot. Significant p_n-values below the α' level are marked by small red triangles. For the late session (session 7), mean, median, and standard deviation of the reaction times of the hit responses are indicated as continuous vertical red line, dashed vertical red line, and horizontal red line, respectively. The green area marks the time range in which pattern classification was possibly interfering with the electrical stimulus artifact (see figure 28 for further details).

From the epochs of significant pattern classification it could be inferred that there existed patterns in the spatial distributions of cortical β- and γ-band activity within these epochs, which contained information about the CS+ and the CS- (see above). Concurrently with the early epoch of highly significant pattern classification, which

occurred in the first 100 ms after stimulus onset in nearly all sessions and animals, a large negative wave occurred in the electrically evoked potential around 30 ms after stimulus onset. Although the topography of this early negative wave could not be determined due to the electrical stimulus artifacts, the largest peak amplitudes were apparently distributed around the stimulation site (figure 21, 22, 23, and 27). Thus, this early epoch of significant pattern classification probably reflected the discernible spatial patterns of the early negative wave evoked by the electrical pulse trains which were delivered as CS+ and CS-, respectively. To which extent the spatial variation of the electrical stimulus artifact contributed to pattern classification in the early epochs, could not be determined.

On the other hand, there was no stimulus evoked activity in the temporal ensemble averages of the ECoG which could be related to the late epochs of significant pattern classification in the time between the end of the electrical stimulus and the behavioral response (figure 25, 26, and 27). Therefore, significant pattern classification in the late epochs apparently relied on spatial activity patterns in the β- and γ-band emerging from the ongoing cortical dynamics.

Further analysis on the late cortical activity patterns was carried out in the 180 ms time window from which the highest significant pattern classification performance, i.e. the lowest significant p_n-value, was obtained in the time interval between the end of the electrical stimulus and the behavioral response. The time of the behavioral response was defined as the median of the hit reaction times. In figure 30, several examples from different animals and sessions illustrate the temporal relationship between this time window of maximum significant pattern classification (blue arrow heads) and the temporal distribution of the reaction times of the hit responses (red bars). Most of the hit responses occurred in the time after the maximum of significant classification performance. The maxima of the distributions of the reaction times were found at various latencies to the maxima of significant pattern classification. From this it can be inferred that the late patterns preceded the behavioral response and were not precisely time-locked to it. Also, this indicates that significant pattern classification was not based on movement artifacts related to the hit response.
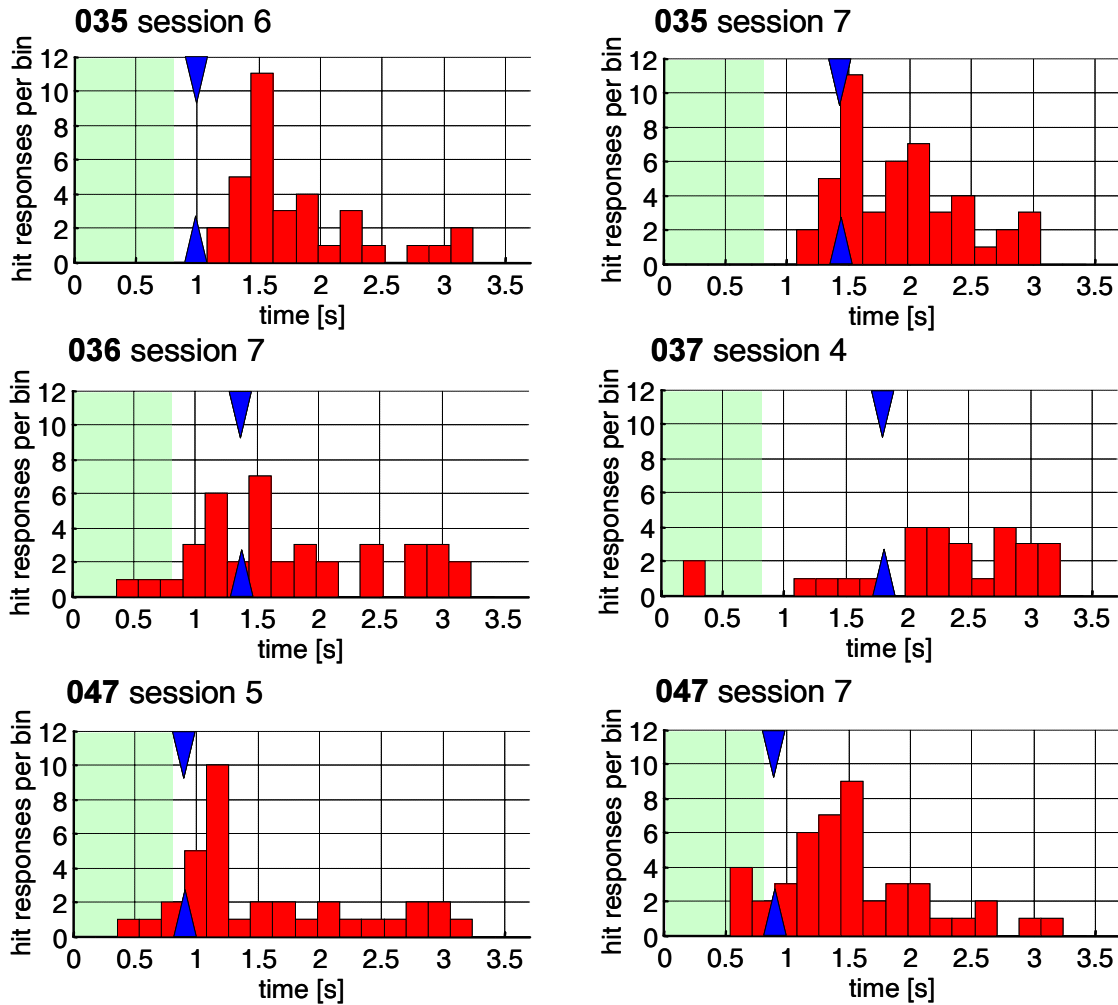
Figure 30: Temporal relationship between the occurrence of late cortical activity patterns and the reaction times of the hit responses. Typical examples are shown from training sessions of animals 035, 036, 037, and 047, in which significant pattern classification was observed in late epochs between the end of the electrical stimulus and the behavioral response, which was defined as the median of the hit reaction times. Blue arrow heads in each plot mark the 180 ms classification time window from which maximum significant pattern classification performance was obtained in the late epochs. The temporal distribution of reaction times of the hit-responses is shown by the red histogram (bin width 180 ms) in each plot. Time (horizontal axis) is referenced to stimulus onset (t=0). The green area marks the time interval possibly interfering with the electrical stimulus artifact.

4.6.2. Correlation between behavioral discrimination performance and ECoG pattern classification performance

If the late cortical activity patterns were related to discrimination learning, one would expect that the patterns occurred in relation to correct behavioral responses (hits and correct rejections). As the frequency of correct behavioral responses increased with learning, the frequency of occurrence of cortical activity patterns related to the stimulus classes should have also increased. Therefore, as the behavioral discrimination performance increased over training sessions, pattern classification performance should have increased over sessions concomitantly.

Behavioral discrimination performance was measured by the discriminability index d'. For each session and animal, pattern classification performance in late epochs was quantified by the maximum of percent correct classification derived from a post-stimulus time interval between the end of the electrical stimulus and the median of the hit reaction times of about 1 s length (see subsection 3.4.5.). In sessions where the animals showed less than six hit responses, maximum percent correct classification was determined in a post-stimulus interval of 2 s. As a control for classification at chance level, maximum percent correct classification values were derived for each session and animal from a pre-stimulus interval of a length corresponding to the post-stimulus interval. Only classification time windows in which interference with the stimulus artifact could be excluded were taken into account.

In the following, data were pooled from the four animals, in which significant pattern classification was found in late epochs between the end of the electrical stimulus and the behavioral response, which was defined by the median of the hit reaction times (animal 035, 036, 037, and 047). In part A of figure 32, the discriminability index d' averaged across the four animals is plotted over session. In part B of figure 32, average maximum percent correct classification across the four animals is plotted over sessions for the pre- (blue bars) and the post-stimulus (red bars) intervals. It can be seen that both the average discriminability index d' and the average maximum percent correct classification derived from the post-stimulus intervals (red bars) followed a similar progression with a concomitant increase from the fourth session on. On the other hand, average maximum percent correct classification obtained from the pre-stimulus intervals (blue bars) was rather constant over sessions and

never exceeded the significance level of about 65% percent correct. In part C of figure 32, average maximum percent correct classification values are plotted session-wise against their corresponding average d' values for the pre- and post-stimulus intervals. The plot shows that ECoG pattern classification performance after the electrical stimulus (red squares) increased from the fourth session on (white numbers) together with the behavioral discrimination performance. Pattern classification performance before the onset of the electrical stimulus (blue squares) stayed at about the same level for all average d' values.
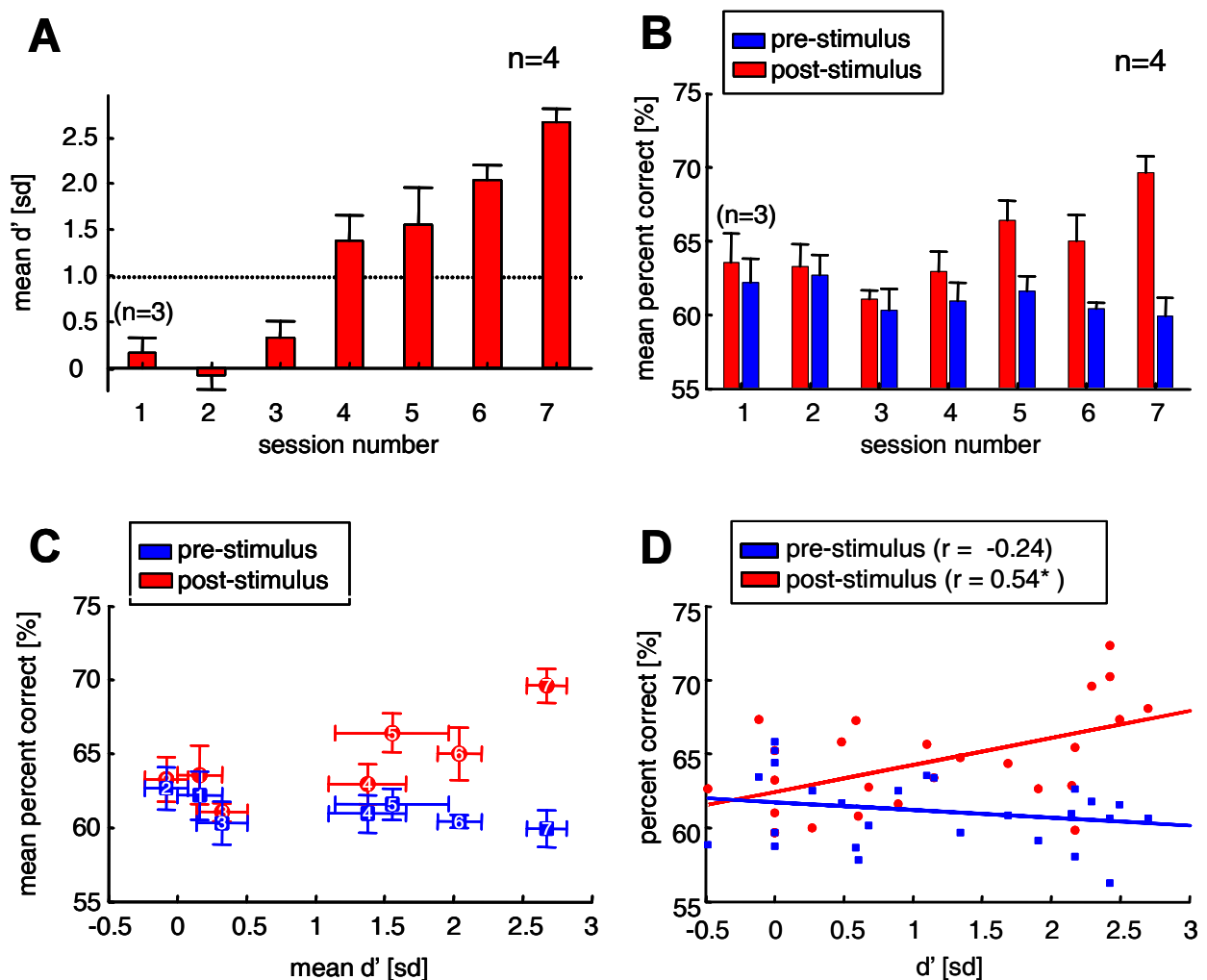
Figure 31: Relationship between ECoG pattern classification performance and behavioral discrimination performance. Data were pooled from the animals, in which late epochs of significant pattern classification were observed in the time between the end of the electrical stimulus and the behavioral response, which was defined as the median of the hit reaction times. Behavioral discrimination performance was quantified by the discriminability index d' and ECoG pattern classification was measured as percent correct classification. For each session and animal, maximum percent correct classification was derived from a pre- and a post-stimulus time

interval of corresponding length (see text). Values of d' larger than one indicated significant discrimination performance.

(A)   The mean and the standard error of the discriminability index d' across the four animals is plotted over all training sessions.

(B)   Maximum percent correct values of pattern classification in the pre- (blue) and the post-stimulus (red) time intervals averaged across the four animals are plotted over all training sessions. Standard errors are indicated by the errorbars.

(C)   Average maximum percent correct values in the pre- (blue squares) and the post-stimulus (red circles) time intervals plotted as a function of their corresponding average discriminability indices d'. Training sessions are indicated by the white number within the markers.

(D)   For each animal and each session, maximum percent correct values in the pre- (blue squares) and the post-stimulus (red circles) time intervals are plotted as a function of their corresponding discriminability indices d'. Common correlation coefficients were calculated for pre- and post-stimulus intervals and are given in the legend above the plot. Regression lines are plotted on the basis of the pre- (blue) and the post-stimulus (red) common correlation coefficient, respectively.

In order to quantify the relationship between behavioral discrimination performance and ECoG pattern classification performance in the late epochs, common correlation coefficients were calculated between maximum percent correct classification values and discriminability indices d' over training sessions across the four animals (see subsection 3.4.5.). A significant positive correlation ($p < 0.01$) was found for the post-stimulus intervals ($r = 0.54$), but not for the pre-stimulus intervals ($r = -0.24$). Part D of figure 32 displays the relationship between single maximum percent correct classification values and their corresponding d' values for the pre- and the post-stimulus interval. Data were pooled over sessions 1 to 7 of animals 035, 036, 037, and 047. Regression lines derived from the common correlation coefficients are also shown. The positive slope of the regression line calculated for the post-stimulus intervals illustrates the concomitant increase of pattern classification performance and discrimination performance in the late epochs. The positive correlation between behavioral discrimination performance and maximum pattern classification performance in the late epochs indicates that the late activity patterns were induced by learning.

In order to test whether the early epochs of highly significant pattern classification in the first 100 ms after the onset of the electrical stimulus (see subsection 4.6.1.) were related to learning, too, common correlation coefficients were calculated between the d' values and the maximum percent correct classification values derived from the time interval 200 ms after stimulus onset over sessions, as specified above (see also

subsection 3.4.5.). No significant correlation was found ($r = -0.08$, $p < 0.05$) indicating that the early epochs of highly significant pattern classification occurring directly after stimulus onset were not related to the increasing discrimination performance and thus to learning. Increases in pattern classification performance over training sessions were also observed at later times during the delivery of the trains of electrical current pulses between 200 ms and 600 ms after stimulus onset (figure 28, see subsection 4.6.1.). However, these increases seemed not to be related to the increase of behavioral discrimination performance, as no significant common correlation over sessions ($r = 0.36$, $p < 0.05$) was found between d' and maximum percent correct classification values derived from a time interval ranging from 200 ms to 600 ms after stimulus onset.

As movement artifacts in the ECoG occurring around the time when the animal crosses the hurdle of the shuttle-box would increase with the number of hit responses and thus with discrimination performance, it had to be ruled out that the positive correlation between behavioral discrimination performance and ECoG pattern classification performance in the late epochs relied on movement artifacts. Thus, for each animal and session, the number of hit responses occurring in a 600 ms interval, centered at the time of maximum significant pattern classification in the late epochs between the end of the electrical stimulus and the median of the hit reaction times, was counted. Common correlation coefficients across animals were calculated between the maximum percent correct classification values at that time and the corresponding numbers of hit responses in the aforementioned 600 ms interval over sessions (see subsection 3.4.5.). No significant common correlation was found ($r = 0.36$, $p < 0.05$) rendering it unlikely that ECoG pattern classification performance was solely based on movement artifacts related to the behavioral response of the animal.

4.6.3. Spatial organization of patterns in the ongoing ECoG

Spatial organization of late cortical activity patterns emerging with discrimination learning was inferred from the spatial distribution of information relevant for the classification described above by discriminant analysis based on a bootstrapping procedure (see subsection 3.4.6.). Analysis was carried out in the four animals (035,

036, 037, and 047) in which late cortical activity patterns emerged with learning in late epochs after the end of the electrical stimulus (see subsection 4.6.2.). The training sessions when the animals entered the plateau phase of their learning curves (session 7 in all animals) were selected for analysis, because all animals were in a well defined behavioral state in this session. Again, late cortical activity patterns were analyzed in the 180 ms time window, from which maximum significant pattern classification performance was obtained in the post-stimulus interval between the end of the electrical stimulus and the median of the hit reaction times. Pattern classification in this classification time window was carried out repeatedly after removing combinations of $n_r = \{0, 1, 2, …, 17\}$ recording channels corresponding to electrodes in the 3x6 recording array.

Figure 32 shows for each number of remaining recording channels (18 - n_r) the minimum, the median, and the maximum values of percent correct classification across each ensemble of 200 channel combinations of n_r removed recording channels. Since the combination of channels to be removed was selected randomly, the median conveys information about the "density" of recording channels required to capture the discriminant information about the two stimuli, CS+ and CS-, in the spatial cortical activity distributions within the 180 ms classification time window. A gradual decline of the median values of percent correct classification (figure 32, open triangles) was observed for decreasing numbers of recording channels remaining in the classification procedure. Clearly, classification performance depended on the size of the set of recording channels used for classification. However, no rapid fall off was observed that would have indicated that a particular channel set size was critical to maintain classification performance.

The minimum values of percent correct classification in 200 repetitions of the removal of n_r recording channels (figure 32, open circles) declined parallel to the median values from 17 to 8 remaining recording channels. Between 8 to 3 remaining channels, a sigmoid decline was found with a point of inflection at around 6 remaining channels. Thus there seemed to be at least one set of 6 remaining channels, which contained no discriminant information about CS+ and CS-. Vice versa a set of 12 recording channels contributed maximally to the discriminant potential of the pattern. With three remaining channels, minimum classification performance across 200 repetitions of channel removal reached the chance level.
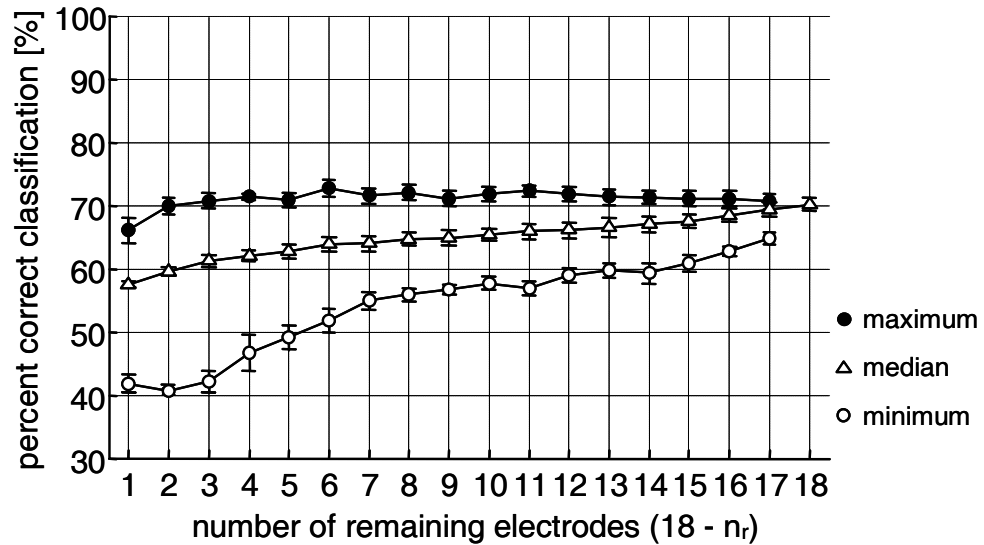
Figure 32: Classification performance for late cortical activity patterns as a function of the number of remaining recording channels (18 - n_r) after channel removal. Training session 7 was selected for analysis, because all animals entered the plateau phase of their learning curves in this session and were thus in a well defined behavioral state (see also figure 16). Data were pooled from the animals (035, 036, 037, and 047), in which late epochs of significant pattern classification were observed in the time between the end of the electrical stimulus and the behavioral response. For each animal, a late cortical activity pattern was identified in the 180 ms time window, from which the maximum significant classification performance was obtained in a late epoch between the end of the electrical stimulus and the median of the hit reaction times. Shown are the minimum (open circles), the median (open triangles) and the maximum (filled circles) values of percent correct classification in the so determined 180 ms time window across 200 (2 to 16 remaining electrodes) or 18 (1 and 7 remaining electrodes) repetitions of removing a combination of n_r recording channels. Minimum, median and maximum percent correct classification values were averaged across the four animals. Standard errors are given by the errorbars. For cases of 18 remaining electrodes, the open triangle corresponds to the average percent correct classification observed for the complete pattern.

With more than two remaining recording channels, maximum values of percent correct classification in 200 repetitions of the removal of n_r recording channels (figure 32, filled circles) constantly retained the discriminant potential of the complete channel set. With only one remaining recording channel, maximum classification performance dropped slightly. This indicates that significant classification could be obtained already with two properly selected recording electrodes in the 3x6 epidural surface array. In some animals, even single recording channels were sufficient to retain the significant classification potential of the full pattern.

107

In order to find out, how single electrodes at different locations contributed to pattern classification, percent correct classification values were calculated by using only one recording channels at a time. This calculation was carried out for each of the four selected animals, separately. The resulting percent correct classification values at the electrode positions corresponding to the recording channels were spatially interpolated between electrode positions. In figure 33, the so determined spatial distribution of single channel classification performance is displayed in a color plot for each of the analyzed animals. The spatial distribution of classification performance across single remaining recording channels displayed focal maxima and minima (figure 33). In three animals (035, 037 and 047) a focal maximum of classification performance was found in the caudal half of the array. In two of the animals (035 and 047), some of these electrodes displayed a classification performance above the significance level. In rostral direction to this focal maximum, classification performance declined steeply towards a focal minimum with classification performance at chance level. In two animals (036 and 047), high values of single channel classification performance were also found with electrodes close to the rostral edge of the array.

However, the contribution of single electrodes to classification performance is not sufficient to describe the spatial organization of cortical activity patterns, because a pattern is defined by the relationship of the cortical activity at every recording site to cortical activity at every other recording site. Therefore, to identify the electrodes in the recording array, which contributed maximally to a spatial activity pattern identified by the classification procedure, the channel combinations yielding the minimum value of percent correct classification among the 200 removed combinations was determined for each animal and for each number of removed electrodes n_r. For $n_r = \{0, 17\}$, the same analysis was performed using all possible 18 combinations of channel removal. The electrodes corresponding to the channel combinations associated with minimum classification performance are plotted for n_r removed recording channels in figure 34 with $n_r = \{10,11,12,13\}$. The numbers of removed channels (n_r) were chosen about the size of the set of channels contributing maximal information about stimulus classes (about 12, see above).
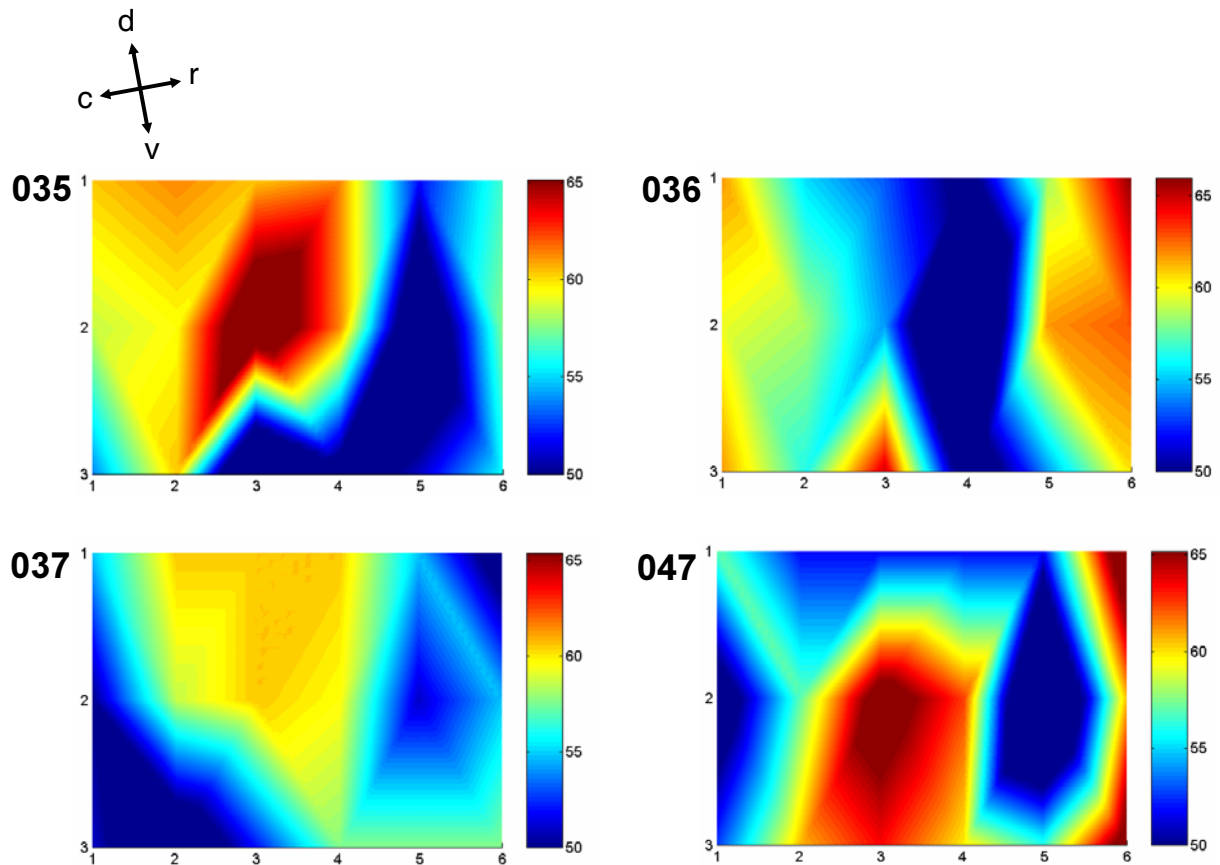
Figure 33: Spatial distribution of classification performance obtained with single recording channels. Training session 7 was selected for analysis, because all animals entered the plateau phase of their learning curves in this session and were thus in a well defined behavioral state (see also figure 16). Data were pooled from the animals (035, 036, 037, and 047), in which late epochs of significant pattern classification were observed in the time between the end of the electrical stimulus and the behavioral response. For each animal, a late cortical activity pattern was identified in the 180 ms time window, from which the maximum significant classification performance was obtained in a late epoch between the end of the electrical stimulus and the median of the hit reaction times. The classification procedure was repeated for each single recording channel. Percent correct classification values at the positions of the recording electrodes corresponding to the recording channels were spatially interpolated. For each of the four analyzed animals, the resulting spatial distribution of single channel classification performance over the two dimensions of 6x3 epidural surface array is displayed in a color plot. Significant pattern classification according to a binomial statistics (percent correct classification values around 65 %) is indicated by the darkest red. Anatomical directions dorsal (d), ventral (v), rostral (r), and caudal (c) are indicated by the orientation cross on top of the figure.
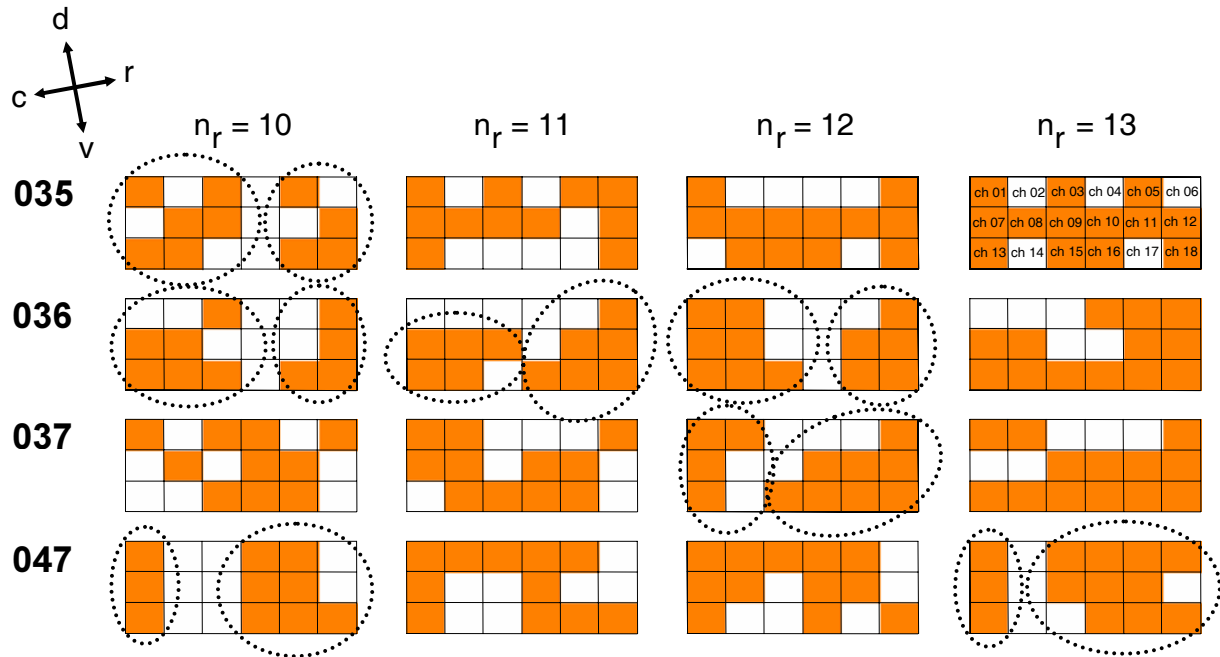
Figure 34: Spatial organization of late cortical activity patterns determined by the spatial arrangement of most discriminating electrodes. Small rectangles represent the electrodes of the 6x3 epidural surface array. Channel indices for each electrode are shown in the upper right panel. Combinations of most discriminating n_r electrodes are marked in orange. Training session 7 was selected for analysis, because all animals entered the plateau phase of their learning curves in this session and were thus in a well defined behavioral state (see also figure 16). Data were pooled from the animals (035, 036, 037, and 047), in which late epochs of significant pattern classification were observed in the time between the end of the electrical stimulus and the behavioral response. For each animal, a late cortical activity pattern was identified in the 180 ms time window, from which the maximum significant classification performance was obtained in a late epoch between the end of the electrical stimulus and the median of the hit reaction times. For each animal and each number of removed electrodes n_r, the most discriminating combination of electrodes was the one which resulted in minimum classification performance in the set of 200 removed electrode combinations. The numbers of removed electrodes (n_r) were chosen about the size of the set of electrodes contributing information about stimulus classes. Anatomical directions dorsal (d), ventral (v), rostral (r) and caudal (c) with reference to the animal are indicated by the orientation cross on top of the figure.

Figure 34 shows the arrangement of electrodes in the 3x6 array with corresponding channel indices given in the top right panel. For each of the four analyzed animals and each n_r, the one combination of electrodes is marked in orange, which was associated with the minimum value of percent correct classification in a set of 200 randomly drawn electrode combinations. Accordingly, this electrode combination contributed maximally to the discriminant power of the spatial pattern. Most discriminating electrodes were always found in connected sets displaying a focal

spatial organization of the late cortical activity patterns. In each animal, at least one of these sets of the size n_r was subdivided into two clusters (marked by dotted circles), one located in the caudal and the other in the rostral part of the 3x6 epidural surface array. The borders of the clusters were separated by two or three interelectrode distances corresponding to 1.2 or 1.8 mm. However, by their location and their spacing to each other, the focal clusters could not be precisely matched to the positions of the stimulation sites. Interestingly, the sets of most discriminating electrodes with different numbers of removed electrodes were not inclusive. This means that in sets of most discriminating electrode of increasing size, i.e. increasing numbers of removed recording channels, the smaller sets were not always subsets of the larger sets (figure 34). This indicates that the spatial information contributing to pattern classification was distributed over a larger set of electrodes than would have been inferred from the focal clusters.

In summary, cortical activity patterns were identified by significant pattern classification in late epochs between the end of the electrical stimulus and the behavioral response. These late cortical activity patterns emerged from the ongoing cortical dynamics in the β- and γ-band of the ECoG. Maximum classification performance in the late epochs was significantly correlated with behavioral discrimination performance, which suggests that the late cortical activity patterns were induced by learning. The spatial organization of the late cortical activity patterns displayed focal clusters. However, there was no clear relationship between the clusters and the site of electrical stimulation.

Significant pattern classification was also obtained from early epochs during the presentation of the electrical stimulus. Early epochs of highly significant pattern classification in the first 100 ms after stimulus onset were time-locked to the electrical stimulus. They were found in all sessions and animals, independent from the learning history of the animals. Significant pattern classification in these early epochs either relied on the topographies of the electrically evoked potentials, which displayed focal patterns around the different stimulation sites in response to CS+ and CS-, or on the spatial variation of the electrical stimulus artifact.

5. Discussion

The following discussion of the results will start with methodological aspects (5.1.). In this section, questions of biosafety of the applied intracortical microstimulation (ICMS) will be addressed (5.1.1.). Also, the proper positioning of the stimulation electrodes in relation to the functional topography of the auditory cortex (5.1.2.) and the difficulties in the analysis of the recorded cortical signals arising from the prominent electrical stimulus artifacts (5.1.3.) will be accounted for. Then, the physiological and biophysical processes leading to cortical activation in response to ICMS will be characterized, and the spatial and temporal specificity of ICMS will be inferred from theoretical considerations (5.2.1.) and from the analysis of electrically evoked potentials (5.2.2.). In the next section (5.3.), the attempt is made to relate the observed behavioral dynamics during discrimination learning of intracortical electrical stimuli to perceptual states underlying the meaningful behavioral interpretation of these stimuli by the animal. In the final sections (5.4., 5.5., 5.6., and 5.7.) it is attempted to go a step beyond the traditional coding approach to cortical neuroprostheses. It will be discussed, how the cortical dynamics further unfolds from the electrically evoked artificial sensory input. Cortical states manifesting in the observed spatiotemporal cortical activity patterns will be referred to sensory and perceptual processes involved in the meaningful behavioral interpretation of the electrical stimuli through discrimination learning (5.4.1.). Patterns emerging from the ongoing cortical activity with the discrimination learning of central, electrical stimuli in the present study will be compared to similar patterns emerging with discrimination learning of peripheral stimuli found by other studies (5.4.2.). Differences observed in the spatial organization of these patterns will be examined. Plastic cortical reorganization induced by learning and by ICMS itself and its role in the formation of cortical activity patterns will be also discussed (5.5.). After the conclusions (5.6.), an outlook is given on future experiments, which are necessary to test the hypotheses derived from the results presented in this work (5.7.).

5.1. Methodological aspects

5.1.1. Tissue reactions to electrode implantation and noxious effects of chronic intracortical microstimulation

Although the study of biosafety of a cortical neuroprosthesis was not in the main focus of this work (Heiduschka & Thanos, 1998), noxious effects of the implantation of stimulation electrodes and chronic intracortical microstimulation (ICMS) were assessed by histological analysis after the termination of the experiments. Such noxious effects could impair the proper functioning of the cortical implant and would have great influence on the results presented here. Small local lesions were found in Nissl stained horizontal sections of the right temporal cortex at the expected locations of the implanted stimulation electrodes. The lesions consisted of agglomerates of densely packed cells. Due to their morphology most of these cells appeared to be glial cells. Glial cells could be easily distinguished from neurons in the Nissl staining, but it was very difficult to differentiate between astrocytes and microglia. As most of the densely packed cells had rather oval shaped nuclei, typical for astrocytes, the agglomerates seemed to consist mainly of astrocytes (Ahrens et al., 1990). Otherwise, the brain tissue within the horizontal sections appeared to be normal at distances more than 0.21 mm away from the centers of the lesions.

In some cases a small lumen remained in the center of the agglomerates, which apparently marked the electrode track. However, most electrode tracks probably collapsed with the removal of the stimulation electrodes, because the brain was not fixated before explantation of stimulation electrodes and Nissl staining. The lesion patterns described above often could be traced over several consecutive sections along the tracks of the stimulation electrodes. Proceeding from dorsal to ventral sections the lesion pattern became more pronounced and vanished then abruptly. In the most ventral sections the lesion sites corresponded well to the expected locations the electrode tips, i.e. the actual stimulation sites.

Traumatic responses of brain tissue to the implantation of needle shaped substrates have been studied with various materials like teflon-insulated platinum-iridium wires (Campbel et al., 1989), silicon probes (Schmidt et al., 1993; Turner et al., 1999, Szarowski et al. 2003) and plastic needles (Stensaas & Stensaas, 1976) by using

traditional histology and immunocytochemical techniques. Independent of the materials used, an encapsulation of the implants by a multilayered sheath of glial cells was observed forming a so called glial scar. In general such glial scars are made up by autologues material, i.e. proteins absorbed onto the surface of the implant (Andrade & Hlady, 1987), reactive astrocytes and activated microglia. To demonstrate histological morphology, most of these studies used hematoxylin and eosin (H&E) staining after perfusion with a fixative like paraformaldehyde or glutaraldehyde. The lesion patterns found in the H&E stained sections in these studies were very similar to the lesions found in the Nissl stained sections prepared from non-fixated brains in the present study. By the immunecytochemical identification of reactive astrocytes and microglia (Turner et al. 1999; Szarowski et al. 2003) it was demonstrated that reactive astrocytes are a major component of the tissue reaction leading to glial scar formation, but that microglia also takes part in this process. Thus, the local agglomerates of cells found in the Nissl stained section of the present study were probably mainly consisting of such reactive astrocytes forming a glial scar.

It was further demonstrated (Turner et al., 1999; Szarowski et al., 2003) that after two or four weeks of implantation reactive astrocytes and microglia formed a loosely organized 50 µm to 100 µm thick sheath around the implant, sometimes consisting of only 2 layers of cells. In regions up to 500 µm away from the implantation site, the numbers of a reactive astrocytes and microglial cells were increased. As they did not find any increase of mitosis in the tissue after implantation, Turner et al. (1999) concluded that the glial cells forming the sheath appeared to have migrated from nearby tissue. Also, a strong adhesion of cells to the implant was found at the first weeks after implantation. After more than 6 weeks after implantation, the glial scar became thinner and more compact, and only a few reactive astrocytes were found in the surrounding region. From that time on, the cells adhered stronger to each other than to the implant. Therefore, it was proposed that the traumatic tissue response may involve to independent processes (Turner et al., 1999; Szarowski et al. 2003): An early reaction is initiated by the damage of brain vasculature or other cellular damage due to the insertion of the implant. This early process is dependent on the implant size, its shape, its surface and the insertion method. After about 2 weeks, a sustained active process comes into play, which maintains a compact glial scar, independent of the magnitude of the early reaction.

All histologically analyzed animals in the study presented here had been carrying their implant for less than 6 weeks. According to the results reviewed above, glial scar formation was likely to be in its initial phase in these animals. Accordingly, the local agglomerates of cells found in the Nissl stained sections of the present study were loosely organized having only a few layers of cells. Interestingly, an elevated density of glial cells was found in the tissue surrounding the glial scar often forming "fingers" protruding from them. This histological pattern possibly reflected the migration of reactive astrocytes towards the glial scar. Also brain tissue was sometimes ruptured after explantation, indicating a strong adhesion of cells to the implanted stimulation electrode, as it was found in the early phase of glial scar formation by Turner an colleagues (1999).

Besides the lesions induced by the implantation of stimulation electrodes, prolonged ICMS can also lead to tissue damage (Agnew et al., 1986). The threshold of electrical simulation causing neural injury is determined both by the charge density at the surface of the stimulation electrode and by the amount of charge injected per phase (McCreery et al. 1990). Agnew and coworkers (1986) histologically evaluated neural damage occurring with ICMS. Identical to the present study, they used charge balanced biphasic current pulses with a phase-duration of 200 µs, and delivered the pulses through platinum-iridium electrodes with a surface area of 0.002 mm^2. Current pulses were continuously applied at a rate of 20 pps for 23 hours per day over 7 days. Even down to the level electron microscopy, no structural changes were found in the brain tissue with amounts of current below 80 µA, which corresponded to a charge density of 8000 nC/mm^2 and an amount of charge of 16 nC/phase. However, neural damage occurred with an amount of current of 320 µA (32000 nC/mm^2, 64 nC/phase) as it was determined from histology showing shrunken neurons, widespread extracellular edema and swollen axons and dendrites.

With amounts of current always below 80 µA, ICMS in the present study could be regarded as save. Accordingly, no changes of neuronal morphology were found around the stimulation electrodes in the present study that were comparable to those found by Agnew and coworkers (1983; 1986) with higher amounts of current. The rim of reduced neuronal cell density around the glial scar, sometimes seen in the present study, could be due to neuronal cell death resulting from toxic products of irreversible electrode reactions (Brummer et al., 1983) or from neuronal hyper-excitation in

response to the applied trains of current pulses, but reduced neuronal densities were also reported around implanted substrates without electrical stimulation (Edell et al., 1992).

In the present study, neural damage to prolonged ICMS seemed to be rather small, although noxious effects of ICMS could not be separated from the glial scar formation induced by the implantation of the stimulation electrodes Recent studies in the auditory cortex of cats (Rousche & Normann, 1999) and in the visual cortex of the macaques (Troyk et al. 2003) applied ICMS with stimulus parameters very similar to those of the present work (15 nC/phase and 9535 nC/mm^2 for the standard stimulus in Rousche & Normann, 1999). Neural activity could be recorded in these studies before and after multiple stimulation sessions over months. This indicates that many of the cortical neurons in the vicinity of the stimulation electrodes remained intact even after prolonged ICMS. In conclusion, the lesion patterns reported in the present study seemed to mainly reflect the glial scar formation in response to the chronically implanted stimulation electrodes.

To address the important question of the biosafety of a cortical neuroprosthesis, a more detailed analysis of the reaction of brain tissue to electrode implantation and chronic intracortical microstimulation is necessary. This would afford a more refined histological analysis than can be achieved by Nissl staining, e.g. by employing immunehistochemical techniques.

Finally, it should be noted that functional impairment of brain tissue can already occur with charge densities and amounts of charge which are not accompanied by histological damage. McCreery and coworkers (1986; 1997; 2002) demonstrated that the excitability of neurons can be largely reduced already with amounts of currents well below the thresholds of histological damage. After prolonged electrical stimulation, thresholds of neural excitation remained elevated for several days, although they finally returned to control levels when the amount of current had been kept below the thresholds for histological damage. Such a reduction of excitability, even when occurring transiently, can have a strong influence on the functioning of a cortical neuroprosthesis. Therefore, these effects should be monitored in future experiments by determining the thresholds of electrically evoked potentials before and after the continuous presentation of electrical stimuli, e.g. before and after each training session during which ICMS is applied.

5.1.2. Positioning of the electrodes

In the present study, it was tried to separately activate populations of neurons in the input layer IV at two different sites along the tonotopic gradient of primary auditory cortex AI (Thomas et al., 1993; Scheich et al., 1993). As the functional properties of neural responses could not be determined from recordings during the implantation procedure, anatomical landmarks were used to position the electrodes. Histological analysis after the termination of the experiments showed that in four animals the stimulation electrodes, as intended, were located in close radial proximity of layer IV along the rostrocaudal tonotopic gradient of the primary auditory field AI. In three of these animals (035, 038 and 047) the rostral stimulation electrode was close to the common high frequency border of the primary auditory field AI and the anterior auditory field AAF. Thus a direct excitation of AAF through rostral electrodes could not be excluded in these animals. However, in two animals (038 and 046) it was unclear whether the stimulation electrodes were properly positioned within AI due to their large ventral offset along the dorsoventral axis. Additionally, in animal 046, the electrodes were found at a radial depth medial to layer IV corresponding to the border between layers V and VI.

With one exception (037), all interelectrode distances were found between 0.6 and 0.7 mm as expected from the spatial arrangement of the stimulation electrodes in the 2x1 array. Spatial resolution in AI has been shown to be about 0.4 mm per octave for frequencies smaller than 1 kHz and about 0.2 mm per octave for frequencies larger than 1 kHz (Thomas et al., 1993; Scheich et al., 1993; Budinger et al., 2000a). Accordingly, the interelectrode distances included about two or three octaves within the frequency representation of AI, with frequencies increasing from positions of the caudal to the rostral stimulation electrode. In animal 037 an interelectrode of about 1.0 mm was found being larger than it was expected from the layout of the 2x1 array. Apparently, the stimulation electrodes were deformed during the process of implantation in this animal.

Clearly, electrode positioning could be improved by recording neural activity from the stimulation electrodes in the depth of cortex. The tuning properties of neurons determined from single- and multiunit recordings could be used to guide the stimulation electrodes to specific isofrequency contours of AI (Thomas et al., 1993).

The radial cortical depth along the tangential track of the stimulation electrodes could be inferred from polarity inversions of the acoustically evoked potential during electrode implantation.

The position of the 3x6 epidural surface array for recording the electrocorticogram (ECoG) could not be determined from the histology of the present work. The positioning of the 3x6 recording array on the epidural surface could be improved by determining the spatial topography of the P1 and N1 component of the pure-tone-evoked potential, which reflects the tonotopic organization of AI in the Mongolian gerbil (Ohl et al., 2000a).

5.1.3. Electrical stimulus artifacts in the electrocorticogram (ECoG)

Delivery of current pulses through a stimulation electrode leads to fast voltage changes at the input of the amplifiers and their analog filters resulting in an impulse response at their output, which is superimposed as an artifact on the ECoG recording. In the worst case, the amplitudes of these voltage changes are so large that the amplifiers leave their linear range of operation resulting in temporally extended complicated artifact waveforms. It also should be noted that digital filtering can temporally extend the artifact, depending on the length of the filter kernel used.

Electrical stimulus artifacts are a great obstacle to the analysis of neural activity during intracortical microstimulation. For this reason, most of the analysis presented here was carried out in the time after the end of the electrical stimulus. As it can be seen from the temporal and spatial ensemble averages of the ECoG (see section 4.5.), the delivery of a biphasic current pulse, either as single pulse or within a pulse train, was accompanied by an electrical stimulus artifact in the ECoG. The artifacts could not be separated from the physiological response to the electrical stimulation by the ECoG ensemble averages alone. However, due to its invariance and its temporal properties, a characteristic waveform was considered an electrical stimulus artifact. The waveform consisted of a fast negative peak invariantly followed by a slower positive peak with the whole waveform lasting less than 10 ms.

In order to investigate neural activity during the delivery of intracortical microstimulation the electrical stimulus artifact has to be removed at early stages of

data analysis. For a successful artifact removal, it is necessary to record the artifact within the operating range of the amplifiers, without clipping them. As this was not always the case in the recordings of the present study, artifact rejection was precluded. If the artifact can be fully recorded together with the neural signal, there exist many different strategies to remove the artifact waveforms. At first the artifact has to be reconstructed, e.g. by fitting exponential functions to artifact segments (Harding, 1991), by peak detection algorithms (O'Keefe et al., 2001), by independent component analysis (Jung et al, 2000), or by building a template (Hashimoto et al., 2002). Then the reconstructed artifact can be subtracted them from the recording. In any case, the electrical stimulus artifact has to be minimized by optimizing the recording reference. Also the artifact itself should be analyzed to a greater detail. For this, it is necessary to record the electrical stimulus artifact separately from any physiological response within saline or even better from inactive brain tissue.

5.2. Spatial and temporal specificity of intracortical microstimulation (ICMS)

To determine the spatial and temporal specificity of ICMS in relation to the functional organization of the cortex is of great importance, not only for the proper coding of electrical stimuli. It is equally important in the study of the interaction between ICMS and the ongoing cortical dynamics, as it characterizes the artificial sensory input imposed onto the ongoing cortical activity from which the cortical dynamics further unfolds. Neural activation in response to ICMS depends on two major processes: the direct excitation of neural elements due to the effective current spread and the transsynaptic activation of populations of neurons caused by these directly excited neural elements.

5.2.1. Direct neural excitation in response to intracortical microstimulation

Which elements are excited in electrical stimulation of the mammalian central nervous system (CNS)? Although already posed more than 20 years ago in a paper by Ranck (1975), there is still no fully satisfactory answer to this question. According

to Ranck (1975), the process of excitation by extracellularly applied electrical stimuli is not trivial often leading to counterintuitive results, as a given current pulse can both excite and block neural activity. One of the first, who devised a quantitative model of excitation caused by extracellular electrical stimulation in the CNS was Rattay (1998). He simulated direct neural excitation by using multi-compartment models of neurons showing that the most excitable part of the neuron to a given applied field is the myelinated axon. This had been already suggested in earlier experimental studies (Gustafson & Jankowska, 1976). The most important factors for the direct excitation in this theoretical study were the geometry of the neuron and its position and orientation relative to the electrode.

Direct excitation of neural elements was not observable by the type of recordings made in the present study. Hence, the spatial specificity of direct excitation was characterized by a theoretical estimate of the effective current spread (Tehovnik, 1996), i.e. the distance from the stimulation site within which neurons of a certain threshold are excited by a single electrical current pulse (see subsection 3.2.). Stoney and colleagues (1968) studied current-distance relationships in detail by recording action potentials from pyramidal tract neurons of cats in response to ICMS. In accordance with earlier studies (Asanuma & Sakata, 1967), they found that the amount of current needed for the direct excitation of a neuron is proportional to the square of the distance between the neuron and the electrode tip. They also determined the constants of proportionality, the so called current-distance constants, which is direct proportional to the thresholds of neural excitation. The estimation of effective current spread in the present study relied on the current-distance constants found by Stoney and colleagues (1968) assuming that the range of these constants is basically the same in the auditory cortex of the Mongolian gerbil and in the motor cortex of the cat. With an effective current spread ranging between 0.43 mm and 0.51 mm for low-threshold neurons in the present study and an interelectrode of about 0.7 mm, there was a considerable spatial overlap between populations of low-threshold neurons activated through the caudal or the rostral stimulation electrode. Further, assuming a cortical cell density of about 40000 neurons/mm^3 (Braitenberg & Schütz, 1998), between 290 and 460 high-threshold neurons and between 13322 and 22226 low-threshold neurons were activated by a single current pulse delivered

through one of the stimulation electrodes (Tehovnik, 1996). However, this estimate makes only sense under the premise that it was cells or their axon initial segments that were directly excited by the ICMS.

Recent advances in the question of direct neural excitation have been made by Nowak and Bullier (1998a, b) studying ICMS in slices of rat visual cortex. From analyzing chronaxies (see section 2.4.) of electrically evoked neural responses (Nowak & Bullier, 1998a) and from pharmacological blocking experiments (Nowak & Bullier, 1998b), they concluded that mainly axonal branches were directly excited by ICMS, whereas axonal initial segments contributed much less to the directly evoked neural responses.

In cortical grey matter, axonal fibers are much more abundant than axon initial segments. Thus, it is likely that ICMS in the present study to a large extent excited axonal fibers masking the excitation of layer IV axon initial segments. The fibers that terminate in layer IV are mainly of thalamic origin, and their excitation would lead to a transsynaptic activation similar to thalamic input. However, it is likely that also fibers bypassing the stimulation site were excited. The action potentials evoked in a conglomerate of such fibers would activate postsynaptic neurons both in the orthodromic and in the antidromic direction of the fibers by invading their axonal branches, although antidromic evasion seems not to play a major role in the generation of excitatory cortical activity in response to ICMS (Butovas & Schwarz, 2003). According to the interconnectivity of the cortex, action potentials would then spread widely via radial connections to superior and infragranular layers, to other cortical (Budinger et al., 2000a) and subcortical (Budinger et al., 2000b) areas, and, via intrinsic horizontal connections, to other sites within the cortical area. Thus, ICMS at a specific point in space leads to a spatially extended activation conveyed by a conglomerate of directly excited excitatory and inhibitory axonal fibers (Butovas & Schwarz, 2003). In this way, the spatial specificity of ICMS is rather determined by the intrinsic cortical connectivity than by the effective current spread.

The temporal specificity of direct neural excitation itself is largely determined by the membrane time constants of the excited neural elements, which are primarily the axonal branches (Nowak & Bullier, 1998a, b). Temporal summation, as it likely occurs with the trains of current pulses applied at high pulse rates in the present study, depends on these time constants. The chronaxie of direct neural activation is

related to these membrane time constants (see section 2.4.) and should be determined in future experiments from strength-duration curves measured by single pulse electrically evoked potentials.

5.2.2. Transsynaptically evoked activity in response to intracortical microstimulation

Although directly excited activity in axonal branches can in principle contribute to the potential fields recorded from the epidural surface, the electrically evoked potentials reported were probably generated dominantly by neural activity postsynaptic to these directly excited elements. This is because synaptic currents flowing through the dendrites of cortical pyramidal neurons are the main source of the ECoG recorded from the cortical surface (Mitzdorf, 1985).

Electrically evoked potentials in response to single current pulses were recorded before the start of the training procedure. A typical waveform was observed for these potentials which resembled a frequency modulated damped oscillation with rapidly decaying amplitude and a frequency decreasing from about 80 Hz to about 20 Hz within the first 150 ms after the delivery of the current pulse. Thus, an electrical stimulus delivered at a well defined point in time already lead to a temporally extended cortical response. Such impulse responses of cortical systems are well understood on theoretical grounds (Freeman, 1975). Accordingly, the oscillatory waveforms found in response to single pulse electrical stimulation can be explained by closed loop feedback interaction within and between sets of mutually connected excitatory and inhibitory neurons. The temporal characteristics of the resulting oscillations are governed by the activity dependent gains of the different limbs of the feedback loops (Freeman, 1975), which are related to the delays and the efficacies of axonal and synaptic conveyance between the neuronal sets.

Studies on cortical evoked potentials in response to intracortical microstimulation (ICMS) are rare (Bishop & Clare, 1953). On the other hand, potentials evoked by electrical single pulse stimulation of the cortical surface have been studied extensively (Creutzfeldt et al., 1966). The generators of this so called direct cortical response (DCR) (Adrian, 1936) have been determined from their radial profile by

current source density (CSD) analysis (Mitzdorf, 1985; Barth & Sutherling, 1988; Barth & Di, 1991a; Harding, 1992). The results of these studies somewhat diverge from each other, which might be related to the difficulty of properly controlling the effective current spread by electrical stimulation applied to the cortical surface. According to Barth and coworkers (Barth & Sutherling, 1988; Barth & Di, 1991a), the generation of the DCR starts with a fast excitatory input to proximal parts of supragranular pyramidal apical dendrites reflected by a positive wave (DCR-P1) around 5 ms after pulse delivery. This is followed by a fast excitatory synaptic input to distal apical dendrites of supra- and infragranular pyramidal cells in the rising phase of the short latency large negative wave of the DCR (DCR-N1). This fast excitatory input is subsequently displaced by a recurrent inhibition of infra- and maybe also supragranular cell bodies at the peak and in the falling phase of the DCR-N1 lasting to about 25 ms post-stimulus time. It follows a positive wave (DCR-P2) in the DCR generated either by afterhyperpolarization of distal apical dendrites or late recurrent excitation of proximal apical dendrites. A superimposed inhibitory input to deeper lying infragranular cell bodies and basilar dendrites gives rise to a slow negative wave (DCR-N2) with a longer latency lasting up to 200 ms after pulse delivery. Similar response sequences consisting of early excitation, feed-forward and feedback inhibition, and rebound excitation were also found with short peripheral stimuli (Barth & Di, 1991b) and are archetypal for neocortical pyramidal neurons (Steriade, 1984).

The waveform of the potentials evoked by single pulse ICMS in the present study was highly similar to the waveform of the DCR reported in the literature (Barth & Sutherling, 1987; Barth & Dia, 1991a; Harding, 1992). A short latency positive wave around 5 ms after pulse delivery corresponding to the DCR-P1 was difficult to detect, because it largely interfered with the electrical stimulus artifact. According to their peak latencies, peak amplitudes, and peak widths relative to each other, the following short latency negative wave with a large peak around 12 ms after stimulus onset and the smaller and slower positive wave with a peak latency of about 20 ms probably corresponded to the DCR-N1 and the DCR-P2, respectively. The subsequent negative wave resembled the DCR-N2. This close similarity in the waveforms suggests that the sequence lying at the source of the electrically evoked potentials in response to single pulse ICMS consisted of a similar sequence of excitation and inhibition as in the DCR. Preliminary results from CSD analysis in the primary

auditory cortex of the Mongolian gerbil (Breindl, 2001) provide some evidence for this. In a recent study of Butovas and Schwarz (2003), a similar sequence of excitation and inhibition was found at the single neuron level by recording single and multiunit responses to near-threshold ICMS from the rat somatosensory cortex. A short latency excitation consisting only of a single spike or a doublet of spikes was invariably followed by an inhibition with a fixed duration of 100 ms to 150 ms. Sometimes, with stronger stimulation, a variable rebound excitation occurred after the inhibition that could last for several hundreds of milliseconds.

The short latency negative wave of the electrically evoked potential in response to single pulse ICMS reflected the early transsynaptic activation within the cortex. The topography of its peak amplitude most often displayed a single focus of activation. In such cases, the spatial activity focus was colocalized with the position of the stimulation electrode delivering the current. The focus of activation extended over distances between 0.6 mm and 1.8 mm from the stimulation site corresponding on average to 3 octaves in the low-frequency range and to 6 octaves in the high-frequency range of the tonotopic gradient of AI (Thomas et al., 1993; Scheich et al., 1993; Budinger et al., 2000a). Thus, the spatial extent of the short latency negative peak in the electrically evoked potential exceeded the theoretically estimated effective current spread, which maximally ranged over a distance of 0.51 mm. Interestingly, axon collaterals of pyramidal neurons in the primary sensory cortices extend over about 1.5 mm (Szentagothai, 1975). The direct excitation of these axon collaterals could therefore account for the spatial extent of the short latency negative peak. This corresponds to the view that the spatial specificity of early transsynaptic activation within the cortex in response to ICMS is rather determined by the intrinsic cortical connectivity than by the effective current spread. Yet, it should be noted that the true spatial extent of the electrically evoked activity in the depth of the cortex was probably overestimated by the electrically evoked potentials recorded from the cortical surface due to distortions by volume conduction (Freeman, 1980). Also, the spatial spread of later parts of the electrical stimulus artifact might have contributed to the observed foci of activation (see subsection 5.1.3.). However, a study at the level of single neurons in the somatosensory cortex of the rat demonstrated that even at stimulus intensities near threshold significant excitatory neuronal activation can be found over distances up to about 1.35 mm from the stimulation site (Butovas & Schwarz, 2003). Significant inhibitory effects in the

single and multiunit recordings were found up to 1.80 mm around the stimulation site near threshold. These distances were independent of the anatomical direction, did not reflect any patchiness of the intrinsic horizontal connectivity of the cortex, and the time course of activation did not significantly change over these distances. The spatial range of the focal activation found for the short latency negative peak in the electrically evoked potential corresponded to the spatial range activation reported by Butovas and Schwarz (2003) at the single neuron level, despite the fact that the amounts of current applied in the present study were well above threshold and at a factor of about 10 higher as in the study of Butovas and Schwarz (2003). A possible explanation for this rather constant spread of electrically evoked activity with largely varying amounts of current could be the postsynaptic interplay of directly excited excitatory and inhibitory fibers. A wider effective current spread with larger amounts of current leads to a wider spread of direct electrical excitation carried both by excitatory and inhibitory axonal fibers. The resulting wider spread of inhibition could thereby spatially restrict the wider spread of excitation at the postsynaptic side (Butovas & Schwarz, 2003). This again suggests that the intrinsic cortical connectivity was the major determinant of the spatial spread of early transsynaptic activation evoked by ICMS in the cortex. Though, differences in cortical areas under study and species specific differences between the rat and the Mongolian gerbil might complicate the comparison between the findings in the present study and the findings by Butovas and Schwarz (2003).

For the short latency negative wave in the single pulse electrically evoked potential, the distance between the spatial maxima of focal activity evoked at stimulation electrode S1 and S2 corresponded to the interelectrode distance of about 0.7 mm. As already discussed (see subsection 5.1.2.), these distance includes about two or three octaves along the tonotopic gradient of AI, with frequencies increasing from positions of the caudal to the rostral stimulation site. According to the spatial extent of the activity foci, there was a considerable spatial overlap between early transsynaptic activation evoked at stimulation electrode S1 and S2.

In two cases the topography of the short latency negative peak in the electrically evoked potential displayed two foci of activation distributed along the rostrocaudal axis of the auditory cortex. The locations of the foci could not be referred to any of the two stimulation electrodes. Possibly, the excitation of bypassing horizontal fibers

connecting different patches along rostrocaudal axis of AI lead to these two foci of activation. Alternatively, the excitation of homotopic connections passing by the stimulation site could have evoked focal activity in AI and a neighboring cortical field (Budinger et al., 2000a, b).

The topography of the smaller positive peak in the electrically evoked potential at about 20 ms after pulse delivery, which followed the short latency negative peak, was difficult to interpret. Between one and three foci were found in the spatial activity distributions. In most cases no apparent relationship could be determined between stimulation sites and the locations of the foci. For a clear interpretation of the activity foci found in the topography of the different peaks in the electrically evoked potential, the functional anatomy of the cortex beneath the epidural recording array should be determined in future experiments, e.g. by recording acoustically evoked potentials in response to different pure-tones (Ohl et al.,2000a).

Electrically evoked potentials in response to trains of current pulses applied as CS+ and CS- during training were difficult to analyze due to the large electrical stimulus artifact. However, the fast artifact waveforms were apparently superimposed to a slower waveform, which was considered as an electrically evoked potential. The single current pulses of a train were not accompanied by evoked components that could have been attributed to a single pulse evoked potential. Instead a slower frequency modulated damped oscillation was observed with frequencies decaying form about 20 Hz to about 5 Hz. A large negative peak around 30 ms after stimulus onset was followed by positive and negative peaks of decaying amplitude. Sometimes this oscillation outlasted the train length. The overall waveform was similar to that obtained from stimulation with single current pulses, but it was larger in amplitude and temporally dispersed. At the single neuron level, Butovas and Schwarz (2003) showed that with pulse trains at rates higher than 10 pps, inhibition formed an almost uniform continuous background from which the fast excitatory responses to each pulse in the train could be clearly separated. At the higher pulse rates (100 pps) and with the higher amounts of currents applied in the present study, the potentials evoked by trains of current pulses were presumably generated by the temporal summation of fast excitatory events in response to each single pulse. The observed decay of the peak amplitudes eventually reflected an inhibitory background increasing over the length of electrical pulse train. A possible mechanism for this

could be the stronger depression of excitatory synapses than of inhibitory synapses with prolonged electrical stimulation as it was observed in slices of the rat neocortex (Galaretta & Hestrin, 1998). That in some cases the electrically evoked potential outlasted the pulse train for about 500 ms, could be explained by afterhyperpolarizations, and/or by afterdischarges as they were found in response to ICMS at the level of single neurons (Butovas and Schwarz, 2003). The spatial maximum of the negative evoked peak in the electrically evoked potential around 30 ms after the onset of the pulse train seemed to be colocalized with the stimulation site, although a detailed analysis of its topography was again precluded by the large electrical stimulus artifact. A possible relationship between the observed slight increase in overall amplitude of the electrically evoked potentials over training sessions to ICMS induced plastic reorganization of the cortex will be discussed below (see subsection 5.5.)

The findings reported above indicate that ICMS, although spatially and temporally confined, lead to a spatiotemporal "blur" of transsynaptically evoked activity caused by the direct excitation of conglomerates of fibers of passage (see section 5.2.). The major determinant of the spatial and temporal specificity of ICMS thereby seemed to be the intrinsic cortical interconnectivity, i.e. the projection range and geometry of the directly activated excitatory and inhibitory axonal fibers and the postsynaptic interplay between excitation and inhibition succeeding direct electrical excitation (Butovas & Schwarz, 2003). This resulted in a considerable spatial overlap between neuron population transsynaptically activated at the two different stimulation sites within the auditory cortex.

5.3. Meaning and perceptual relevance of intracortical electrical stimuli

Although the meaning of stimuli can be experienced only by a perceiving, conscious subject and cannot be measured directly, it can be indirectly inferred from the use of the stimuli for the successful adaptation to the environment in a behavioral context. Cortical activity related to the meaningful interpretation of the stimuli by the animal often makes only sense, when the behavioral context, i.e. the learning history, the

127

expectation, the attentiveness and the motivation of the subject is sufficiently controlled. For this reason the investigation of the interaction between ongoing cortical dynamics and intracortical microstimulation (ICMS), in the present study, was carried out in freely behaving learning animals.

Despite the considerable overlap of neuron populations transsynaptically activated at the low- and the high-frequency sites along the tonotopic gradient of the auditory cortex, the animals were able to behaviorally discriminate between intracortical microstimulation (ICMS) applied to the one or the other site. From the increase of the hit responses relative to the false alarm responses in the learning curves, it was concluded that all animals learnt this discrimination within four or five sessions of training. However, the GO/NO-GO avoidance paradigm employed here had the drawback that in contrast to the CS+ the animals could only passively avoid the CS- by staying in their shuttle-box compartment. Therefore, the low false-alarm-rate could have simply reflected the behavioral ineffectiveness of the electrical stimulus applied as CS-. However, the biphasic time course of the false-alarm rates found in most of the animals indicates that these animals generalized between CS+ and CS- during early training sessions. This demonstrates that the animals were generally able to behaviorally respond to the CS-. The successful retraining of two animals after a contingency reversal also shows that the animals could make use of ICMS at both stimulation sites. Thus, the GO and the NO-GO responses leading to an avoidance of US and error shock were apparently part of a discrimination strategy acquired by the animal within the first four or five sessions of training (Stark et al., 2004). Altogether, from the analysis of discrimination learning it can be inferred that the animals were able to behaviorally interpret the intracortical electrical stimuli in a meaningful way.

Discrimination performance measured by the discriminability index d' increased over sessions. With the fourth or fifth session, it exceeded the value of one, at the same time when the animals showed significantly larger hit-rates compared to false-alarm rates for the first time. In session 7, the learning curves of most of the animals reached a plateau phase. Though, discrimination performance measured by the discriminability index d' did not seem to approach an upper asymptote indicating that the animals could have further improved their discrimination performance with extended training. Two animals (038 and 046) showed a slightly different learning

dynamics with a delayed increase of discrimination performance. Interestingly, the positions of the stimulation electrodes in these animals could not be clearly assigned to the primary auditory field AI according to their large ventral offset along the dorsoventral axis (see subsection 5.1.2.). Additionally, in animal 046, the stimulation electrodes were located medially distant to layer IV at the border of layer V and VI. Although both animals finally reached significant discrimination performance, the activation of neural elements different from those activated by the stimulation electrodes positioned close to layer IV within AI in the other animals had a measurable behavioral effect, as can be seen from the delayed learning dynamics.

The behavioral part of the study presented here was largely based on the work of Scheich and Breindl (2002). Using a similar preparation and a similar behavioral paradigm, they demonstrated that Mongolian gerbils can rapidly learn to discriminate two sites of electrical stimulation within their primary auditory cortex at an interelectrode distance of about 1.0 mm. Whereas the animals used by Scheich and Breindl (2002) were deafened before the start of the training procedure, the present study was carried out with normal hearing animals, because auditory deprived Mongolian gerbils often show behavioral abnormalities when trained over a longer period, e.g. largely increased spontaneous compartment changes. Comparing the learning curves of deafened and normal hearing animals, no major differences were found suggesting that the deaf and normal hearing animals relied on the same cues to solve the task. This is supported by the finding that in human subjects, electrical stimulation of visual and auditory cortex evokes qualitatively similar sensations in blind and normal sighted subjects or in deaf and hearing subjects, respectively (Dobelle et al., 1973; Bak et al., 1990; Schmidt et al., 1996).

Behavioral discrimination of different cortical stimulation sites has also been demonstrated by earlier studies (Grosser and Harrison, 1960). For example, Doty and his coworkers have extensively studied conditioned behavioral responses to electrical stimulation at the surface and in the depth of various cortical areas of the cat and the Macaque (Doty et al., 1956; Doty, 1965). In the macaque Doty (1965) showed that the animals were able to discriminate between electrical stimuli applied at different sites within a cortical area less than 1 to 3 mm apart. Successful discrimination learning was obtained from stimulation sites within visual, auditory, inferiotemporal and prefrontal cortical areas.

Charge per phase thresholds for the detection of ICMS in the Mongolian gerbil are not known, but such thresholds have been recently determined for the cat primary auditory cortex by Rousche and Normann (1999). In their study, trains of current pulses were delivered through single electrodes of an Utah Intracortical Electrode Array (UIEA) consisting of multiple penetrating silicon micro-electrodes coated with platinum at their tips. Using trains of current pulses (150 µs phase duration, 100 µs inter-phase interval, 250 pps pulse rate and 0.6 s train length) thresholds were found to be about 10 nC/phase on average with a minimum of 1.5 nC/phase and a maximum of 26 nC/phase. The parameters of ICMS used by Rousche and Normann (1999) were very similar to those used in the present study allowing for a good comparison with respect to charge density and amount of charge delivered through the stimulation electrodes. Charge levels in the present study were chosen between 10 nC/phase and 14 nC/phase, which is close to the threshold levels found by Rousche and Normann (1999). However, Rousche and Normann (1999) stated that their behavioral paradigm seemed to have produced somewhat elevated thresholds. Although possible species specific differences between cat and gerbil auditory cortex make a precise comparison quite difficult, charge levels applied in the present study were most likely set to the lower suprathreshold range (see section 2.4.).

Discrimination learning with acoustic stimuli was investigated in Mongolian gerbils by using a GO/NO-GO avoidance paradigm similar to the present study (Wetzel et al., 1998b; Ohl et al., 1999). With the asymptotic increase of the hit-rates and the biphasic time course of the false-alarm-rates, the shape of the learning curves found in these studies was similar to the shape of the learning curves reported in the present study. However, discrimination learning of simple tones or rising versus falling frequency-modulated tones seemed to be faster, as significant discrimination performance was often found already with the second or third session of training in these studies. In the present study, transient break-ins of learning performance were occasionally observed during a single session in the course of training. This was also found during acoustic training. Thus, the observed transient break-ins of learning performance seem to be inherent to the formation of a discrimination strategy and could be related to a revaluation of the task by the animal (Stark et al., 2004).

The rapid learning of the animals suggests that ICMS at different sites within AI induced percepts that were immediately discriminable after the animals had learnt the procedural aspects of the task, e.g. changing the shuttle-box compartments. Although crucial, the question about the subjective quality of the electrically evoked percepts is difficult to tackle. The possibility that the discrimination performance of the animals in the present study relied on pain, as it can result from the stimulation of pain receptors in the dura mater and the cerebral blood vessels (Doty et al., 1956), can be ruled out by the fact, that the response rates to the CS- remained very low. This indicates that the CS- was not aversive in itself, as it would have been expected with a painful stimulus.

Several studies have shown that animals can make use of electrical stimulus attributes different from stimulation site. For example, Scheich and Breindl (2002) demonstrated that Mongolian gerbils can learn to discriminate electrical stimuli with different temporal structure by using upward and downward rate-modulated trains of current pulses as CS+ and CS-, respectively. Furthermore, the Mongolian gerbils were able to learn to discriminate a sequence of short pulse trains (100 pps constant rate, 0.3 s train duration) delivered subsequently to two cortical stimulation sites from the reverse sequence. Also, in secondary cortical areas like visual area MT, ICMS can influence perception. For example, Salzman et al. (1990) found that perception of the direction of a moving stimulus could be biased by ICMS towards the direction to which the MT neurons at the site of stimulation were tuned (see also Cohen & Newsome, 2004 for a review).

Carrying out transfer learning experiments, Scheich and Breindl (Scheich & Breindl, 2002; Breindl, 2001) suggested that ICMS in the auditory cortex evokes modality-specific auditory percepts. Normal hearing animals were trained to detect ICMS within auditory cortex until they reached a 75% response criterion over 6 consecutive sessions. After this pre-training, ICMS in auditory cortex was replaced by ICMS applied to the visual cortex in one group of animals. In the other group, ICMS within auditory cortex was replaced by a sequence of six tones (1 kHz , 0.7 s tone duration). Animals transferred to tone stimulation retained the 75% criterion level within 10 trials after a slight decrease in response rate. Although ICMS applied to the visual cortex had been shown to be equally effective as ICSM in the auditory cortex, the response rate in animals transferred to visual cortex stimulation dropped

to 30 % and remained there for at least 30 trials. Thus, the percept evoked by ICMS applied to the auditory cortex appeared to be more similar to a percept evoked by acoustic stimulation than to a non-specific percept or a percept polysynaptically evoked in another modality (Breindl, 2001).

The question remains which kind of perceptual cues the animals used for the discrimination of the two different sites of ICMS within auditory cortex. Although reports on sensations evoked by electrical stimulation of the human auditory cortex are rare, a few subjects have described sensation evoked by electrical surface stimulation of Heschl's gyrus or of the lateral superior temporal gyrus as "buzzing", "knocking", "humming" or "wavering" (Penfield & Perot, 1963; Howard et al., 2000). Varying with the site of electrical stimulation, the spectral quality thereby seemed to be the most salient aspect of these sensations (Dobelle et al., 1973; Brugge, personal communication). In the present study, ICMS applied as the CS+ and the CS- was directed towards sites representing different frequencies along the tonotopic gradient of AI. Thus, it could well be that the animals exploited some kind of place pitch as a cue for discrimination learning. Although the amount of current at the two stimulation electrodes was adjusted to yield similar electrically evoked potentials, the possibility remains that the electrical stimuli evoked sensations at different intensities. Therefore, the animals could have rather relied on an intensity discrimination than on a pitch discrimination. However, this seems unlikely, as several studies have shown that animals readily generalize a conditioned response to cortical stimulation to a variety of stimulus intensities (Doty, 1969; Rousche et al. 2003). For example, Rousche et al. (2003) investigated the dynamic range of ICMS within rat auditory cortex by measuring behavioral generalization gradients. Animals trained to detect an electrical stimulus of 90 µA thereby showed high generalization to an untrained test stimulus of 70 µA.

In order to uncover the nature of the perceptual cues used by the animals in the discrimination learning of intracortical electrical stimuli, one could measure the perceptual similarity between electrical and peripheral stimuli by determining their generalization gradients along different stimulus dimensions. Romo et al. (2000), for example, were able to demonstrate that in monkeys, trained to discriminate the difference in frequency between two mechanical flutter stimuli delivered sequentially on the fingertips, the psychophysical performance was nearly unchanged when flutter

stimuli were replaced by ICMS applied without training to the somatosensory cortex at the same rate as the fluttering rate of the mechanical stimuli. Yet, with a few exceptions (Romo et al., 2000; Breindl, 2001; Scheich & Breindl, 2002), experiments involving generalization between cortical electrical stimulation and peripheral stimuli have been rather unsuccessful (Doty & Rutledge, 1959; John & Kleinman, 1973). Troyk and colleagues (2003) have recently demonstrated that in macaques trained to make saccades towards illuminated spots in the visual field, the visual stimuli could be replaced by ICMS applied to the visual cortex. The endpoints of the ICMS induced saccades in the visual field were correlated with the receptive field locations of the neurons recorded from the stimulation electrode. However, there was no immediate generalization between visual and electrical stimuli, as the animals needed about two weeks to relearn the task after being switched from visual to electrical stimulation. The failure of most transfer learning experiments might be due to subtle differences in the percepts emerging from peripheral and intracortical electrical stimuli. Also, transfer learning experiments are highly prone to flaws (John & Kleinman, 1973). Another opportunity to investigate the perceptual scaling of intracortical electrical stimuli is offered by behavioral paradigms involving category learning (Wetzel et al., 1998a). To introduce such an approach into the research on cortical neuroprosthesis would be of great value.

Finally, it should be noted that the behavioral response of an animal in a shuttle-box does not only consist of a compartment change, which defines the CR. There is a whole sequence of behavioral elements in response to the CS like an attention response or an orienting response towards the hurdle preceding the actual CR (Bischof et al., 2001). A detailed analysis of this fast behavioral dynamics within a trial and its changes in the course of learning will shed more light on the question of how the animals perceive the electrical stimuli.

5.4. Cortical activity patterns in relation to the meaningful interpretation of intracortical electrical stimuli

5.4.1. Early and late cortical activity patterns

From epochs of significant pattern classification observed in the β- and γ-band (15 Hz to 80 Hz) of the ECoG, it was inferred that there existed spatial cortical activity patterns within these epochs, which were associated with the stimulus classes CS+ and CS-. Early epochs of significant pattern classification were found during electrical stimulus presentation and late epochs emerged in the time between the end of the electrical stimulus and the behavioral response.

Early cortical activity patterns were identified in early epochs during the first 100 ms of the electrical stimulus time-locked to its onset. They were found throughout all training sessions and their frequency of occurrence was not correlated with learning performance. Coexisting with these early patterns, a large negative peak occurred in the electrically evoked potential around 30 ms after the onset of the electrical pulse trains. Although the large electrical stimulus artifact obstructed a detailed spatial analysis of the potentials electrically evoked by the pulse trains, the negative peak, as determined by visual inspection, seemed to have a focal topography with a spatial maximum at the stimulation site. The spatial distribution of the negative peak at a latency of 30 ms in the electrically evoked potential therefore represented a pattern, which was highly discriminable between CS- and the CS+. Thus, the high classification performance seen in the first 100 ms after stimulus onset obviously relied on the focal activation patterns imposed onto the cortical activity by ICMS representing the artificial sensory input to the cortex.

Epochs of significant pattern classification also indicated cortical activity patterns at later times during electrical stimulus presentation emerging over training sessions. However, the increase of classification performance at that time over sessions was not correlated with learning performance. Also, there seemed to be no clear relationship of these patterns to later parts of the electrically evoked potential whose frequency at that time had already dropped below 15 Hz, outside the analyzed β- and γ-band (15 Hz to 80 Hz). How these patterns could relate to ICMS induced plastic cortical reorganization will be discussed below (see subsection 5.5.).

It cannot be ruled out that the spatial distribution of the electrical stimulus artifacts caused by the delivery of electrical current through the different stimulation electrodes with CS+ and CS- contributed to pattern classification during stimulus presentation (see subsection 5.1.3.). Also, changes in the impedances of the stimulation electrodes, as it is often found due to glial scar formation over the first weeks after implantation (see subsection 5.1.1.), could have lead to more discernable spatial distributions of the stimulus artifact, which could also explain the increase of pattern classification performance over sessions at the time of current delivery. A more reliable analysis of the early patterns will certainly afford the development of appropriate techniques for removing the electrical stimulus artifacts (see subsection 5.1.3.).

In contrast to the early patterns, late cortical activity patterns in the β- and γ-band were identified by epochs of significant pattern classification in the time between the end of the electrical stimulus and the behavioral response. No stimulus evoked activity was observed in the β- and γ-band at that time, which could have contributed to the classification. Instead, the ECoG in the late epochs displayed an aperiodic oscillatory waveform shared across all recording channels, which largely varied from trial to trial. Pattern classification in the late epochs relied on the separation of spatial amplitude modulations carried by these aperiodic oscillations, which were associated with the behaviorally relevant stimulus classes CS+ and the CS-. As the ECoG is generated by the vector sum of synaptic currents of thousands of cortical neurons (Mitzdorf, 1985) providing a measure of the local mean field of neuronal ensembles (Freeman, 2000a), the aperiodic waveforms carrying the pattern reflected the cooperative dynamics of large sets of neurons bound together by widespread synaptic interactions. Altogether, this suggests that the late cortical activity patterns emerged from a spatially distributed ongoing cortical dynamics (Freeman & Barrie, 2000).

Pattern classification performance was not continuously elevated over the time between stimulus and response, but was structured into peaks. From this it can be inferred that the spatial activity patterns emerged only transiently. The peaks marked epochs of significant pattern classification which occurred at various latencies between the end of the electrical stimulus and the behavioral response indicating that the patterns were neither precisely time-locked to the stimulus, nor to the behavioral

response. Even if significant, pattern classification performance in the late epochs remained rather low, never exceeding 75% correct classification. This refers to a major drawback of the classification procedure applied in the work presented here. Classification performance values were derived from fixed interval time steps relative to stimulus onset across trials. That the emergence of the late patterns was not time-locked to the stimulus would thus account for the observed low values of classification performance. Ohl et al. (2001) developed a method that permitted them to identify stimulus related activity patterns within single trials. They showed that late learning induced cortical activity patterns occurred at random times between the acoustic stimulus and the behavioral response. Thus, the development of single trial methods for pattern identification that can be suitably applied to the present data will be an important next step.

Moreover, late cortical activity patterns emerged in the course of training. The maximum pattern classification performance in the time between stimulus and behavioral response increased concomitantly with the behavioral discrimination performance and was significantly correlated with it. This suggests that the late cortical activity patterns were induced by learning. As the electrical stimuli remained the same over training sessions, the late patterns were rather related to the behavioral interpretation of the electrical stimuli by the animal than to the sensory processing of the physical properties of the electrical stimulus.

In two animals (038 and 046) no learning induced late cortical activity patterns were found in the time between the end of the electrical stimulus and the behavioral response. Interestingly, in both animals, the positions of the stimulation electrodes could not be clearly assigned to primary auditory cortex due to their large ventral offset along the dorsoventral axis (see subsection 5.1.2.). Also, these animals exhibited a slightly delayed learning dynamics (see subsection 5.3.). It seems that the neural activation in response to ICMS in animals 038 and 046 did not recruit the same cortical processes as in the other animals. Nevertheless, both animals learned to behaviorally discriminate the site of ICMS. In animal 038, delayed epochs of significant pattern classification were found after the behavioral response. Cortical activity patterns in this animal possibly emerged in a different cortical area and were transmitted to AI with a delay. In animal 046, early pattern classification performance during stimulus presentation was low, as well. Accordingly, the amplitudes of the

electrically evoked potentials were small both with single and trains of current pulses. As the stimulation electrodes in this animal were located at a greater radial cortical depth, close to the border of layer V and VI, this suggests that ICMS in this animal was not as effective in eliciting a cortical response as in the other animals. Discrimination learning in animal 046 was eventually based on the transsynaptic activation of subcortical structures by the excitation of cortical output neurons situated in the layers V and VI of the primary auditory cortex.

At this point, the difficult question arises which role the auditory cortex plays in the discrimination learning of intracortical electrical stimuli. Is discrimination learning solely based on electrically evoked intracortical activity or does it necessarily involve stimulus-evoked activity in subcortical structures (Budinger et al., 2000b)? As an extreme, it is conceivable that the auditory cortex only relayed the electrically evoked activity to subcortical structures, which then played the major role in discrimination learning. For example, Ohl et al. (1999) have shown that after bilateral ablation of the complete auditory cortex, Mongolian gerbils can still learn to discriminate simple tones. Pharmacological inactivation experiments (Sandkühler et al., 1987; Kraus & McGee, 1995; Tehovnik & Sommer, 1997) in combination with activity dependent histological staining (Goldschmidt et al. 2004; Scheich et al., 1993) could give an answer to this question.

5.4.2. Comparison between cortical activity patterns emerging with discrimination learning of central and peripheral stimuli

Early and late cortical activity patterns related to the discrimination learning of peripheral stimuli have been recently described by Freeman and colleagues in the sensory cortices of rabbits (Barrie et al., 1996; Freeman & Barrie, 2000). By developing the multivariate classification method which was also applied in the present study, they were able to identify early and late cortical activity patterns in response to acoustic, visual, and somatosensory stimuli in the corresponding sensory cortices. Early cortical activity patterns occurring during the first 300 ms after stimulus onset were time-locked to the stimulus and were already found in naïve, untrained animals. They coexisted with the stimulus evoked potentials and reflected the stimulus specific sensory input. Late cortical activity patterns emerged from the

ongoing cortical activity with olfactory, somatosensory, visual, and acoustic discrimination learning. They occurred at variable points in time around 1 s after stimulus onset and were not time-locked to the stimulus. The learning induced late patterns described by Barrie et al. (1996) showed a lack of invariance with respect to physical stimulus properties (see subsection 1.4.2.). They were individual for each animal, and they changed with the behavioral situation, the behavioral context, and the learning history of the animal. According to Freeman and colleagues (Barrie et al., 1996; Freeman & Barrie, 2000), these patterns are related to the meaning of the stimulus to the animal. In the auditory cortex of Mongolian gerbils, Ohl and colleagues (2001) found early and late cortical activity patterns in response to frequency modulated (FM) tones during categorization learning. Early patterns reflected the tonotopic organization of the early evoked cortical activity (Ohl et al., 2000a, b), whereas late learning induced cortical activity patterns were related to the categories learnt by the animal. In particular, the late patterns in this study possessed a metric that reflected the individual animal's perceptual scaling and sorting of the stimuli into the categories, in a manner that abstracted from the precise physical composition of the stimuli.

The cortical activity patterns found with central, electrical stimulation in the present work resemble the activity patterns induced by peripheral stimuli in many ways. Early patterns were probably evoked by site specific ICMS, and the resulting focal transsynaptic activation patterns were highly discernable between CS+ and CS-. In contrast, late cortical activity patterns were rather related to the meaningful interpretation of the stimuli than to the physical features of the electrical stimuli. Therefore, the late patterns found in the present work apparently reflected the subjective perceptual sorting of the electrical stimuli into the behaviorally relevant classes.

However, comparing late cortical activity patterns emerging with discrimination learning of central, electrical stimuli applied to the auditory cortex in the present study and late patterns emerging with discrimination learning of acoustic stimuli in the auditory cortex, marked differences were found regarding their spatial organization. In the auditory cortex of the Mongolian gerbil, Ohl and colleagues analyzed the spatial organization of early and late cortical activity patterns emerging with the discrimination learning of FM tones to a greater detail (Ohl et al. 2003a, b). One of

their studies (Ohl et al. 2003a) permits a good comparison, because they used basically the same methods for pattern analysis as in the present study. As in the present study, the spatial organization of cortical activity patterns was obtained by discriminant analysis, which was based on a bootstrapping procedure. Classification was carried out repeatedly after removing randomly selected combinations of recording channels and evaluating the classification performance for each combination. Sets of most discriminating electrodes were inferred from the combinations of removed channels yielding minimum classification performance.

The results showed that early patterns in response to acoustic stimuli were focal and topographically organized. The location of the foci was correlated with the distinctive parts of the topography of the mid-latency evoked potentials elicited by rising and falling FM tones (Ohl et al. 2000b). Thus, similar to the early patterns evoked by the electrical stimuli, stimulus-specific differences in the cortical input where responsible for the classification potential of the early pattern in response to the acoustic stimuli.

In contrast, the late patterns emerging with discrimination learning of the FM tones displayed a nonfocal and nontopographical spatial organization. The set of most discriminating electrodes was disconnected and apparently randomly distributed over the recording array. No correlation was found with the stimulus specific thalamic input. Apparently, the spatial information contained in the topographic sensory input disseminated by the dynamic operation of constructing the late pattern. The spatial organization of these late patterns resembled the interference pattern of a hologram (Pribram, 1971), as the same information was present at every electrode, and the classification performance was only dependent on a critical number of electrodes. Thus, the initiating early pattern of sensory input was discarded at that time and could not be reconstructed from the late pattern anymore.

In the present study, the spatial organization of the learning induced late cortical activity patterns was different. The patterns appeared to be focally organized with the most discriminating electrodes always arranged in one or two connected sets. Clusters of most discriminating electrodes were found in the caudal and rostral parts of the recording array. Also, an optimally selected electrode could retain the classification potential of the full pattern, and the spatial distribution of classification performance derived from single recording channels displayed a focal maximum of high classification performance in the caudal part of the recording array and a focal

minimum in the rostral part of the recording array. This focal spatial organization cannot be explained alone by the focal nature of the artificial sensory input. Although the cortical input evoked by FM tones traversing a large tonotopic range was spatially extended (Ohl et al., 2000b), there was no systematic relationship between the spatial organization of this input and the distributed spatial organization of the late cortical activity patterns emerging with the discrimination learning of the FM tones (Ohl et al., 2003a). Furthermore, distributed late cortical activity patterns emerged also from discrimination learning of pure tones with rather focal tonotopic input to the auditory cortex (Barrie et al., 1996).

The clusters of most discriminating electrodes were located along the rostrocaudal axis of the auditory cortex, but their positions could not be matched to the rostral and caudal stimulation sites. Thus, the late patterns induced by electrical stimulation were nontopographically organized with respect to the artificial sensory input. It is possible that different cortical areas were activated by ICMS at the caudal and the rostral stimulation site. Especially the anterior auditory field AAF could have been directly or indirectly excited by some of the rostral stimulation electrodes positioned close to the common high frequency border of AI and AAF. Accordingly, it cannot be excluded that the caudal and rostral cluster of most discriminating electrodes were correlated with focal activity in AI and AAF, respectively. However, due to the positioning of the epidural surface array, only a few rostral electrodes should have recorded signals from AAF. As the rostral clusters also covered large central parts of the array, it is unlikely that pattern classification relied on the separate activation of the fields AI and AAF, respectively.

Despite the focal spatial organization of the patterns induced by electrical stimulation, discriminant analysis provided some evidence that the auditory cortex still operated in a distributed mode. Similar to the distributed late patterns and unlike the focal early patterns found with acoustic discrimination learning, the sets of most discriminating electrodes with different numbers of removed electrodes were not inclusive in the present study. This means that in most discriminating sets of increasing size, the smaller sets were not always subsets of the larger sets. This is also evident from the spatial distribution of single channel classification performance, which did not fully conform to the clusters of most discriminating electrodes. Therefore, the spatial information about the stimulus classes was carried by various different sets of

electrodes. One might speculate that the distributedness of the late cortical activity patterns emerging with electrical stimulation might have been masked by the focal activation. A distributed mode of operation could serve as a mechanism for spatiotemporal integration of cortical activity within a radius of several millimeters (Freeman, 2000a; Freeman & Barrie, 2000). This way, the animals might have extracted the behaviorally relevant cues from the spatially extended activity transsynaptically evoked by ICMS (see section 5.2.). If the animals could be trained to sort electrical stimuli applied to different cortical sites into the same category (Ohl et al. 2001), one should be able to determine the spatial aspects of the pattern pertaining to the perceptual scaling rather than to the stimulus specific input.

It will be interesting to see, how the spatial organization of the cortical activity patterns changes with varying stimulus parameters. Especially varying the length of the pulse trains could shed some light the nature of these patterns. Libet et al. (1964), for example, has shown that in the somatosensory cortex of humans a train length of at least 100 ms and at near-threshold intensities up to 500 ms is required to evoke a conscious sensation (for a review see Libet, 1982). Similar results have been reported in studies of the human visual (Ray et al., 1999) and auditory (Howard et al., 2000) cortex. In cats trained to detect ICMS applied to the auditory cortex, Rousche et al. (1999) showed that the behavioral detection probability reliably fell below 50 % at train lengths of shorter than 100 ms. Investigating late cortical activity patterns induced by pulse trains close to this train length in a discrimination task could give more insight in the behavioral and perceptual relevance of these patterns. Interestingly, the train length has a strong influence on the behavioral outcome of ICMS. For example, in the motor cortex of monkeys, short trains of electrical current pulses evoke muscle twitches, whereas longer trains lasting for about 500 ms can evoke coordinated, complex postures involving many joints (Graziano et al., 2002).

The emergence of the late cortical activity patterns could also be influenced by cortical states preceding the stimulus. This pertains to the more general question of how ICMS interferes with the changing states of the ongoing cortical activity (see 1.4.2.). Several studies have shown that the timing of stimuli relative to the ongoing cortical activity has great influence on perception (Pöppel, 1994; Varela, 1981). However, such states cannot be detected by the classification method applied in the

present study, because only patterns are identified with this procedure that can be assigned either to the CS+ or the CS-. The development of a classification method, which is independent from an external reference would be of great value.

5.5. Neuroplasticity related to the use of a cortical neuro-prosthesis

It is well known that perceptual learning can induce plastic changes in the functional maps of the sensory cortex. For example, Recanzone et al. (1993) found that in monkeys performing a perceptual learning task, tonal frequency discrimination performance within a small frequency range was positively correlated with the size of the representation of this frequency range within auditory cortex. Similar plastic changes can be also induced by ICMS itself due to the highly synchronous activation it exerts on a large population of neurons (Nudo, 1990; Recanzone et al. 1992; Dinse et al. 1993). Several studies have shown that after applying trains of weak current pulses (< 10 µA) for 1 or 4 h to the auditory cortex the cortical representation of the particular frequencies around the stimulation site were enlarged, and the tuning bandwidth of neurons responding to tonal stimuli was increased (Maldonado & Gerstein 1996a; Sakai & Suga, 2002; Valentine & Eggermont, 2003).

It was found some evidence that ICMS, as it was applied during training in the present study, also lead to such a plastic cortical reorganization. Besides the early epochs of highly significant pattern classification during the first 100 ms after stimulus onset, which were found from the first training session on, epochs of significant pattern classification emerged over training session at later times during the presentation of the electrical stimuli. As the increase of classification performance at that time was not significantly correlated with behavioral discrimination performance, these patterns were possibly induced by ICMS itself (see subsection 4.6.1. and 4.6.2.). Similar to the discernable focal patterns seen in the topography of the early negative peak of the electrically evoked potential from the first training sessions on, ICMS itself could have induced plastic changes around the stimulation site, from which discernable spatial patterns emerged in the topographies of later peaks over sessions. The increase in overall amplitude of the electrically evoked potential over

training sessions, both in response to the CS+ and the CS- pulse trains (see subsection 4.5.3.), also indicated ICMS induced plastic changes. As it was hypothesized, ICMS induced plastic effects are due to the decrease of intracortical inhibition leading to an unmasking of subthreshold excitatory connections by the resulting disinhibition (Valentine & Eggermont, 2003). Due to the decreased intracortical inhibition, electrical stimulation would recruit a larger number of cells, which could account for the increase of the peak amplitudes of the electrically evoked potentials. Furthermore, Maldonado and Gerstein (1996b) reported an increased level of correlated neuronal activity within the enlarged frequency representation around the stimulation site. This could also produce an increase in the amplitude of the electrically evoked potential.

ICMS induced plastic changes in the auditory cortex lasted only temporary disappearing within a few hours (Maldonado 1996a, b; Sakai & Suga, 2002). The increase of amplitudes of the electrically evoked potentials over days of training would be difficult to explain by such a local short-term plasticity. However, in the visual cortex of the cat, Godde and colleagues (2002) demonstrated that ICMS can in principle induce persistent, large scale plastic reorganization. They found non-recovering plastic changes in the orientation preference maps in regions up to 4 mm around the stimulation site. One might speculate that the larger amounts of current used in the present study have yielded such a long lasting, large scale rearrangement in the auditory cortex. Although, as not much is known about how plastic changes in the cortex depend on the parameters of ICMS, a systematic investigation of the dependence of plastic changes on different stimulus parameters would be of great importance at this point.

ICMS induced plastic reorganization of the cortex might also account for the observed focal organization of the late cortical activity patterns. According to Freeman (2000a), new cortical activity patterns are established by learning induced plastic changes of the intracortical synaptic connectivity. It could well be that plastic cortical reorganization induced by ICMS itself, independent from learning, distorted the spatial organization of the learning induced cortical activity patterns. For example, Valentine and Eggermont (2003) found evidence that ICMS applied for 1 h can result in a diminished lateral intracortical inhibition in cat auditory cortex. Effects that could be related to such a reduced intracortical inhibition were most pronounced at

distances of 0.5 mm to 2 mm from the stimulation site. Also these effects were observable in the spontaneous activity without acoustic stimulation. In the present study, diminished lateral inhibition induced by ICMS could have distorted the late cortical activity patterns in regions rostral and caudal to the stimulation sites, which might be reflected by the clusters of most discriminating electrodes found in the rostral and caudal parts of the recording array. This would also explain why the positions of the clusters could not be matched to the stimulation sites.

Whether the plastic reorganization of the sensory cortex induced by ICMS is behaviorally relevant, remains a question of debate. In a study of Talwar and Gerstein (2001), ICMS induced frequency specific reorganization of AI in the rat did no alter frequency discrimination behavior. In contrast to all the studies reporting plastic reorganization induced by ICMS, the electrical stimuli in the present study were attached with behavioral significance. Applied in a context meaningful to the animals, plastic cortical reorganization could have played a significant role in discrimination learning (Talwar & Gerstein, 2001). The experimental approach of the present study would offer the opportunity to investigate the relevance of plastic cortical reorganization for the discrimination learning by comparing the changes induced by behaviorally relevant ICMS with changes induced either by passively delivered ICMS or by ICMS applied during a pseudo-training procedure.

Investigating neuroplasticity related to the use of a cortical neuroprosthesis is fundamental for the development of such a device for blind or deaf persons. Deprivation of sensory cortices leads to plastic reorganization changing both its physiology and its morphology (for a review see Hardie, 1998). These changes are more pronounced early in development. Accordingly, it is currently unknown whether ICMS can evoke even simple sensations like phosphenes or audenes in subjects who never developed normal vision or hearing, e.g. in congenitally blind or deaf subjects. Electrical stimulation of the visual cortex and transcranial magnetic stimulation of the visual cortex (Walsh & Cowey, 1998) have yielded negative results in this respect. In congenitally deaf cats, it was shown by electrical stimulation of the 8th cranial via a cochlear implant that the deprived auditory cortex functioned only rudimentary, with later stages of intracortical processing being impaired (Klinke et al., 1999; Kral et al., 2000). If young congenitally deaf kittens were chronically stimulated via the cochlear implant, cortical functioning became similar to normal hearing

controls after several weeks due to neural plasticity and maturational changes. Synaptic efficacy in the cortex increased, and long latency responses indicating intracortical processing developed over time. With the cats becoming mature, this recruitment of cortical processing was largely reduced demonstrating that there existed a sensitive period for this reorganization of the cat's auditory system (Kral et al., 2002). The crucial question is, whether ICMS can lead to similar plastic and maturational restorative effects as seen with the cochlear implants. This is complicated by the fact that ICMS can induce plastic changes in the cortex by itself which might rather disturb these restorative, reorganizational processes.

Even if deprivation occurred late in development, the functional integration of a cortical neuroprosthesis has to rely on the capacity of the cortex to reorganize through learning. Based on a better understanding of the interaction between ICMS and the ongoing cortical dynamics, training and stimulation protocols could be devised that promote such a functional integration of a cortical neuroprosthesis.

5.6. Conclusions

From the analysis of electrically evoked potentials, it was inferred that spatially and temporally confined intracortical microstimulation (ICMS) lead to spatiotemporally extended transsynaptic activation within the cortex. Early transsynaptic activation reflected by a short latency negative wave in the single pulse electrically evoked potentials displayed a focal topography around the stimulation site. The spatial extent of this focal activation exceeded the theoretically estimated effective current spread. Altogether, this indicates that the major determinants of the spatial and temporal specificity of ICMS were the intrinsic cortical interconnectivity, i.e. the projection range and geometry of the directly activated excitatory and inhibitory axonal fibers, and the succeeding postsynaptic interplay between excitation and inhibition (Butovas & Schwarz, 2003).

Despite this spatiotemporal "blur" of the artificial sensory input, all animals were able to learn to discriminate high- from low-frequency sites of ICMS along the tonotopic gradient of the auditory cortex within four or five sessions of training. This demonstrates that the animals were able to behaviorally interpret the electrical stimuli

in a meaningful way. Using a multivariate pattern classification procedure, cortical activity patterns in the β- and γ- band of the electrocorticogram (ECoG) were identified in early epochs during the presentation of the electrical stimuli and in late epochs in the time between the end of the electrical stimuli and the behavioral response. Early cortical activity patterns could be related to the discernable focal patterns of transsynaptic activation found in the topographies of the electrically evoked potentials, which were highly discriminable between CS+ and CS-. Thus, the early patterns reflected the focal artificial sensory input evoked by ICMS. Late cortical activity patterns emerged over training sessions from the ongoing cortical activity and were related to the meaningful behavioral interpretation of the electrical stimuli. They were similar to late cortical activity patterns found in the β- and γ- band of the ECoG with discrimination learning of acoustic stimuli, which were also learning induced, not time-locked to the stimulus and occurred in the time between the stimulus and the behavioral response. However, a marked difference was found with respect to the spatial organization of late cortical activity patterns emerging with discrimination learning of electrical and acoustic stimuli. Whereas learning induced cortical activity patterns emerging with discrimination learning of acoustic stimuli were spatially distributed, patterns emerging with electrical stimulation were more focal, although the focal organization of the patterns could not be related to the focal transsynaptic activation around the stimulation sites. This indicates principle differences in the modes how cortical dynamics is recruited to form discernable percepts when using acoustic or electrical stimuli.

It is possible that the highly synchronous activity imposed by ICMS onto a large, mixed population of neurons was responsible for this altered mode of cortical functioning. Additionally, by the highly synchronous activation, ICMS can induce a plastic reorganization of the cortex, which could distort cortical activity patterns emerging with learning (Maldonado & Gerstein, 1996; Sakai & Suga, 2002; Valentine & Eggermont, 2003). The observed increase in overall amplitude of the electrically evoked potentials over training sessions could indicate such plastic changes induced by ICMS. Also, epochs of significant pattern classification emerged over training session at later times during the presentation of the electrical stimuli. As the increase of classification performance at that time was not significantly correlated with behavioral discrimination performance, the patterns underlying the classification were possibly induced by ICMS itself. Finally, it has to be taken into account that, in

bypassing the afferent sensory pathways, ICMS applied through an unidirectionally operating cortical interface is not properly timed with respect to the ongoing cortical state transitions (Ohl et al., 2001). This could also account for different modes of cortical functioning.

5.7. Outlook: towards an interactive cortical neuro-prosthesis

The hypothesis that the modes how the cortical dynamics is recruited to form discernable percepts when using acoustic or electrical stimuli is different, needs further investigation. The question must be addressed how plastic reorganization induced by intracortical microstimulation (ICMS) interferes with the learning induced formation of cortical activity patterns. Therefore, experiments have to be devised by which learning induced plasticity can be separated from plasticity induced by ICMS itself, e.g. by comparing early and late cortical activity patterns emerging in the course of discrimination training, pseudo-training and passive electrical stimulation. Also, a more profound understanding of the biophysics giving rise to cortical activity patterns is highly needed. This could be achieved by determining the generators underlying both the early, stimulus evoked and late, learning induced patterns in making use of current source density analysis (Mitzdorf, 1985) and by analyzing multiple single unit firing patterns related to the learning with electrical stimuli. Also, the analysis of spatial patterns of phase could shed light on the fast dynamics from which these patterns emerge (Freeman & Barrie, 2000).

A crucial factor for yielding meaningfully structured percepts from ICMS might be the proper timing between state changes in the ongoing cortical dynamics and the incoming electrical stimuli. In order to test the principle relevance of a proper timing of ICMS, it would be necessary to interact with cortical dynamics instantaneously in a freely behaving animal. The monitoring of cortical state changes necessarily involves the real-time analysis of brain signals. With a cortical neuroprosthesis operating in a unidirectional mode, the coincidence of the neuroprosthetic stimulation and the occurrence of brain states open for correct processing of the artificial sensory input would occur only by chance. An interactive cortical neuroprosthesis could guarantee

for the proper timing and shaping of the electrical stimuli conditional on the momentary cortical state, and by this improve the perceptual interpretation of stimuli delivered by the neuroprosthetic device. With a better understanding of the interaction between neuroprosthetic stimulation and the ongoing cortical dynamics, it might be possible to approach the crucial step in the development of a cortical neuroprosthesis: the generation of meaningfully structured perception by patterned multi-site electrical stimulation.

6. References

Abeles M., Bergman H., Gat I., Meilijson I., Seidemann E., Tishby N., & Vaadia E. (1995) Cortical activity flips among quasi-stationary states. *Proc. Natl. Acad. Sci. USA* 92: 8616-8620.

Adrian E. D. (1936) The spread of activity in the cerebral cortex. *J. Physiol.* 88: 127-161.

Agnew W. F., Yuen T. G., & McCreery D. B. (1983) Morphologic changes after prolonged electrical stimulation of the cat's cortex at defined charge densities. *Exp. Neurol.* 79: 397-411.

Agnew W. F., Yuen T. G., McCreery D. B., & Bullara L. A. (1986) Histopathologic evaluation of prolonged intracortical electrical stimulation. *Exp. Neurol.* 92: 162-185.

Ahrens P., Schleicher A., Zilles K., & Werner L. (1990) Image analysis of Nissl-stained neuronal perikarya in the primary visual cortex of the rat: automatic detection and segmentation of neuronal profiles with nuclei and nucleoli. *J. Microsc.* 157 (Pt 3): 349-365.

Alteheld N., Roessler G., Vobig M., & Walter P. (2004) The retina implant--new approach to a visual prosthesis. *Biomed.Tech. (Berl.)* 49: 99-103.

Andrade J. D. & Hlady V. (1987) Plasma protein adsorption: the big twelve. *Ann. N. Y. Acad. Sci.* 516: 158-172.

Arieli A., Sterkin A., Grinvald A., & Aertsen A. (1996) Dynamics of ongoing activity: explanation of the large variability in evoked cortical responses. *Science* 273: 1868-1871.

Asanuma H. & Sakata H. (1967) Functional organization of a cortical efferent system examined with focal depth stimulation in cats. *J. Neurophysiol.* 30: 35-54.

Bach Y. Rita P., Collins C. C., Saunders F. A., White B., & Scadden L. (1969) Vision substitution by tactile image projection. *Nature* 221: 963-964.

Bach Y. Rita P. (2004) Tactile sensory substitution studies. *Ann. N. Y. Acad. Sci.* 1013: 83-91.

Bak M., Girvin J. P., Hambrecht F. T., Kufta C. V., Loeb G. E., & Schmidt E. M. (1990) Visual sensations produced by intracortical microstimulation of the human occipital cortex. *Med. Biol. Eng. Comput.* 28: 257-259.

Barrie J. M., Freeman W. J., & Lenhart M. D. (1996) Spatiotemporal analysis of prepyriform, visual, auditory, and somesthetic surface EEGs in trained rabbits. *J. Neurophysiol.* 76: 520-539.

Barth D. S. & Sutherling W. (1988) Current source-density and neuromagnetic analysis of the direct cortical response in rat cortex. *Brain Res.* 450: 280-294.

Barth D. S. & Di S. (1991) Laminar excitability cycles in neocortex. *J. Neurophysiol.* 65: 891-898.

Basar E., Basar-Eroglu C., Karakas S., & Schurmann M. (2000) Brain oscillations in perception and memory. *Int. J. Psychophysiol.* 35: 95-124.

Bavelier D. & Neville H. J. (2002) Cross-modal plasticity: where and how? *Nat. Rev. Neurosci.* 3: 443-452.

Beer R. D. (2000) Dynamical approaches to cognitive science. *Trends Cogn. Sci.* 4: 91-99.

Bischof A., Stark H., Blumenstein R., Wagner T., Brechmann A., & Scheich H. (2001) A semiautomatic method for adding behavioral data to videotape records in combination with the Noldus Observer system. *Behav. Res. Methods Instrum. Comput.* 33: 549-555.

Bishop G. H. & Clare M. H. (1953) Responses of cortex to direct electrical stimuli applied at different depths. *J. Neurophysiol.* 16: 1-19.

Bortz J. (1999) Statistik für Sozialwissenschaftler. Springer, Berlin.

Braitenberg V. & Schütz A. (1998) Cortex: Statistics and Geometry of Neuronal Connectivity. 2nd edn., Springer, Berlin.

Breindl A. (2001) Kodierungsmöglichkeiten durch Elektrostimulation bei einer auditorischen Cortexprothese: Untersuchungen in der Mongolischen Wüstenrennmaus (Meriones unguiculatus). Dissertation, Otto-von-Guericke-Universität, Magdeburg.

Brindley G. S. & Lewin W. S. (1968) The sensations produced by electrical stimulation of the visual cortex. *J. Physiol.* 196: 479-493.

Brindley G. S., Donaldson P. E., Falconer M. A., & Rushton D. N. (1972) The extent of the region of occipital cortex that when stimulated gives phosphenes fixed in the visual field. *J. Physiol.* 225: 57P-58P.

Brooks R. A. (1999) Cambrian Intelligence: The Early History of the New AI. Bradford Books.

Brummer S. B., Robblee L. S., & Hambrecht F. T. (1983) Criteria for selecting electrodes for electrical stimulation: theoretical and practical considerations. *Ann. N. Y. Acad. Sci.* 405: 159-171.

Budinger E., Heil P., & Scheich H. (2000a) Functional organization of auditory cortex in the Mongolian gerbil (Meriones unguiculatus). III. Anatomical subdivisions and corticocortical connections. *Eur. J. Neurosci.* 12: 2425-2451.

Budinger E., Heil P., & Scheich H. (2000b) Functional organization of auditory cortex in the Mongolian gerbil (Meriones unguiculatus). IV. Connections with anatomically characterized subcortical structures. *Eur. J. Neurosci.* 12: 2452-2474.

Butovas S. & Schwarz C. (2003) Spatiotemporal effects of microstimulation in rat neocortex: a parametric study using multielectrode recordings. *J. Neurophysiol.* 90: 3024-3039.

Button J. & Putnam T. (1962) Visual responses to cortical stimulation in the blind. *J. Iowa Med. Soc. LII* 1: 1-21.

Buzsaki G. (2002) Theta oscillations in the hippocampus. *Neuron* 33: 325-340.

Campbell P. K., Normann R. A., Horch K. W., & Stensaas S. S. (1989) A chronic intracortical electrode array: preliminary results. *J. Biomed. Mater. Res.* 23: 245-259.

Cao Q., Benton R. L., & Whittemore S. R. (2002) Stem cell repair of central nervous system injury. *J. Neurosci. Res.* 68: 501-510.

Cha K., Horch K. W., & Normann R. A. (1992a) Mobility performance with a pixelized vision system. *Vision Res.* 32: 1367-1372.

Cha K., Horch K., & Normann R. A. (1992b) Simulation of a phosphene-based visual field: visual acuity in a pixelized vision system. *Ann. Biomed. Eng.* 20: 439-449.

Cha K., Horch K. W., Normann R. A., & Boman D. K. (1992c) Reading speed with a pixelized vision system. *J. Opt. Soc. Am. A* 9: 673-677.

Chapin J. K., Moxon K. A., Markowitz R. S., & Nicolelis M. A. (1999) Real-time control of a robot arm using simultaneously recorded neurons in the motor cortex. *Nat. Neurosci.* 2: 664-670.

Chapin J. K. & Moxon K. A. (2001) Neural Prostheses for Restoration of Sensory and Motor Function. CRC Press LLC.

Chapin J. K. (2004) Using multi-neuron population recordings for neural prosthetics. *Nat. Neurosci.* 7: 452-455.

Chiel H. J. & Beer R. D. (1997) The brain has a body: adaptive behavior emerges from interactions of nervous system, body and environment. *Trends Neurosci.* 20: 553-557.

Clark A. (1999) An embodied cognitive science? *Trends Cogn. Sci.* 3: 345-351.

Clynes M. E. & Kline N. S. (1960) Cyborgs and Space. *Astronautics* 26-27.

Cohen M. R. & Newsome W. T. (2004) What electrical microstimulation has revealed about the neural basis of cognition. *Curr. Opin. Neurobiol.* 14: 169-177.

Creutzfeldt O. D., Watanabe S., & Lux H. D. (1966) Relations between EEG phenomena and potentials of single cortical cells. I. Evoked responses after thalamic and erpicortical stimulation. *Electroencephalogr. Clin. Neurophysiol.* 20: 1-18.

DeMott D. W. (1966) Cortical micro-toposcopy. *Med. Res. Eng.* 5: 23-29.

Dinse H. R., Recanzone G. H., & Merzenich M. M. (1993) Alterations in correlated activity parallel ICMS-induced representational plasticity. *Neuroreport* 5: 173-176.

Dobelle W. H., Stensaas S. S., Mladejovsky M. G., & Smith J. B. (1973) A prosthesis for the deaf based on cortical stimulation. *Ann. Otol. Rhinol. Laryngol.* 82: 445-463.

Dobelle W. H., Mladejovsky M. G., & Girvin J. P. (1974a) Artifical vision for the blind: electrical stimulation of visual cortex offers hope for a functional prosthesis. *Science* 183: 440-444.

Dobelle W. H. & Mladejovsky M. G. (1974b) Phosphenes produced by electrical stimulation of human occipital cortex, and their application to the development of a prosthesis for the blind. *J. Physiol.* 243: 553-576.

Dobelle W. H., Mladejovsky M. G., Evans J. R., Roberts T. S., & Girvin J. P. (1976) "Braille" reading by a blind volunteer by visual cortex stimulation. *Nature* 259: 111-112.

Dobelle W. H., Turkel J., Henderson D. C., & Evans J. R. (1979a) Mapping the representation of the visual field by electrical stimulation of human visual cortex. *Am.J Ophthalmol.* 88: 727-735.

Dobelle W. H., Quest D. O., Antunes J. L., Roberts T. S., & Girvin J. P. (1979b) Artificial vision for the blind by electrical stimulation of the visual cortex. *Neurosurgery* 5: 521-527.

Dobelle W. H. (2000) Artificial vision for the blind by connecting a television camera to the visual cortex. *ASAIO J.* 46 (1): 3-9.

Donoghue J. P. (2002) Connecting cortex to machines: recent advances in brain interfaces. *Nat. Neurosci.* 5 Suppl: 1085-1088.

Doty R. W., Larsen R. M., & Ruthledge L. T., Jr. (1956) Conditioned reflexes established to electrical stimulation of cat cerebral cortex. *J. Neurophysiol.* 19: 401-415.

Doty R. W. & Rutlege L. T. (1959) Generalization between cortically and peripherally applied stimuli eliciting conditioned reflexes. *J. Neurophysiol.* 22: 428-435.

Doty R. W. (1965) Conditioned reflexes elicited by electrical stimulation of the brain in macaques. *J. Neurophysiol.* 28: 623-640.

Doty R. W. (1969) Electrical stimulation of the brain in behavioral context. *Annu. Rev. Psychol.* 20: 289-320.

Edell D. J., Toi V. V., McNeil V. M., & Clark L. D. (1992) Factors influencing the biocompatibility of insertable silicon microshafts in cerebral cortex. *IEEE Trans. Biomed. Eng.* 39: 635-643.

Epstein W., Hughes B., Schneider S., & Bach Y.Rita P. (1986) Is there anything out there? A study of distal attribution in response to vibrotactile stimulation. *Perception* 15: 275-284.

Epstein W., Hughes B., Schneider S. L., & Bach Y.Rita P. (1989) Perceptual learning of spatiotemporal events: evidence from an unfamiliar modality. *J. Exp. Psychol. Hum. Percept. Perform.* 15: 28-44.

Fine I., Wade A. R., Brewer A. A., May M. G., Goodman D. F., Boynton G. M., Wandell B. A., & MacLeod D. I. (2003) Long-term deprivation affects visual perception and cortex. *Nat. Neurosci.* 6: 915-916.

Förster O. (1929) Beitrage zur Pathophysiologie der Sehsphäre. *J. Psychol. Neurol.* 39: 463-485.

Freeman W. J. (1975) Mass Action in the Nervous System. Academic Press, New York.

Freeman W. J. (1980) Use of spatial deconvolution ot compensate for distortion of EEG by volume conduction. *IEEE Trans. Biomed. Eng.* 27: 421-429.

Freeman W. J. (1994) Characterization of state transitions in spatially distributed, chaotic, nonlinear, dynamical systems in cerebral cortex. *Integr. Physiol. Behav. Sci.* 29: 294-306.

Freeman W. J. (2000a) Mesoscopic neurodynamics: from neuron to brain. *J. Physiol. Paris* 94: 303-322.

Freeman W. J. (2000b) Neurodynamics: An Exploration in Mesoscopic Brain Dynamics (Perspectives in Neural Computing). Springer, London.

Freeman W. J. (2000c) Emotion is Essential to All Intentional Behaviors. In: *Emotion, Development, and Self-Organization: Dynamic Systems Approaches to Emotional Development* (eds. Lewis M. D. and Granic I.) pp. 209-235. Cambridge University Press, Cambridge, UK.

Freeman W. J. & Barrie J. M. (2000) Analysis of spatial patterns of phase in neocortical gamma EEGs in rabbit. *J. Neurophysiol.* 84: 1266-1278.

Fritsch G. & Hitzig E. (1870) Über die elektrische Erregbarkeit des Grosshirns. *Archiv für Anatomie, Physiologie und wissenschaftliche Medicin* 300-332.

Fromherz P. (2002) Electrical interfacing of nerve cells and semiconductor chips. *Chemphyschem.* 3: 276-284.

Gage F. H. (2002) Neurogenesis in the adult brain. *J. Neurosci.* 22: 612-613.

Galarreta M. & Hestrin S. (2002) Electrical and chemical synapses among parvalbumin fast-spiking GABAergic interneurons in adult mouse neocortex. *Proc. Natl. Acad Sci. USA* 99: 12438-12443.

Godde B., Leonhardt R., Cords S. M., & Dinse H. R. (2002) Plasticity of orientation preference maps in the visual cortex of adult cats. *Proc. Natl. Acad. Sci. USA* 99: 6352-6357.

Goldschmidt J., Zuschratter W., & Scheich H. (2004) High-resolution mapping of neuronal activity by thallium autometallography. *Neuroimage.* 23: 638-647.

Graziano M. S., Taylor C. S., & Moore T. (2002) Complex movements evoked by microstimulation of precentral cortex. *Neuron* 34: 841-851.

Green D. M. & Swets J. A. (1966) Signal Detection Theory and Psychophysics. Wiley, New York.

Grosser G. S. & Harrison J. M. (1960) Behavioral interaction between stimulated cortical points. *J. Comp. Physiol. Psychol.* 53: 229-233.

Gustafsson B. & Jankowska E. (1976) Direct and indirect activation of nerve cells by electrical pulses applied extracellularly. *J. Physiol.* 258: 33-61.

Haraway D. F. (1991) Simians, Cyborgs and Women. Routledege, New York.

Hardie N. A. (1998) The consequences of deafness and chronic intracochlear electrical stimulation on the central auditory pathways. *Clin. Exp. Pharmacol. Physiol.* 25: 303-309.

Harding G. W. (1991) A method for eliminating the stimulus artifact from digital recordings of the direct cortical response. *Comput. Biomed. Res.* 24: 183-195.

Harding G. W. (1992) The currents that flow in the somatosensory cortex during the direct cortical response. *Exp. Brain Res.* 90: 29-39.

Harrower T. P. & Barker R. A. (2004) Is there a future for neural transplantation? *BioDrugs* 18: 141-153.

Hashimoto T., Elder C. M., & Vitek J. L. (2002) A template subtraction method for stimulus artifact removal in high-frequency deep brain stimulation. *J. Neurosci. Methods* 113: 181-186.

Hayes J. S., Yin V. T., Piyathaisere D., Weiland J. D., Humayun M. S., & Dagnelie G. (2003) Visually guided performance of simple tasks using simulated prosthetic vision. *Artif. Organs* 27: 1016-1028.

Heeger D. Signal detection theory. 2003. http://www.cns.nyu.edu/~david/sdt/sdt.html

Heiduschka P. & Thanos S. (1998) Implantable bioelectric interfaces for lost nerve functions. *Prog. Neurobiol.* 55: 433-461.

Hess A. & Scheich H. (1996) Optical and FDG mapping of frequency-specific activity in auditory cortex. *Neuroreport* 7: 2643-2647.

Howard M. A., Volkov I. O., Mirsky R., Garell P. C., Noh M. D., Granner M., Damasio H., Steinschneider M., Reale R. A., Hind J. E., & Brugge J. F. (2000) Auditory cortex on the human posterior superior temporal gyrus. *J. Comp. Neurol.* 416: 79-92.

Hutzler M. & Fromherz P. (2004) Silicon chip with capacitors and transistors for interfacing organotypic brain slice of rat hippocampus. *Eur. J. Neurosci.* 19: 2231-2238.

John E. R. & Kleinman D. (1975) "Stimulus generalization" between differentiated visual, auditory, and central stimuli. *J. Neurophysiol.* 38: 1015-1034.

Jung T. P., Makeig S., Humphries C., Lee T. W., McKeown M. J., Iragui V., & Sejnowski T. J. (2000) Removing electroencephalographic artifacts by blind source separation. *Psychophysiology* 37: 163-178.

Kahana M. J., Seelig D., & Madsen J. R. (2001) Theta returns. *Curr. Opin. Neurobiol.* 11: 739-744.

Kay L. M., Lancaster L. R., & Freeman W. J. (1996) Reafference and attractors in the olfactory system during odor recognition. *Int. J. Neural Syst.* 7: 489-495.

Kay L. M. & Freeman W. J. (1998) Bidirectional processing in the olfactory-limbic axis during olfactory behavior. *Behav. Neurosci.* 112: 541-553.

Kempermann G., Wiskott L., & Gage F. H. (2004) Functional significance of adult neurogenesis. *Curr. Opin. Neurobiol.* 14: 186-191.

Kennedy P. R., Mirra S. S., & Bakay R. A. (1992) The cone electrode: ultrastructural studies following long-term recording in rat and monkey cortex. *Neurosci. Lett.* 142: 89-94.

Kennedy P. R. & Bakay R. A. (1998) Restoration of neural output from a paralyzed patient by a direct brain connection. *Neuroreport* 9: 1707-1711.

Klinke R., Kral A., Heid S., Tillein J., & Hartmann R. (1999) Recruitment of the auditory cortex in congenitally deaf cats by long-term cochlear electrostimulation. *Science* 285: 1729-1733.

Köhler W. (1967) Gestalt psychology. *Psychol. Forsch.* 31: 18-30.

Kral A., Hartmann R., Tillein J., Heid S., & Klinke R. (2000) Congenital auditory deprivation reduces synaptic activity within the auditory cortex in a layer-specific manner. *Cereb. Cortex* 10: 714-726.

Kral A., Hartmann R., Tillein J., Heid S., & Klinke R. (2002) Hearing after congenital deafness: central auditory plasticity and sensory deprivation. *Cereb. Cortex* 12: 797-807.

Kraus N. & McGee T. (1995) The middle latency response generating system. *Electroencephalogr. Clin. Neurophysiol. Suppl.* 44: 93-101.

Krause F. & Schum H. (1931) Die epileptischen Erkrankungen. In: *Neue Deutsche Chirurgie* (ed. Kuttner H.). pp. 482-486. Enke, Stuttgart.

Krieg W. (1953) In: *Functional Neuroanatomy.* pp. 207-208. Blakiston, New York

Kruger J. (1982) A 12-fold microelectrode for recording from vertically aligned cortical neurones. *J. Neurosci. Methods* 6: 347-350.

Kuchta J. (2004) Neuroprosthetic hearing with auditory brainstem implants. *Biomed. Tech. (Berl.)* 49: 83-87.

Le Van Quyen M., Martinerie J., Navarro V., Boon P., D'Have M., Adam C., Renault B., Varela F., & Baulac M. (2001) Anticipation of epileptic seizures from standard EEG recordings. *Lancet* 357: 183-188.

Lehnertz K., Andrzejak R. G., Arnhold J., Kreuz T., Mormann F., Rieke C., Widman A. G., & Elger C. E. (2001) Nonlinear EEG analysis in epilepsy: its possible use for interictal focus localization, seizure anticipation, and prevention. *J. Clin. Neurophysiol.* 18: 209-222.

Lenarz M., Matthies C., Lesinski-Schiedat A., Frohne C., Rost U., Illg A., Battmer R. D., Samii M., & Lenarz T. (2002) Auditory brainstem implant part II: subjective assessment of functional outcome. *Otol. Neurotol.* 23: 694-697.

Lenarz T., Moshrefi M., Matthies C., Frohne C., Lesinski-Schiedat A., Illg A., Rost U., Battmer R. D., & Samii M. (2001) Auditory brainstem implant: part I. Auditory performance and its evolution over time. *Otol. Neurotol.* 22: 823-833.

Lenay C., Gapenne O., Hanneton S., Marque C., & Genouëlle C. (2003) Sensory substitution: limits and perspectives.
http://www.utc.fr/gsp/publi/Lenay03-Sensory%20substitution.pdf

LeRoy C. (1755) Où l'on rend compte de quelques tentatives que l'on a faites pour guérir plusieurs maladies par l'électricité. *Hist. Acad. Roy. Sciences (Paris) M´emoires Math. Phys.* 87-95.

Libet B., Alberts W. W., Wright E. W., Jr., Delattre L. D., Levin G., & Feinstein B. (1964) Production of threshold levels of conscious sensation by electrical stimulation of human somatosensory cortex. *J. Neurophysiol.* 27: 546-578.

Libet B. (1982) Brain stimulation in the study of neuronal functions for conscious sensory experiences. *Hum. Neurobiol.* 1: 235-242.

Lilly J. C. (1954) Instantaneous relations between the activities of closely spaced zones on the cerebral cortex; electrical figures during responses and spontaneous activity. *Am. J. Physiol.* 176: 493-504.

Lilly J. C., Hughes J. R., Alvord E. C., Jr., & Galkin T. W. (1955) Brief, noninjurious electric waveform for stimulation of the brain. *Science* 121: 468-469.

Livanov M. N. (1977) Spatial Organization of Cerebral Processes. Wiley, New York.

Löwenstein K. & Borchardt M. (1918) Symptomatologie und elektrische Reizung bei einer Schußverletzung des Hinterhauptlappens. *Dtsch.Z.Nervenheilkd.* 58: 264-292.

Macmillan N. A. & Creelman C. D. (1991) Detection theory: A user's guide. Cambridge University Press, Cambridge, UK.

Maldonado P. E. & Gerstein G. L. (1996a) Reorganization in the auditory cortex of the rat induced by intracortical microstimulation: a multiple single-unit study. *Exp.Brain Res.* 112: 420-430.

Maldonado P. E. & Gerstein G. L. (1996b) Neuronal assembly dynamics in the rat auditory cortex during reorganization induced by intracortical microstimulation. *Exp. Brain Res.* 112: 431-441.

McCreery D. B., Bullara L. A., & Agnew W. F. (1986) Neuronal activity evoked by chronically implanted intracortical microelectrodes. *Exp. Neurol.* 92: 147-161.

McCreery D. B., Agnew W. F., Yuen T. G., & Bullara L. (1990) Charge density and charge per phase as cofactors in neural injury induced by electrical stimulation. *IEEE Trans. Biomed. Eng.* 37: 996-1001.

McCreery D. B., Yuen T. G., Agnew W. F., & Bullara L. A. (1997) A characterization of the effects on neuronal excitability due to prolonged microstimulation with chronically implanted microelectrodes. *IEEE Trans. Biomed. Eng.* 44: 931-939.

McCreery D. B., Agnew W. F., & Bullara L. A. (2002) The effects of prolonged intracortical microstimulation on the excitability of pyramidal tract neurons in the cat. *Ann. Biomed. Eng.* 30: 107-119.

McIntyre C. C., Savasta M., Kerkerian-Le Goff L., & Vitek J. L. (2004a) Uncovering the mechanism(s) of action of deep brain stimulation: activation, inhibition, or both. *Clin. Neurophysiol.* 115: 1239-1248.

McIntyre C. C., Savasta M., Walter B. L., & Vitek J. L. (2004b) How does deep brain stimulation work? Present understanding and future questions. *J. Clin. Neurophysiol.* 21: 40-50.

Merleau-Ponty M. (1962) Phenomenology of Perception. Humanities Press, New York.

Mitzdorf U. (1985) Current source-density method and application in cat cerebral cortex: investigation of evoked potentials and EEG phenomena. *Physiol. Rev.* 65: 37-100.

Nicolelis M. A. (2003) Brain-machine interfaces to restore motor function and probe neural circuits. *Nat. Rev. Neurosci.* 4: 417-422.

Normann R. A., Maynard E. M., Rousche P. J., & Warren D. J. (1999) A neural interface for a cortical vision prosthesis. *Vision Res.* 39: 2577-2587.

Nowak L. G. & Bullier J. (1998a) Axons, but not cell bodies, are activated by electrical stimulation in cortical gray matter. I. Evidence from chronaxie measurements. *Exp. Brain Res.* 118: 477-488.

Nowak L. G. & Bullier J. (1998b) Axons, but not cell bodies, are activated by electrical stimulation in cortical gray matter. II. Evidence from selective inactivation of cell bodies and axon initial segments. *Exp. Brain Res.* 118: 489-500.

Nudo R. J., Jenkins W. M., & Merzenich M. M. (1990) Repetitive microstimulation alters the cortical representation of movements in adult rats. *Somatosens. Mot. Res.* 7: 463-483.

Nunez R. & Freeman W. J. (2000) Reclaiming Cognition: The Primacy of Action, Intention and Emotion. Imprint Academic, Thorverton, UK.

O'Keeffe D. T., Lyons G. M., Donnelly A. E., & Byrne C. A. (2001) Stimulus artifact removal using a software-based two-stage peak detection algorithm. *J. Neurosci. Methods* 109: 137-145.

O'Regan J. K. & Noë A. (2001) A sensorimotor account of vision and visual consciousness. *Behav. Brain Sci.* 24: 939-973.

Odeh R. E. & Evans J. O. (1965) In: *Handbook of Mathematical Functions* (eds M. Abramowitz and I. A. Stegun) pp. 358. Dover, New York.

Ohl F. W. & Scheich H. (1996) Differential frequency conditioning enhances spectral contrast sensitivity of units in auditory cortex (field AI) of the alert Mongolian gerbil. *Eur. J. Neurosci.* 8: 1001-1017.

Ohl F. W. & Scheich H. (1997) Orderly cortical representation of vowels based on formant interaction. *Proc. Natl. Acad. Sci. USA* 94: 9440-9444.

Ohl F. W., Wetzel W., Wagner T., Rech A., & Scheich H. (1999) Bilateral ablation of auditory cortex in Mongolian gerbil affects discrimination of frequency modulated tones but not of pure tones. *Learn. Mem.* 6: 347-362.

Ohl F. W., Scheich H., & Freeman W. J. (2000a) Topographic analysis of epidural pure-tone-evoked potentials in gerbil auditory cortex. *J. Neurophysiol.* 83: 3123-3132.

Ohl F. W., Schulze H., Scheich H., & Freeman W. J. (2000b) Spatial representation of frequency-modulated tones in gerbil auditory cortex revealed by epidural electrocorticography. *J. Physiol. Paris* 94: 549-554.

Ohl F. W., Scheich H., & Freeman W. J. (2001) Change in pattern of ongoing cortical activity with auditory category learning. *Nature* 412: 733-736.

Ohl F. W., Deliano M., Scheich H., & Freeman W. J. (2003a) Early and late patterns of stimulus-related activity in auditory cortex of trained animals. *Biol. Cybern.* 88: 374-379.

Ohl F. W., Deliano M., Scheich H., & Freeman W. J. (2003b) Analysis of evoked and emergent patterns of stimulus-related auditory cortical activity. *Rev. Neurosci.* 14: 35-42.

Oster G. (1970) Phosphenes. *Sci. Am.* 222: 82-87.

Penfield W. & Rasmussen T. (1950) The Cerebral Cortex in Man. Macmillan, New York.

Penfield W. & Jasper H. (1954) Epilepsy and the Functional Anatomy of the Human Brain. Churchill, London.

Penfield W. & Perot P. (1963) The Brain's record of auditory and visual experience. A final summary and discussion. *Brain* 86: 595-696.

Peterman M. C., Noolandi J., Blumenkranz M. S., & Fishman H. A. (2004) Localized chemical release from an artificial synapse chip. *Proc. Natl. Acad. Sci. USA* 101: 9951-9954.

Peterson D. A. (2004) Stem cell therapy for neurological disease and injury. *Panminerva Med.* 46: 75-80.

Picard-Riera N., Nait-Oumesmar B., & Baron-Van Evercooren A. (2004) Endogenous adult neural stem cells: limits and potential to repair the injured central nervous system. *J. Neurosci. Res.* 76: 223-231.

Pollen D. A. (1975) Some perceptual effects of electrical stimulation of the visual cortex in man. In: *The Nervous System* (ed. Tower D. B.) pp. 519-528. Raven Press, New York.

Port R. F. & van Gelder T. (1995) Mind as Motion: Explorations in the Dynamics of Cognition. Bradford Books, The MIT Press, Cambridge, Massachusetts, USA.

Pöppel E. (1994) Temporal mechanisms in perception. *Int. Rev. Neurobiol.* 37: 185-202.

Pribram K. H. (1971) Languages of the Brain; Experimental Paradoxes and Principles in Neuropsychology. Prentice-Hall, Englewood Cliffs, N.J.

Prochazka A., Mushahwar V. K., & McCreery D. B. (2001) Neural prostheses. *J. Physiol.* 533: 99-109.

Ranck J. B., Jr. (1975) Which elements are excited in electrical stimulation of mammalian central nervous system: a review. *Brain Res.* 98: 417-440.

Rattay F. (1998) Analysis of the electrical excitation of CNS neurons. *IEEE Trans. Biomed. Eng.* 45: 766-772.

Ray P. G., Meador K. J., Smith J. R., Wheless J. W., Sittenfeld M., & Clifton G. L. (1999) Physiology of perception: cortical stimulation and recording in humans. *Neurology* 52: 1044-1049.

Recanzone G. H., Merzenich M. M., & Dinse H. R. (1992) Expansion of the cortical representation of a specific skin field in primary somatosensory cortex by intracortical microstimulation. *Cereb. Cortex* 2: 181-196.

Recanzone G. H., Schreiner C. E., & Merzenich M. M. (1993) Plasticity in the frequency representation of primary auditory cortex following discrimination training in adult owl monkeys. *J. Neurosci.* 13: 87-103.

Romo R., Hernandez A., Zainos A., Brody C. D., & Lemus L. (2000) Sensing without touching: psychophysical performance based on cortical microstimulation. *Neuron* 26: 273-278.

Rousche P. J. & Normann R. A. (1999) Chronic intracortical microstimulation (ICMS) of cat sensory cortex using the Utah Intracortical Electrode Array. *IEEE Trans. Rehabil. Eng.* 7: 56-68.

Rousche P. J., Otto K. J., Reilly M. P., & Kipke D. R. (2003) Single electrode micro-stimulation of rat auditory cortex: an evaluation of behavioral performance. *Hear. Res.* 179: 62-71.

Rubinstein J. T. & Miller C. A. (1999) How do cochlear prostheses work? *Curr. Opin. Neurobiol.* 9: 399-404.

Ryan A. (1976) Hearing sensitivity of the mongolian gerbil, Meriones unguiculatis. *J. Acoust. Soc. Am.* 59: 1222-1226.

Sachs L. (1992) Angewandte Statistik, 7th edn. Springer, Berlin.

Sacks O. (1998) The Man Who Mistook His Wife For A Hat: And Other Clinical Tales. Touchstone, New York.

Sakai M. & Suga N. (2002) Centripetal and centrifugal reorganizations of frequency map of auditory cortex in gerbils. *Proc. Natl. Acad. Sci. USA* 99: 7108-7112.

Salzman C. D., Britten K. H., & Newsome W. T. (1990) Cortical microstimulation influences perceptual judgements of motion direction. *Nature* 346: 174-177.

Sandkühler J., Maisch B., & Zimmermann M. (1987) The use of local anaesthetic microinjections to identify central pathways: a quantitative evaluation of the time course and extent of the neuronal block. *Exp. Brain Res.* 68: 168-178.

Scheich H., Heil P., & Langner G. (1993) Functional organization of auditory cortex in the mongolian gerbil (Meriones unguiculatus). II. Tonotopic 2-deoxyglucose. *Eur. J. Neurosci.* 5: 898-914.

Scheich H., Stark H., Zuschratter W., Ohl F. W., & Simonis C. E. (1997) Some functions of primary auditory cortex in learning and memory formation. *Adv. Neurol.* 73: 179-193.

Scheich H. & Breindl A. (2002) An animal model of auditory cortex prostheses. *Audiol. Neurootol.* 7: 191-194.

Schmidt E. M., Bak M. J., Hambrecht F. T., Kufta C. V., O'Rourke D. K., & Vallabhanath P. (1996) Feasibility of a visual prosthesis for the blind based on intracortical microstimulation of the visual cortex. *Brain* 119 (Pt 2): 507-522.

Schmidt S., Horch K., & Normann R. (1993) Biocompatibility of silicon-based electrode arrays implanted in feline cortical tissue. *J. Biomed. Mater. Res.* 27: 1393-1399.

Schulze H. & Scheich H. (1999) Discrimination learning of amplitude modulated tones in Mongolian gerbils. *Neurosci. Lett.* 261: 13-16.

Schulze H., Hess A., Ohl F. W., & Scheich H. (2002) Superposition of horseshoe-like periodicity and linear tonotopic maps in auditory cortex of the Mongolian gerbil. *Eur. J. Neurosci.* 15: 1077-1084.

Schwartz A. B. (2004) Cortical neural prosthetics. *Annu. Rev. Neurosci.* 27: 487-507.

Shannon C. E. (1948) A mathematical theory of communication. Bell Telephone System Tech. Publ. Monograph B-1598 , 1-80.

Stark H., Bischof A., Wagner T., & Scheich H. (2000) Stages of avoidance strategy formation in gerbils are correlated with dopaminergic transmission activity. *Eur. J. Pharmacol.* 405: 263-275.

Stark H., Rothe T., Wagner T., & Scheich H. (2004) Learning a new behavioral strategy in the shuttle-box increases prefrontal dopamine. *Neuroscience* 126: 21-29.

Stensaas S. S. & Stensaas L. J. (1978) Histopathological evaluation of materials implanted in the cerebral cortex. *Acta Neuropathol. (Berl.)* 41: 145-155.

Steriade M. (1984) The excitatory-inhibitory response sequence in thalamic and neocortical cells: state-related changes and regulatory systems. In: *Dynamic aspects of Neocortical Function* (eds. Edelman G. M., Gall W. E., and Cowan W. M.) pp. 107-157. Wiley, New York.

Stoney S. D., Thompson W. D., & Asanuma H. (1968) Excitation of pyramidal tract cells by intracortical microstimulation: effective extent of stimulating current. *J. Neurophysiol.* 31: 659-669.

Szarowski D. H., Andersen M. D., Retterer S., Spence A. J., Isaacson M., Craighead H. G., Turner J. N., & Shain W. (2003) Brain responses to micro-machined silicon devices. *Brain Res.* 983: 23-35.

Szentagothai J. (1975) The 'module-concept' in cerebral cortex architecture. *Brain Res.* 95: 475-496.

Talwar S. K. & Gerstein G. L. (2001) Reorganization in awake rat auditory cortex by local microstimulation and its effect on frequency-discrimination behavior. *J. Neurophysiol.* 86: 1555-1572.

Talwar S. K., Xu S., Hawley E. S., Weiss S. A., Moxon K. A., & Chapin J. K. (2002) Rat navigation guided by remote control. *Nature* 417: 37-38.

Tass P. A., Klosterkotter J., Schneider F., Lenartz D., Koulousakis A., & Sturm V. (2003a) Obsessive-compulsive disorder: development of demand-controlled deep brain stimulation with methods from stochastic phase resetting. *Neuropsychopharmacology* 28 Suppl. 1: S27-S34.

Tass P. A. (2003b) A model of desynchronizing deep brain stimulation with a demand-controlled coordinated reset of neural subpopulations. *Biol. Cybern.* 89: 81-88.

Tehovnik E. J. (1996) Electrical stimulation of neural tissue to evoke behavioral responses. *J. Neurosci. Methods* 65: 1-17.

Tehovnik E. J. & Sommer M. A. (1997) Effective spread and timecourse of neural inactivation caused by lidocaine injection in monkey cerebral cortex. *J. Neurosci. Methods* 74: 17-26.

Thomas H., Tillein J., Heil P., & Scheich H. (1993) Functional organization of auditory cortex in the mongolian gerbil (Meriones unguiculatus). I. Electrophysiological mapping of frequency representation and distinction of fields. *Eur.J. Neurosci.* 5: 882-897.

Thompson E. & Varela F. J. (2001) Radical embodiment: neural dynamics and consciousness. *Trends Cogn. Sci.* 5: 418-425.

Troyk P., Bak M., Berg J., Bradley D., Cogan S., Erickson R., Kufta C., McCreery D., Schmidt E., & Towle V. (2003) A model for intracortical visual prosthesis research. *Artif. Organs* 27: 1005-1015.

Turner J. N., Shain W., Szarowski D. H., Andersen M., Martins S., Isaacson M., & Craighead H. (1999) Cerebral astrocyte response to micromachined silicon implants. *Exp. Neurol.* 156: 33-49.

Uhlig C. E., Taneri S., Benner F. P., & Gerding H. (2001) Electrical stimulation of the visual system. From empirical approach to visual. *Ophthalmologe* 98: 1089-1096.

Urban H. (1937) Zur Physiologie der Occipitalregion des Menschen. *Z. Ges. Neurol. Psychiat.* 158: 257-261.

Valentine P. A. & Eggermont J. J. (2003) Intracortical microstimulation induced changes in spectral and temporal response properties in cat auditory cortex. *Hear. Res.* 183: 109-125.

Varela F. J., Toro A., John E. R., & Schwartz E. L. (1981) Perceptual framing and cortical alpha rhythm. *Neuropsychologia* 19: 675-686.

Varela F. J., Thompson E. T., & Rosch E. (1992) The Embodied Mind: Cognitive Science and Human Experience. The MIT Press, Cambridge, Massachusetts, USA.

Varela F. J. (1997) Patterns of life: intertwining identity and cognition. *Brain Cogn.* 34: 72-87.

Varela F. J. & Shear J. (1999) The View from Within: First-person Approaches to the Study of Consciousness. Imprint Academic, Thorverton, UK.

Villa A. E., Tetko I. V., Hyland B., & Najem A. (1999) Spatiotemporal activity patterns of rat cortical neurons predict responses in a conditioned task. *Proc. Natl. Acad Sci. USA* 96: 1106-1111.

Volkmann J. (2004) Deep brain stimulation for the treatment of Parkinson's disease. *J.Clin.Neurophysiol.* 21: 6-17.

Walsh V. & Cowey A. (1998) Magnetic stimulation studies of visual cognition. *TICS* **2**: 103-110.

Wasserman E. A. & Miller R. R. (1997) What's elementary about associative learning? *Annu.Rev.Psychol* 48: 573-607.

Wessberg J., Stambaugh C. R., Kralik J. D., Beck P. D., Laubach M., Chapin J. K., Kim J., Biggs S. J., Srinivasan M. A., & Nicolelis M. A. (2000) Real-time prediction of hand trajectory by ensembles of cortical neurons in primates. *Nature* 408: 361-365.

Wetzel W., Wagner T., Ohl F. W., & Scheich H. (1998a) Categorical discrimination of direction in frequency-modulated tones by Mongolian gerbils. *Behav. Brain Res.* 91: 29-39.

Wetzel W., Ohl F. W., Wagner T., & Scheich H. (1998b) Right auditory cortex lesion in Mongolian gerbils impairs discrimination of rising and falling frequency-modulated tones. *Neurosci. Lett.* 252: 115-118.

Wilson B. S., Lawson D. T., Muller J. M., Tyler R. S., & Kiefer J. (2003) Cochlear implants: some likely next steps. *Annu. Rev. Biomed. Eng.* 5: 207-249.

Zhong Y., Yu X., Gilbert R., & Bellamkonda R. V. (2001) Stabilizing electrode-host interfaces: a tissue engineering approach. *J. Rehabil. Res. Dev.* 38: 627-632.

Acknowledgement

Lebenslauf

Name: Matthias Deliano

Geburtstag: 07.04.1972

Geburtsort: München

Wohnsitz: Steinigstr. 12b, 39108 Magdeburg

Staatsangehörigkeit: deutsch

Fachgebiet der Promotion: Neurowissenschaften

Schulausbildung:

1978-1982   Grundschule Vaterstetten

1982-1991   Gymnasium Vaterstetten
                   Abitur

Wehrersatzdienst:

1991-1992   Altenpflege bei der Arbeiterwohlfahrt in München

Hochschulausbildung:

10/1992-09/1998   *Ludwig-Maximilians-Universität München*
                   Studium der Biologie

06/1997-05/1998   *Laboratoire de Neurosciences Cognitives et Imagerie Cérébral, Centre National de la Recherche Scientifique (CNRS), Paris*
                   Diplomarbeit über Gamma-Oszillationen im menschlichen EEG unter Betreuung von Francisco Varela

06/1998   *Ludwig-Maximilians-Universität München*
                   Diplom in Biologie mit Hauptfach Neurobiologie

ab 03/1999   *Leibniz-Institut für Neurobiologie, Magdeburg*
                   Doktorand unter Betreuung von Prof. Dr. Henning Scheich

Stipendien:

07/1995   Aufnahme in die Studienstiftung des deutschen Volkes

Magdeburg, den 27.03.2006

(Matthias Deliano)

Selbständigkeitserklärung

Hiermit erkläre ich, dass ich die von mir eingereichte Dissertation mit dem Thema

„Neural dynamics and their relationship to learning behavior in response to stimulation with a cortical neuroprosthesis"

selbständig verfasst, nicht schon als Dissertation verwendet habe und die benutzten Hilfsmittel und Quellen vollständig angegeben habe.

Weiterhin erkläre ich, dass ich weder diese noch eine andere Arbeit zur Erlangung des akademischen Grades doctor rerum naturalium (Dr. rer. nat.) an anderen Einrichtungen eingereicht habe.

Magdeburg, den 27.03.2006